

**ALMA MATER STUDIORUM - UNIVERSITÀ DI
BOLOGNA**

School of Science

Department of Industrial Chemistry “Toso Montanari”

Corso di Laurea Magistrale / Master

Advanced Spectroscopy in Chemistry

Classe LM-71 - Scienze e Tecnologia della Chimica Industriale

**FUNCTIONAL DNA NANOSTRUCTURES FOR *IN VITRO*
BIOSENSING IN LIVE CELLS**

Experimental Master Thesis

CANDIDATE :

Isidro Badillo

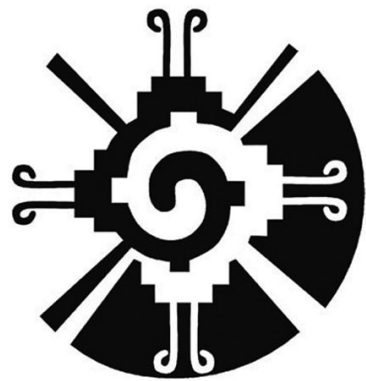
TUTOR:

Dott. Giampaolo Zuccheri



First Session

Academic Year 2013-2014



*Nature is the source of all true knowledge.
She has her own logic, her own laws,
she has no effect without cause
nor invention without necessity.*

Leonardo da Vinci

Preface

This Master thesis is the result, in principle, of my curiosity for going into the Nanoworld to know, discover and research, how DNA nanotechnology is setting the bases for an upcoming revolution in the biomedical scene and many other scientific fields. I believe this is just the beginning of one of the more promising scientific disciplines in human sciences.

In the following pages I present the results of my master thesis internship, performed at the department of Nanobiotechnology under the supervision of Dr. Giampaolo Zuccheri. This thesis concludes my two years of the Master of Science Advanced Spectroscopy in Chemistry as part of the Erasmus Mundus program.

This research is presented in five main parts that includes from the design, synthesis, characterization and functional evaluation of two self-assembled multifunctional DNA nanobiosensors. Each structure was devised in an attempt to perform a specific area of DNA self-assembly that we find promising for the future development of functional DNA sensor nanotechnology.

Abstract

DNA is a fascinating biomolecule that is well known for its genetic role in living systems. The emerging area of DNA nanotechnology provides an alternative view that exploits unparalleled self-assembly ability of DNA molecules for material use of DNA. The pioneering work by Professor Seeman has showed that the self-assembly of synthetic oligonucleotides can be used in order to make nanostructures of arbitrary shape and complexity; such nanostructures can also be endowed with interesting functional properties. After nearly three decades of research efforts, the meaning of DNA nanotechnology has evolved from toylike beautiful nanoscale structures to really useful building blocks for a variety of applications. In this thesis, I report the design, synthesis and characterization of multifunctional fluorescent nanobiosensors by DNA self-assembling. Each structure was designed and implemented to be introduced in live cells in order to give information on their functioning in real-time.

Although many reports exist on the results of DNA self-assembling systems, still few of them focus on the *in vitro* study about the function of such DNA nanostructures in live cells. Due to this, there are still a limited knowledge about the functionality in real time of such designs. To address an aspect of this issue, we designed, synthesized and characterized two main DNA nanostructures with biosensor functionality. In the design effort, we have used computational tools to design a graphic model of two new DNA motifs and to obtain the specific sequences to all the ssDNA molecules in our models, to provide their functionality.

By thermal self-assembly techniques we have successfully synthesized the structure and corroborate their formation by PAGE technique. In addition with this last technique, we have established the conditions to characterize their structural conformation change when they perform their sensor response. The sensing behavior was also accomplished by fluorescence spectroscopy techniques; FRET evaluation and fluorescence microscopy imaging. Providing the evidence about their adequate sensing performance outside and inside the cells detected in real-time.

As a preliminary evaluation we have tried to show the evidence about the localized functionality of our structures in different cancer cell lines with the ability to work as a therapy target sensor. However, still a better understanding in the biomedical correlation process between DNA nanostructures and live systems is required.

Contents

Summary	10
PART I Elements of Nanoscience and DNA nanotechnology	18
1 Introduction to the Nanoworld	19
1.1 Nanoscience and Nanotechnology Definitions	19
1.1.1 Brief History of Nanotechnology	22
1.2 The Creation of Nanoscale Objects	24
1.2.1 Top-Down	24
1.2.2 Bottom-Up	25
1.3 The Nano-Bio Interface	27
1.4 Nanobiotechnology	27
1.4.1 Towards Molecular Nanobiotechnology	29
2 DNA Nanotechnology	31
2.1 Brief History of DNA Nanotechnology	31
2.2 Fundamental DNA Properties	32
2.3 DNA Nucleobase Interactions	37
2.3.1 Sticky Ends	37
3 Hybridization Techniques of Creating Nanostructures	40
3.1 Holliday Junctions	42
3.2 3D DNA Polyhedra	49

3.2.1	Funtionality of DNA Polyhedra	52
3.3	Future Directions	53
References Part I		54
 PART II Strategy of Implementations		58
4	Structural Modelling	59
4.1	The pH Dependent Biosensor	60
4.1.1	The idea	60
4.1.2	The model	61
4.2	The Nucleic-Acid Sensitive Nanostructure	68
4.2.1	The idea	68
4.2.2	The model	69
5	The Sequence Design	71
5.1	NANEV	72
5.2	NUPACK	72
References Part II		76
 PART III Method for Synthesis and Characterizations		78
6	Experimental Synthesis	79
6.1	Annealing DNA Strands to Self-Assemble DNA nanostructures	79

6.2	Non-denaturing PAGE for the Characterization of Self-Assembled DNA Nanostructures	80
7	Characterization of Nanostructures	81
7.1	Spectroscopic and Optical Microscopy Characterizations	81
7.1.1	Fluorescence Spectroscopy	81
7.1.1.1	Quenching or FRET Interactions	81
7.2	Fluorescence Microscopy	84
7.2.1	Imaging Rationale and Image Acquisition	84
7.2.2	Semiautomatic Analysis of Fluorescence Images	85
8	Cell culture and nanostructure delivery to cells	87
	References Part III	89
PART IV	Results and Discussions	90
9	The Nucleic-Acid Sensitive DNA Nanostructure	92
9.1	Characterization of the Self-Assembly DNA Nanostructure	92
9.2	Probing the Binding of Targets Sequences to TT:BAX Structure	95
9.3	The Functionality of the Nucleic-acid DNA Tetrahedron as a Sensor	99
10	The pH Dependent DNA Tetrahedron	106
10.1	Self-Assembly and Characterizations of Nanostructures	106
10.2	Probing the Triple Helix Formation	107

10.3	Probing the Sense Response to pH Changes	111
11	Cell Uptake	117
11.1	The DNA nanostructures internalization by the cells	117
11.2	The internal localization inside the cells	119
12	Re-design of the Nanostructures with the Cy3/Cy5	
	Fluorophore pairs	121
12.1	PAGE gel characterizations	122
12.2	Fluorescence spectroscopy characterizations	124
12.3	Fluorescence microscopy characterization. The cell uptake	125
12.4	The micrograph semi-automatic analysis	131
12.5	TT:BAX15 and Staurosporine for cellular apoptotic evaluation	131
	References Part IV	133
PART V	Conclusions and Appendixes	135
13	Conclusions and outlook	136
13.1	Future Perspectives	139
14	Appendixes	140
15.1	Microscope Filter Characterization	140
15	Acknowledgments	143

Summary

Introduction

The seminal work of Nadrian Seeman has showed that the self-assembly of synthetic oligonucleotides can be used in order to make nanostructures of arbitrary shape and complexity. As oligonucleotides can be chemically derivatized in many ways, such nanostructures can also be endowed with interesting functional properties. This field will certainly lead to a wealth of future applications in sensing and other fields.

The goal of the research performed during this Master's internship is to make multifunctional nanobiosensors by DNA self-assembly. These are intended to be introduced in live cells in order to give information on their functioning in real-time.

Strategy of implementation

We chose to design and realize DNA self-assembled biosensors as modifications of the original DNA tetrahedron design proposed by Andrew Turberfield and coworkers. These are simple and efficiently assembled nanostructures that can be obtained with as few as 4 different oligonucleotides. The tetrahedrons can be made functional in many ways by performing the assembly of chemically-derivatized oligonucleotides.

We postulated the design of 'open' DNA tetrahedral that can close to a compact tetrahedron (triangular pyramid) upon a chemical binding event. This large conformational transition can be coupled with a change in the fluorescence properties (FRET) of fluorophores decorating some of the component oligonucleotides, and thus it can be detected externally.

We propose the design of at least two classes of such nanostructures:

- A pH-sensitive nanostructure, where the conformational 'closing' transition is driven by the formation of an intramolecular CT-motif triple helix. See **Figure 1**.
- A nucleic-acids sensitive nanostructure, where the conformational 'closing' transition is driven by the contemporary binding of a target nucleic acid to two ssDNA tails of the structure. See Figure 2.

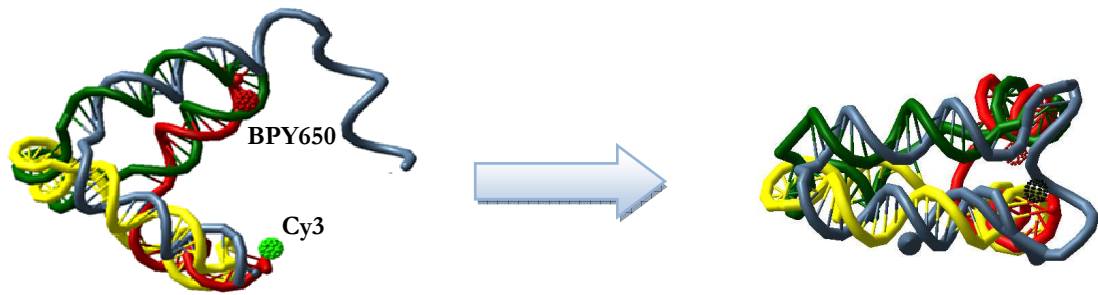


Figure 1: structural model and functioning scheme for the pH sensitive nanostructure (left: high pH state, right, low pH state). FRET between fluorophores decorating the structure vertices is more efficient if the closed conformation.

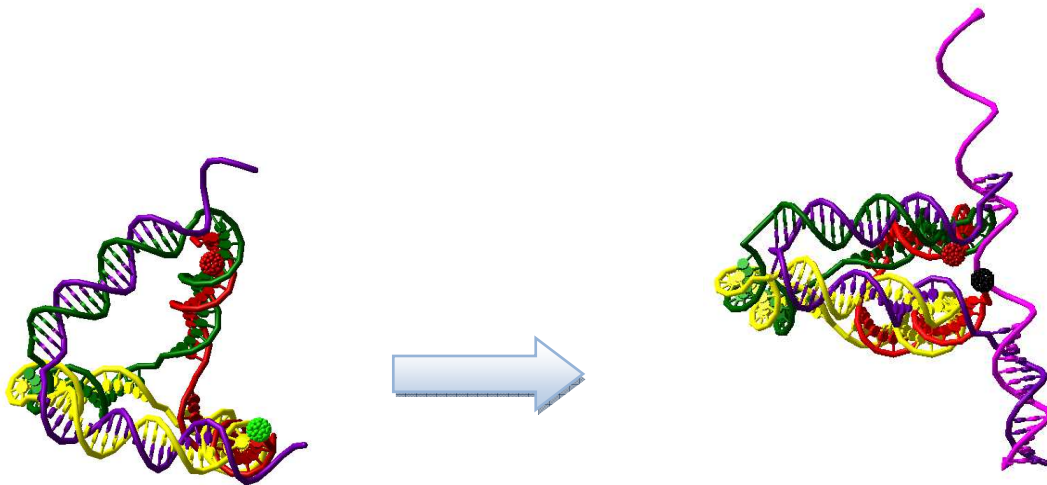


Figure 2: structural model and functioning scheme for the nucleic-acids sensitive nanostructure (left: unbound open state, right, bound closed state). FRET between fluorophores decorating the structure vertices is more efficient if the closed conformation.

Results

We designed and made DNA nanostructures and showed they are function. Then, we treated live cells with them and demonstrated uptake in live human cancer cells.

Design of nanostructures

We successfully designed DNA nanostructures by taking advantage of available software tools and achieved two different nanostructures coded in 4 oligonucleotides each:

- A pH sensitive tetrahedral nanostructure (see **Figure 1**) that contains a double-stranded target and a single-stranded triplex-forming oligonucleotide section that

will assemble in a triple-helix upon reduction of the solution pH. The triplex sequence was obtained previously in the lab and displays a transition point between pH 6 and 7 at 37°C in physiological conditions, so it is apt for measuring changes in the intracellular pH in mammalian cells.

- A nucleic-acids sensitive tetrahedral nanostructure (see **Figure 2**) that contains two single stranded tails that are complementary to two near portions of the BAX transcript RNA. This is the RNA product of a gene that is involved in cell apoptosis and thus it can be triggered by apoptosis-inducing signals.

Two fluorophores are localized at two vertices of the nanostructure where their mutual distance will change the most upon conformational transition (see **Figures 1 and 2**, fluorophores are represented as spheres). We used Cy3 as the donor dye and Bodipy650 or Cy5 as the acceptor dye.

Characterization of nanostructures

We characterized the assembly of the nanostructures by PAGE, so that we can follow the assembly step-wise and test the thermodynamic stability of the structures in physiological conditions.

Assembly characterization

As an example of successful assembly, **Figure 3** below shows the stepwise assembly of two variations of the BAX nucleic-acid sensing nanostructure. PAGE shows that assembly proceeds with high yield. Functional tetrahedrons migrate as single bands and are stable in physiological conditions. Occasionally, the gels show small stoichiometry impairments, but the tetrahedron is always the principal product.

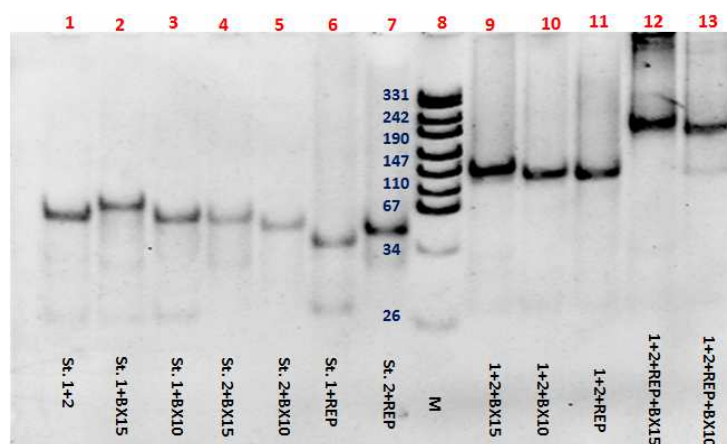


Figure 3. Annealing of oligonucleotide dimers (lanes 1-6), trimers (lanes 9-11) and full tetrahedrons for two variations (lanes 12 and 13) of the nucleic-acids sensor DNA tetrahedron.

Functional characterization

The functional characterization of the dynamic behavior of nanostructures is achieved by PAGE, by changing the conditions (running pH for the pH biosensor and titration with target oligonucleotide for nucleic-acids biosensor) and by spectrofluorimetry.

Nucleic acids biosensor

We demonstrated that the nucleic-acids sensitive tetrahedron is functional. PAGE shows that tetrahedron bind the target and it then migrates as a single band (verifying recognition and association) and that the nanostructure band gets shifted to higher mobility than the unbound state (as it is more compact in shape) as expected. **Figure 4A.**

Tetrahedrons are decorated with donor and acceptor fluorophores that can do energy transfer (FRET) on closing of the structure upon recognition. Upon titration with target nucleic acids of appropriate sequence and sufficient length, the structure undergoes a conformational transition towards a compact, closed structure where FRET is more efficient. Fluorescence spectroscopy shows a significant quenching of the donor dye, and correspondent increase in the acceptor sensitized emission of fluorescence. **Figure 4B.**

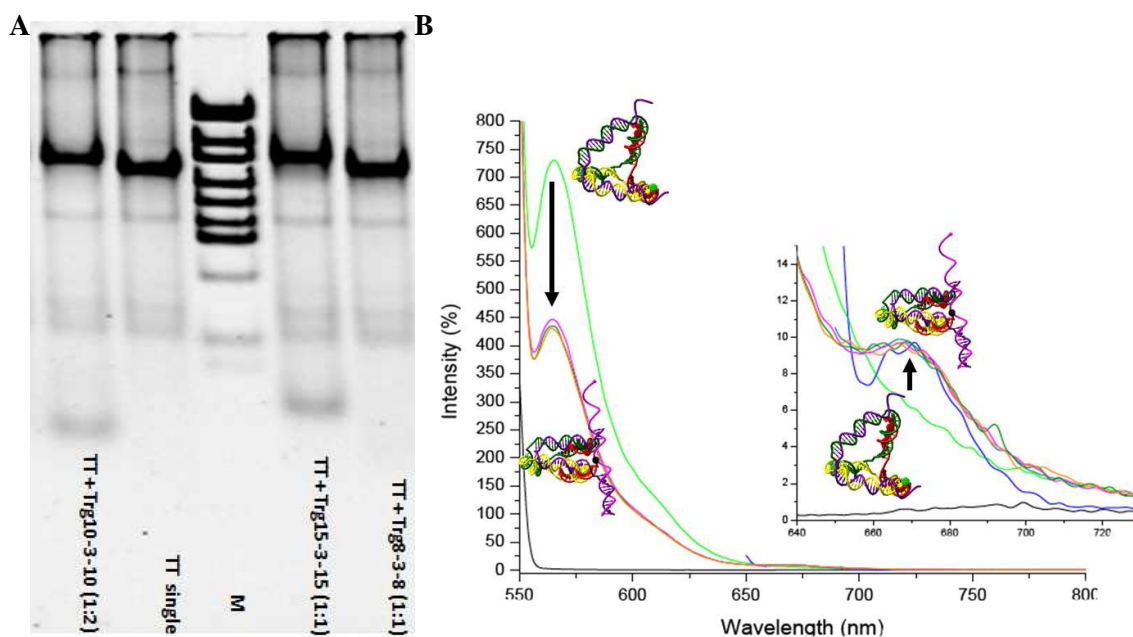


Figure 4. **A)** PAGE showing the shift in mobility of the tetrahedron band (TT) upon binding with specific DNA targets of appropriate sequence and length (20-nt –Trg10-3-10 - or 30-nt - Trg15-3-15 - recognition sequence, in these conditions). Shorter recognition sequences are not stably bound (Trg8-3-8). **B)** Spectrofluorimetric characterization of the conformational transition upon target binding (in the direction of arrows) as evidenced by both the quenching of donor fluorophore emission and the sensitized emission of the acceptor fluorophore (inset).

pH-biosensor

By exploiting the same strategy for functional characterization, we performed PAGE and spectrofluorimetry also in order to characterize the dynamic behavior of the conformational transition of the pH sensitive nanostructure.

In order to better characterize the behavior, we also prepared control pH-insensitive nanostructures: an open DNA tetrahedron that cannot close, and a compact tetrahedron that stays close irrespective of the solution pH. All the 3 specimen (negative ‘open’ control, positive ‘closed’ control and biosensor tetrahedron) are run in PAGE in different pH buffers. At pH 5, the pH-sensitive tetrahedron runs as fast as the positive control, ‘closed’ nanostructure. At pH 8, the pH sensing tetrahedron runs as fast as the negative-control, ‘open’ tetrahedron. **Figure 5A.**

The pH-driven conformational transition can also be checked via spectrofluorimetry, using the same strategy described above. pH-independent donor (Cy3) and acceptor fluorophores (Bodipy650 or Cy5) are brought in proximity by the closing of the tetrahedron at low pH, leading to donor fluorescence quenching and

correlated acceptor sensitized emission. The fluorescence behavior of the control positive and negative nanostructures are not changed with solution pH. Figure 5B. Our measurements show that the behavior of nanostructures is reversible and robust, as they can undergo repetitive transitions by cycling the pH.

Cell uptake

Confirming previous evidence reported by our laboratory and others, we confirmed that this class of nanostructures can spontaneously be taken up by live cells even without the aid of transfecting agents. We tested different cell lines, including HeLa and glioblastoma cells. We have demonstrated uptake by characterizing the cellular fluorescence by epifluorescence microscopy. Nanostructures are also present as a diffuse signal in the cytoplasm, but they are mainly evidenced as a localized signal in lysosomes and possibly mitochondria.

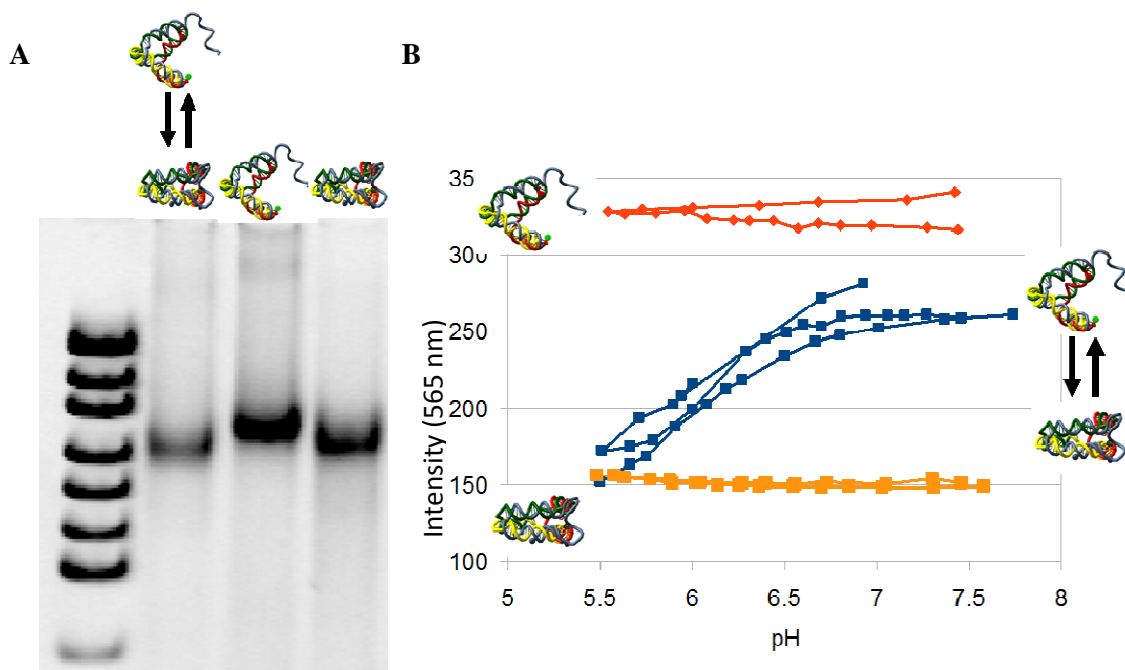


Figure 5. A) PAGE showing the mobility of the pH-sensitive tetrahedron band at acidic pH as a comparison with pH-insensitive control nanostructures. Gel is run at 37°C in physiological conditions. B) Plot of the fluorescence signal due to the emission of the donor (Cy3) dye decorating the nanostructure during cycling of the solution pH. Fluorescence of the pH-sensitive tetrahedral nanostructure gets quenched when the structure is closed by triple helix formation and the donor fluorophore is near the acceptor. Measurements are performed at 37°C in physiological conditions.

pH-biosensor

We characterized the state of the pH-sensitive tetrahedron inside live cultured cells. By characterizing the localization of the FRET signal in the fluorescence microscope, in comparison with the direct excitation signal of the donor and acceptor dye, we evidenced that the higher FRET comes from point-like organelles recognizable as lysosomes. As it is known that these should have their contents at low pH (≤ 5) and thus we conclude that the nanostructure is successfully reporting on intracellular pH variations, see **Figure 6**.

Nucleic acids biosensor

We also proved that our nucleic-acids sensitive nanostructure gets internalized by live glioblastoma cells. These also get localized in the cytoplasm, but mainly in lysosomes and possibly mitochondria.

We made and used nanostructures that were designed to target an RNA transcript involved in the apoptotic pathway. We did a number of attempts but so far we have not been able to show the emergence of the target RNA after induction of apoptosis in the glioblastoma cells.

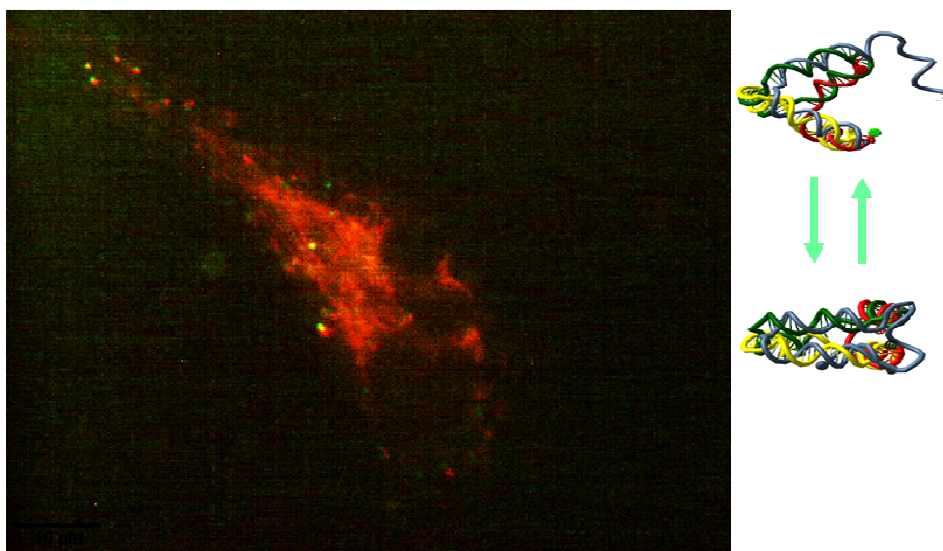


Figure 6. Fluorescence image of a human cultured glioblastoma cell after uptake of the pH-sensitive DNA nanostructure. Here is the display of the overlay of the fluorescence signal of the donor dye represented in red with the signal from the FRET channel, represented in green. Localization of the green signal (or perfect overlay of signals that shows as yellow) reports on the localization of high-FRET states in point-like organelles identifiable as lysosomes.

Conclusions

We have successfully designed and realized functional dynamic DNA nanostructures that can respond to the change in pH or to the presence of specific nucleic acids by changing their conformation in an externally measurable fashion. We have also shown that these nanostructures can be internalized by live human cells in culture and could report on their internal state.

Outlook

Additional experiments and possibly more statistically relevant citofluorimetry experiments will be needed to quantitatively assess the functionality of the nanostructures as intracellular biosensors, especially for the case of the nucleic acid biosensor.

An important factor in the deployment of such biosensor will be the intracellular localization upon uptake. Current evidence seem to show that this could depend on the cell line, on the cell state and possibly also on the type and number of fluorophores that are used to detect the presence and signaling state of the internalized nanostructures. Further studies are needed in order to have a better control on cellular localization.

PART I

Elements of Nanoscience and DNA Nanotechnology

Elements of Nanoscience and DNA Nanotechnology

1. Introduction to the Nanoworld

1.1 Nanoscience and Nanotechnology Definitions

Nowadays the terms nanotechnology, nanoparticles, and nanomaterials are familiar to a broad audience of readers since the term “nano” has revolutionized the way of thinking about the object size. Nanobiotechnology is a multidisciplinary field that covers a vast and diverse array of technologies coming from engineering, physics, chemistry, and biology. It is the combination of these fields that has led to the birth of a new generation of materials and methods of making them. The scope of applications is enormous and every day are discovered new areas of our daily lives where they can find use.

From a general perspective, the prefix nano is derived from the Greek word “νάνος” (nanos) meaning “dwarf”, the quantity of 10^{-9} (one billionth) of a measuring unit. Therefore, the nanoscience is defined as the research field where objects and those phenomena originated by nanoscale objects converge in a range size of 1 to 100 nm. Thus, Nanoscience can be viewed as an highly interdisciplinary that seeks to integrate mature nanoscale technology.

Once nanoscience was defined, it can be possible to define “nanotechnology” in general way as the field of research and fabrication that is on a scale of 1 to 100 nm. In a broad sense, nanotechnology involves the “creation and application of nanomaterials, devices and technical systems whose functions are determined by the presence of nanostructural fragments” [1].

In the way to understand the proper term of nanotechnology, it is helpful to delimit the nanoworld in the context of basic science. Chemistry is the study of atoms and molecules, a real matter of dimensions generally less than one nanometer, while condensed matter physics deals with solids of essentially infinite arrays of bound atoms or molecules of dimensions greater than 100 nm. A significant gap exists between these regimes, which corresponds to the previously defined nanosize region, in other words this gap corresponds to particles of 1 to 100 nm, or about 10 to 10⁶ atoms or molecules per particle [2].

In this nanoscale domain neither quantum chemistry nor classical laws of physics hold. For example, in materials where strong chemical bonding is present, delocalization of valence electrons can be extensive, and the range of delocalization can vary with the size of the system. This effect, coupled with structural changes depending on size, can generate different chemical and physical properties.

Another way to interpret the nanoscale meaning, is to put into visual perspective the atomic, nano, micro and macro domains and compare with other usual objects in our world as it is shown in **Figure 1**. This illustration helps to compare in meters the size of a DNA strand, a bacterium and a regular cell.

The existing definitions of nanotechnology also emerged from the modern achievements and inventions in the area of visualization, manipulation, and analysis of nanometersized structures as well as the controllable creation of new functional materials with unique properties and nanosized devices that provided technological breakthroughs in various industrial fields.

Over time and with the advancement in this field, the definitions of Nanotechnology have become much more robust to integrate almost all the elements that describe better its meaning and understanding. Some of such particular definitions that can be found in literature are:

From the report of the Royal Society & the Royal Academy of Engineering of 2004 [3]. “Nanotechnology is the design, characterization, production and application of structures, devices and systems by controlling shape and size at nanometer scale.”

From the National Nanotechnology Initiative [4]. “Nanotechnology is science, engineering, and technology conducted at the nanoscale, which is about 1 to 100 nanometers. Nanoscience and nanotechnology are the study and application of extremely small things and can be used across all the other science fields, such as chemistry, biology, physics, materials science, and engineering”

The Concept of the Development of Research in the Area of Nanotechnology in Russia until 2010 (approved by the government of the Russian Federation on 18 October 2004) used the following definition: “Nanotechnology is the combination of methods and techniques that provide the possibility of controllable creation and modification of objects that include components with the size of less than 100 nm which have unique properties and can be integrated with complete functioning large-scale systems.”

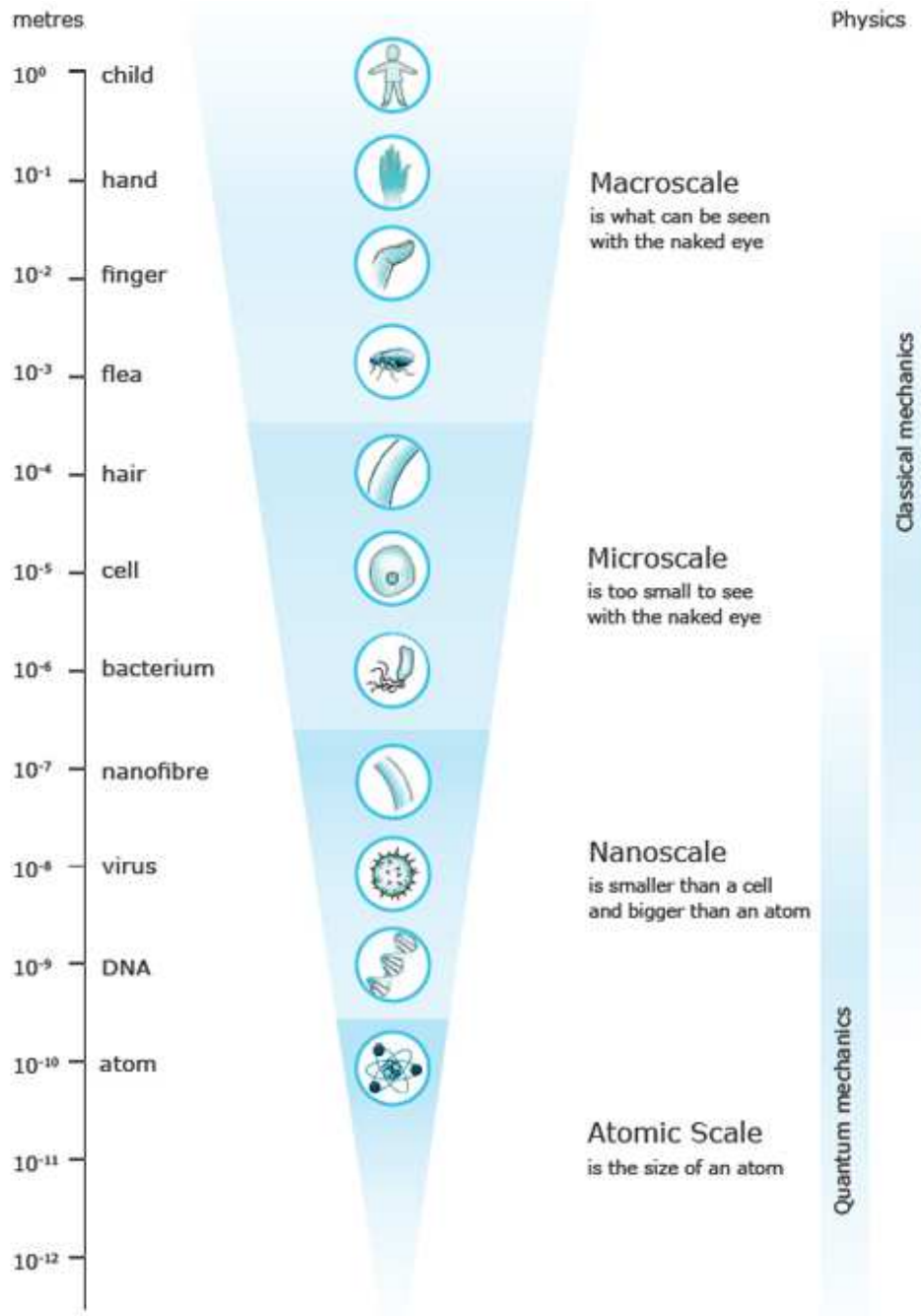


Figure 1. Size comparison of progressively “small” objects in atomic, nano, micro and macro scale

It is obvious that all of the definitions are not perfect and can be subject to criticism, and the rapid development of various branches of nanotechnology will correct and improve them.

1.1.1 Brief History of Nanotechnology

Even though nanotechnology is considered as a relatively new field, it does not mean that technologists and scientists had not been working intuitively in this area before. The ancient Romans empirically used gold nanoparticles to color goblets and other glass products [5]. (This technology was used to create the famous Roman ruby goblets). It is also appropriate to remember that in 1857, M. Faraday was working with a red colloid solution that contained gold nanoparticles with a size of 20 nm.

The primary documented concept of Nanotechnology was presented on December 29, 1959, when Richard Feynman presented his famous lecture entitled “There’s Plenty of Room at the Bottom” at the annual meeting of the American Physical Society at the California Institute of Technology [6]. In this talk, Feynman stated for the first time several ground-breaking concepts, most of which are still relevant today. Even though his speech was completely theoretical, he described how the laws of physics do not limit our ability to manipulate single atoms and molecules. Back then, manipulating single atoms or molecules was not possible because they were far too small for available tools in that time. Nevertheless, he correctly predicted that the time for the atomically precise manipulation of matter would inevitably arrive. Today, that lecture is considered to be the first landmark of science at the nanolevel.

Later, the term nanotechnology was first used by Prof. Norio Taniguchi in 1974 at a conference in Tokyo with his paper “On the Basic Concept of 'Nano-Technology’” defining it as “the processing of, separation, consolidation, and deformation of materials by one atom or one molecule” [7].

On the other hand, the progress in nanotechnology was based on inventions made at the end of the twentieth century. The first of these inventions belongs to Nobel laureates, physicists Gerd Binnig and Heinrich Rohrer from IBM research laboratory, who, in 1981, designed the tunnel scanning microscope that made it possible to see single atoms [8]. The second discovery was made in 1986, when the atoms were not only observed, but also manipulated for the first time with the help of a tunnel microscope enhanced by G. Binnig. The Nobel lecture in 1986 [9] described both the principle of operation of the tunnel microscope and the way of manipulating atoms. On the same

year, Dr. Kim Eric Drexler published a book entitled “Engines of Creation: the Coming Era of Nanotechnology” [10]. This book speculatively explored the concepts proposed by Feynman bringing them to a wide public attention. The concepts used by Drexler about nanotechnology are often referred as “molecular nanotechnology”, that is, the engineering of functional machines at the molecular scale designed and built atom-by-atom.

Summarizing, the principal scheme of integral parts of nanotechnology formed by the end of the twentieth century is illustrated in **Figure 2**. Remarks on this scheme, can be stated that engineering (technical) nanotechnology has started being focused toward solution of the following problems [11].

- Creation of solid materials and surfaces with controllable molecular structures
- Designing new types of chemical compounds with controllable properties (nanoconstructions)
- Creating nanosized self-organizing or self-replicating structures
- Fabrication of devices for various purposes (components of nanoelectronics, nanooptics, nanoenergetics, etc.)
- Integration of nanosized devices with electric systems

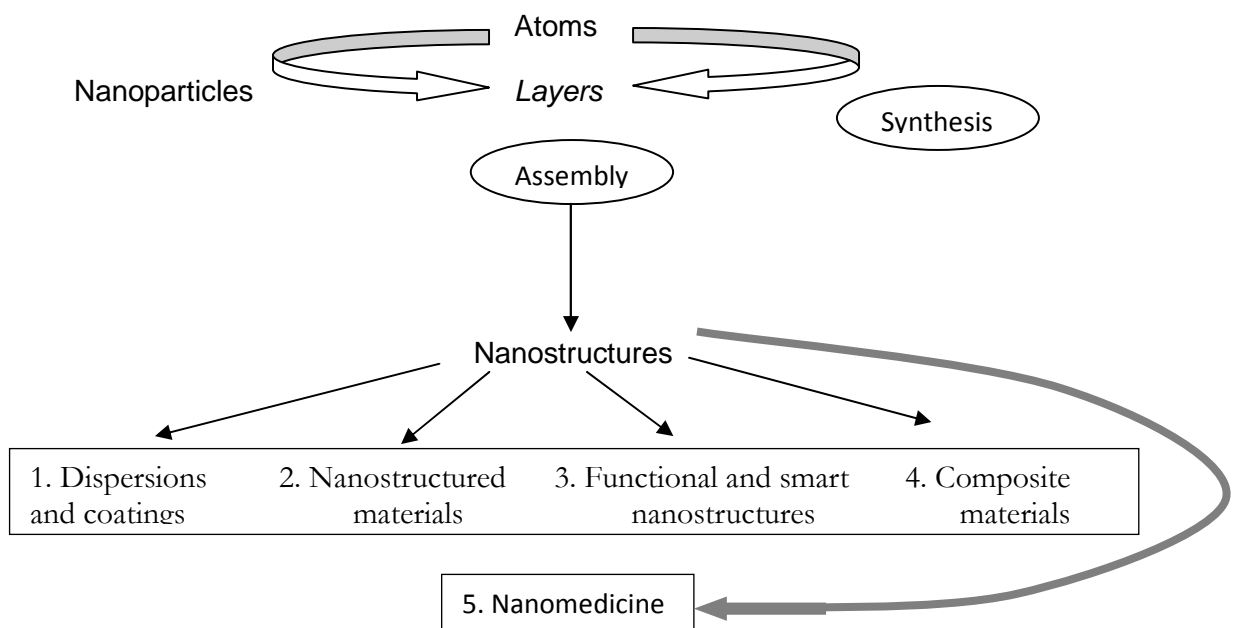


Figure 2. The principal scheme of the basic part of nanotechnology formed to the end of the twentieth century and the main research fields.

In this perspective, the goal in nanotechnology may be described as the ability to assemble molecules into useful objects hierarchically integrated along several length scales and then, after use, disassemble objects into molecules. Nature already accomplishes this in living systems and in the environment.

1.2 The Creation of Nanoscale Objects

The first 30 years of the nanosciences were dedicated mainly to studying and fabricating materials at the nano scale range. In those studies, much effort was focused on shortening the dimension of fabricated materials. It was also a time when the two basic fabrication approaches were defined: “bottom-up” and “top-down” based on the type of action that is needed to go from the starting materials to the desired product. A general view and comparison of these two techniques are shown in **Figure 3**.

1.2.1 Top-Down

The Top-Down approach represents the type of nanofabrication first imagined by Feynman that search to create nanoscale structures or devices by using larger, externally-

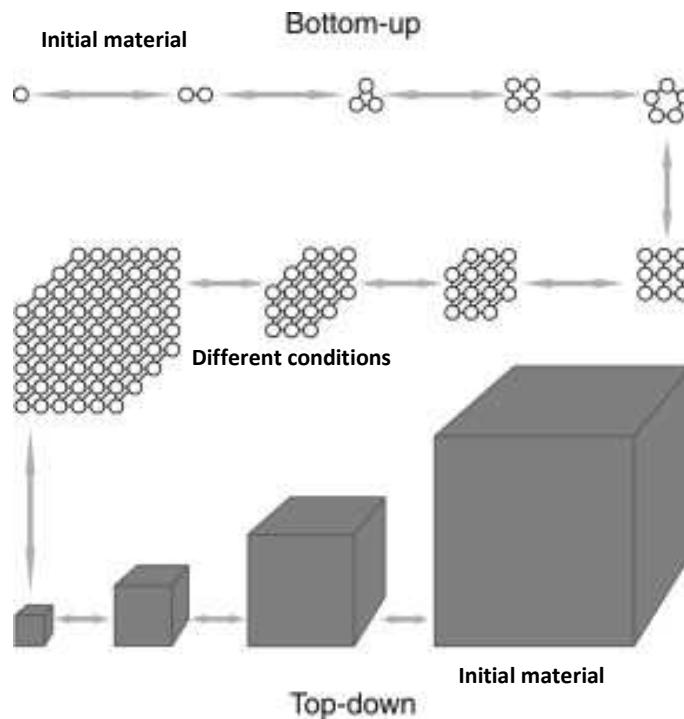


Figure 3. Technological approaches to the creation of nanomaterials: Top-down and bottom-up.

controlled tools to direct their assembly. This technique is referred to the molding, carving, and fabricating of small materials and components by reducing the size of the initial substance or placement of required atoms on the surface of some material in a certain configuration, this is possible by the use of larger objects like mechanical tools and lasers.

Examples of Top-Down nanofabrication include all types of lithography (photo-, electron beam, dip-pen, soft-, nanoimprint-) and etching tools. In all these techniques, the generation of nanoscale features relies on the externally controlled relative movement of a tool and the substrate. The advantage of the top-down technique is that it enables to control the manufacture of smaller, more complex objects, as illustrated by micro and nanoelectronics, for example in the silicon chip fabrication.

1.2.2 Bottom-Up

On the other hand, the bottom-up approach, searches for the means and tools to build nanomaterials (devices) by combining smaller components from desired elements, such as single molecules and atoms, that are integrated into spatial structures as a result of a physicochemical process; generally, those elements are held together by covalent forces.

Theoretically, it can be exemplified by molecular assemblers, where nanomachines are programmed to build a structure one atom or molecule at a time; the strategy is to put the desired elements in a context where they can freely find each other and establish those interactions, without or with very limited external control. In this way, the result of the assembly is ultimately dependent on exactly how sub-component can bind to each other. Since no direct action is taken to drive the components to the position assigned to them, the arrangement will be spontaneously; this process is often called “self-assembly”.

In the context of nanoscience and nanotechnology, the self-assembling components are obviously nano-sized objects, for examples molecules or colloidal particles. Bottom-up approaches based on self-assembly could in principle be able to produce the same structures accessible to top-down methods, with the advantage to be in a highly parallel fashion and much cheaper. In addition, with the bottom-up design, the covalent bonds holding a single molecule together are far stronger than the weak interactions that hold more than one molecule together in the top-down. Thus, this

approach enables to control the manufacture of atoms and molecules and holds far more practical and applicative future potential.

It is necessary to remark that in any variant of the considered technologies described above, the forming nanomaterials will obtain new properties that the initial objects do not possess.

It is clear that the creation of practically significant structures at the nanometer scale is one of the fundamental challenges of science and technology in this century. This means that commercial demand for the production of miniature devices will determine the need to develop building blocks based on concept and principles that are used in nature to create nanosized systems or biosystems. At the same time, the building blocks must have a size that fills the gap between the submicrometric sizes reached by the classical top-down technology and the sizes that can be achieved using the classical bottom-up technology.

Analysis of the fundamental backgrounds of physical chemistry, biochemistry, and synthetic chemistry of biological molecules, considering the requirements for the two aforementioned approaches to obtain nanoobjects leads to the conclusion that, due to their geometric size, two groups of compounds are the most suitable for the creation of nanosized structures [12]:

- 1 Biopolymers (such as nucleic acids and proteins)
- 2 Nanoparticles (nanoclusters) of various origin

The formation of complex spatial objects, using the bottom-up approach, with regulated properties (nanostructures, nanobiomaterials, nanoconstructions) using nucleic acid molecules and their complexes as construction blocks is called nucleic acid based nanodesign or structural nucleic acid nanotechnology [13-15]. At this time, there are two different strategies of nanodesign:

1. Creation of nanostructures using single-stranded polynucleotide (DNA) molecules containing deliberately selected sequences of nucleobases.
2. Creation of nanoconstructions using spatially fixed linear double-stranded DNA molecules (or their complexes)

1.3 The Nano-Bio Interface

Biosystems are governed by complicated nanoscale processes and structures that have been optimized over millions of years. Biologists have been operating for many years at the molecular level, ranging from nanometers (DNA and proteins) to micrometers (cells, bacteria). A typical protein like hemoglobin has a diameter of about 5 nm, the DNA's double helix is about 2 nm wide, and a mitochondrion spans a few hundred nanometers as compared in Figure 1. Therefore, the study of any subcellular entity can be considered "nanobiology." Moreover, the living cell along with its hundreds of nanomachines is considered, today, to be the ultimate nanoscale fabrication system.

Considering that the groundwork of each and every biological system are nanosized molecular building blocks and machinery that cooperate to produce living entities and these elements have been integrated for nanotechnologists in the combination of two disciplines (nano and biotechnology) to give birth of a new science, nanobiotechnology. Nanotechnology provides the tools and technology platforms for the investigation and transformation of biological systems, and biology offers suitable models and bio-assembled components to nanotechnology. The difference between "nanobiology" to "nanobiotechnology" resides in the technology part of the term. Objects that are "man-made" correspond to the technology section of nanobiotechnology. Nanobiotechnology will lead to the design of entirely new classes of micro- and nanofabricated devices and machines, determining the inspiration for which will be based on bio-structured machines, the use of biomolecules as building blocks, or the use of biosystems as the fabrication machinery.

1.4 Nanobiotechnology

The nanoconstruction technology approaches are based on top-down for the construction of nonbiological systems and bottom-up for the molecular level as biological systems. Those constructions are done via a collection of molecular tool kits of atomic resolution that are used to fabricate micro- and macrostructure architectures. Nanobiotechnology, can be described in many ways: one is the incorporation of nanoscale machines into biological organisms for the ultimate purpose of improving the organism's quality of life. To date, there are few methods for synthesizing nanodevices that have the potential to be

used in an organism without risk of being rejected as antigens; another way is the use of biological “tool kits” to construct from nano- to microstructures. However, the broad perspective to define “Nanobiotechnology” is probably the one that will include both and will be defined as: the engineering, construction, and manipulation of entities in the 1- to 100-nm range using biologically based approaches or for the benefit of biological systems. The biological approaches can be either an inspired way of imitate biological structures or the actual use of biological building blocks and building tools to assemble nanostructures.

Nanotechnology and nanobiotechnology could be differentiated by the technique used for the construction of nanostructures and nanodevices. In nanotechnology, the dominant approach is top-down, whereas in nanobiotechnology is bottom-up. The bottom-up approach to nanofabrication has the ambition to learn how to use biological strategies for its ends. Unfortunately, we are currently unable to design from scratch complex information-containing polymers with the same efficiency displayed by nature, not to mention synthesizing them. So one slightly different approach is to use not only the basic strategy, but also the actual molecules found in biological systems, or specific portions of them.

An interesting example of the bottom-up approach is the pioneering work of Seeman and coworkers by the use of the structural properties of DNA to produce target materials with predictable three-dimensional (3D) [16-19]. He uses DNA motifs with specific, structurally well defined, cohesive interactions involving hydrogen bonding or covalent interactions (“sticky ends”) to produce target materials with predictable 2D and 3D structures. The elements for the construction of these structures will be described in more detail in the next sections. These efforts have generated a large number of individual species, including polyhedral catenanes, such as a cube and a truncated octahedron, a variety of single-stranded knots, and Borromean rings. The combination of these constructions with other chemical components is expected to contribute to the development of nanoelectronics, nanorobotics, and smart materials. Therefore, the organizational capabilities of structural DNA nanotechnology are just beginning to be explored, and the field is ultimately expected to be able to organize a variety of species in the material world.

Actually, nanobiotechnology already has an impact on healthcare. Research on biosystems at the nanoscale has created one of the most dynamic science and technology domains at the confluence of physical sciences, molecular engineering, biology,

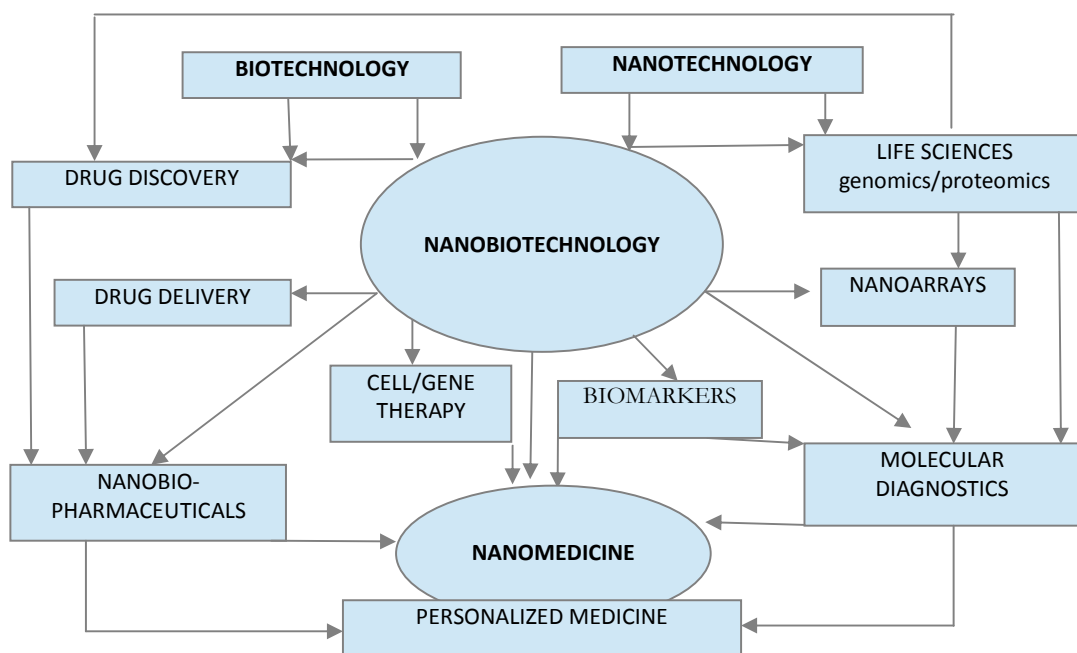


Figure 4. Relationship of Biotechnology and Nanotechnology to Nanomedicine and related technologies.

biotechnology, and medicine [20]. The confluence of nanoscience and biology are contributed to unified new particular fields of study that are even now more frequently to find in the literature such as: Nanomedicine, Nanobiomedicine, Nanobiopharmaceutical, Nanobiosystem science and engineering, Nanotherapy. The relationship of nanotechnology to biotechnology and related technologies is depicted graphically in **Figure 4**.

1.4.1 Towards Molecular Nanobiotechnology

It is clear that Nanotechnology provides investigation tools and technology platforms for biomedicine. Examples include current work in the subcellular environment, investigating and transforming nanobiosystems (for example, the nervous system) rather than individual nanocomponents, and developing new nanobiosensor platforms. Investigative methods of nanotechnology have been implemented in uncovering fundamental biological processes, including self-assembling, subcellular processes, and system biology (for example, the biology of the neural system).

In those days, key improvements have been made in measurements at the molecular and subcellular levels and in understanding the cell as a highly organized

molecular mechanism based on its abilities of information utilization, self-organization, self-repair, and self-replication [21]. Single molecule measurements are providing an improvement on the dynamic and mechanistic properties of molecular biomachines, both in vivo and in vitro, allowing direct investigation of molecular motors, enzyme reactions, protein dynamics, DNA transcription, and cell signaling. Chemical composition has been measured within a cell in vivo.

Another aspect is the transition from understanding and control of a single nanostructure to nanosystems. Scientists are beginning to recognize the interactions of subcellular components and the molecular origins of diseases, influencing areas of medical diagnostics, treatments, and human tissue replacements. Also, spatial and temporal interactions of cells including intracellular forces have been measured for the development of particular techniques. For example, atomic force microscopy has been used to measure intermolecular binding strength of a pair of molecules in a physiological solution, providing quantitative evidence of their cohesive function [22]. In this perspective, flows and forces around cells have been quantitatively determined, and mechanics of biomolecules are better understood. It is accepted that cell architecture and macro behavior are determined by small-scale intercellular interactions.

Some other trends include the ability to detect molecular phenomena and build sensors and systems of sensors that have high degrees of accuracy and cover large domains. For example, fluorescent semiconductor nanoparticles or quantum dots can be used in imaging as markers for biological processes because they photobleach much more slowly than dye molecules and their emission wavelengths can be finely tuned. Also, key challenges are the encapsulation of nanoparticles with biocompatible layers and avoiding nonspecific adsorption. Thus, nanoscience investigative tools help us understand self-organization, supramolecular chemistry and assembly dynamics, and self-assembly of nanoscopic, mesoscopic, and even macroscopic components of living systems [23, 24]

Thereby, emerging areas include developing realistic molecular modeling for “soft” matter, obtaining nonensemble-averaged information at the nanoscale domain, understanding energy supply and conversion to cells (photons and lasers), and regeneration mechanisms. Because the first level of organization of all living systems is at the nanoscale, it is expected that nanotechnology will have a strong consequences in almost all aspects of bio-domains.

2 DNA Nanotechnology

2.1 Brief History of DNA Nanotechnology

The beginning of DNA nanotechnology started in 1953, when James Watson and Francis Crick proposed a double-helical model of the DNA molecule to describe the arrangement of the complementary base sequences (A-T and G-C) in the DNA polymer backbone.

Nadrian Seeman and coworkers proposed innovative ideas of exploiting the unique DNA molecular recognition properties for nanoconstruction in the early 1980s [15, 16]. In their initial work, they constructed artificial nucleic acid architectures using synthetic DNA branched junction motifs containing three and four arms, which has been considered as the foundation work of DNA nanotechnology [14, 25, 26]

The area of DNA nanotechnology grew quickly in the 1990s, partially because of the industrial availability of chemically synthesized DNA molecules with arbitrary sequences. Actually, it is possible to order almost all components needed for DNA nanotechnology, including modified DNA bases. On the other hand, catalyst for the rapid development of DNA nanotechnology came from the invention and commercialization of particular characterization tools, such as atomic force microscopy (AFM). AFM, as a member of scanning probe microscopy (SPM), can readily probe almost any samples deposited at flat surfaces and perform measurements and visualizations in three dimensions of a given sample. AFM, together with more recently developed techniques such as cryo-EM and high resolution fluorescent microscopy, provides a powerful set of toolbox for in-depth characterization of self-assembled DNA nanostructures. With these technological advances, numerous sophisticated DNA nanostructures rapidly appeared, greatly accelerate the growth of this area.

In 1994, Adleman reported a DNA-based “wet-lab” solution for solving a computational problem[27], which can be considered as one of the first applications of DNA nanostructures in biological computing. There was an area full of nice structures without any applications. However, nearly a decade ago, researchers started to rationally control variation of DNA nanostructures with external triggers, which extended the area of DNA nanotechnology from structure to function. One of the most attractive directions is to convert static DNA nanostructures to dynamic, this means the creation of functional

DNA “nanomachines” or DNA “nanodevices.” An elegant example of DNA nanomachines is “DNA tweezers” reported by Turberfield and Simmel in 2000 [28].

Also, the progress of DNA nanotechnology was benefited from the rapid development of another emerging area, functional nucleic acids (FNAs) (aptamers and DNAzymes). Aptamers are artificially in vitro selected single-stranded DNA or RNA with antibody-like high affinity and specificity [29]. Ribozymes or DNA zymes are artificial selected nucleic acid with specific enzyme catalytic activities. The introduction of FNA into DNA nanostructure developed versatile applications of DNA nanotechnology, leading to the construction of functional DNA nanostructures for biosensing, nanoplasmonics, and nanorobotics.

One of the milestone works in DNA nanotechnology was done by Rothermund in 2006 by the introduction of the DNA “origami” technique [30]. This great strategy was inspired by the ancient Asia paper-cutting art origami. In brief, DNA origami involves raster-filling a designed shape using a long single-stranded scaffold oligonucleotide and hundreds of short helper strands. After temperature annealing, the scaffold is kept in place by these staple strands. “Scaffolded DNA origami” has several important advantages as compared to previously used simple self-assembled “tile” strategies. The particular strategy construction techniques will be described in the next sections.

2.2 Fundamental DNA Properties

Before describing the properties of DNA nanostructures, it is necessary to examine the fundamental properties of these molecules that determine the possibility of their application in nanotechnology.

Chromosomes, as part of the cell nucleus of all living systems, include DNA molecules; the genetic code is encrypted in their structures. Watson and Crick proposed a double-helical model to described the DNA molecule (**Figure 5**). In the model they encountered that a DNA molecule is a linear polymer consisting of two sugar-phosphate chains that contain nucleotides—nitrogen bases: adenine (A), guanine (G), cytosine (C), and thymine (T) bound to sugar residues. Two opposite sugar-phosphate chains twist upon each other and form a linear double spiral (double helix). Each chain contains complementary base pairs, such as A-T (with two hydrogen bonds between them) and G-C (with three hydrogen bonds between them) (**Fig. 5b**). The complementarity concept

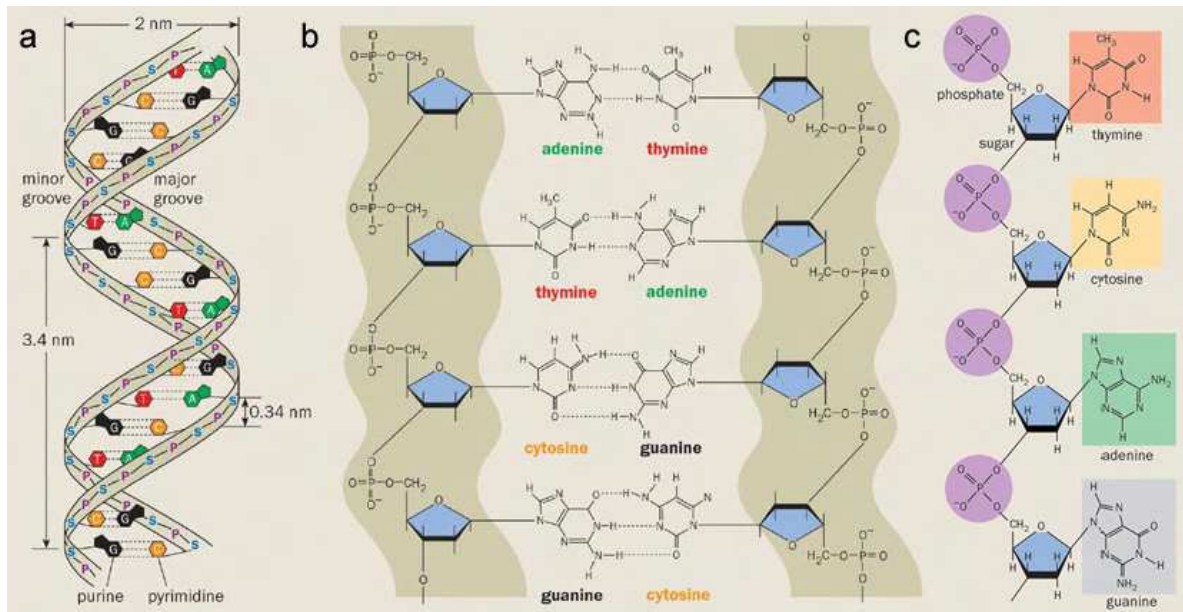


Figure 5 – (a) Scheme of a double-stranded DNA molecule consisting of two hydrogen bonded opposite polynucleotide chains that run in opposite directions and are twisted around each other. Hydrogen bonds hold complementary base pairs together - adenine (green) with thymine (red) and guanine (black) with cytosine (orange), a size of a helical turn (3.4 nm) and the diameter of the helical structure (2 nm) are marked; (b) An untwisted view of the two chains with complementary base pairs that form specific Watson-Crick hydrogen bonds; (c) Structure of a portion of a single strand of DNA. It is a polymeric chain, consisting of a sugar-phosphate backbone with bases attached to the sugar residues. In a single chain, the structure places no restrictions on the sequence in which the bases can occur.

involves the formation of hydrogen bonds between A and T, as well as between G and C, and a precise steric conformity between the surfaces of nitrogen base pairs, and, consequently, the oligonucleotide chains that include these nitrogen bases. In addition to the hydrogen bonds, the double-stranded DNA structure is maintained by hydrophobic interactions between the bases. The hydrophobic nature of the bases means that a single-stranded structure, in which the bases are exposed to the aqueous environment, is unstable. Pairing of the bases allow them to be removed from interaction with the surrounding water.

In contrast to the hydrogen bonding, hydrophobic interactions are relatively non-specific, this means, nucleic acid strands will tend to stick together even in the absence of specific base pairing, although the specific interactions make the association stronger. Negatively charged groups of phosphoric acid residues provide the electrostatic repulsion between chains in a DNA molecule and give the molecule the properties of an acid soluble in standard water-salt solutions (**Fig. 5c**).

The simplicity of the Watson-Crick model has provided a great influence on other areas of science, from law to medicine. This discovery has answered the question

of how genetic information is stored and how it is interpreted and processed in a DNA molecule. Some important facts in the dimension range of a DNA double helix as a nanometric object can be summarized from the (Fig. 5a). The diameter of a molecule is about 2 nm, and the distance between pairs is 0.34 nm. Every helical turn consists from 10 to 10.5 base pairs per turn, so the total size of one turn is about 3.5 nm.

The spatial structure of a double-stranded DNA molecule depends on the base sequence: The changes in the relative orientation of mean planes of the base pair is due to the differences in spatial organization caused by the presence of different pairs in the chain. The mutual orientation of base pairs and their orientation to the axis of a linear DNA molecule are expressed in such terms as base slope angle, base pair helical twist angle, and inclination angle of base pairs (Figure 6).

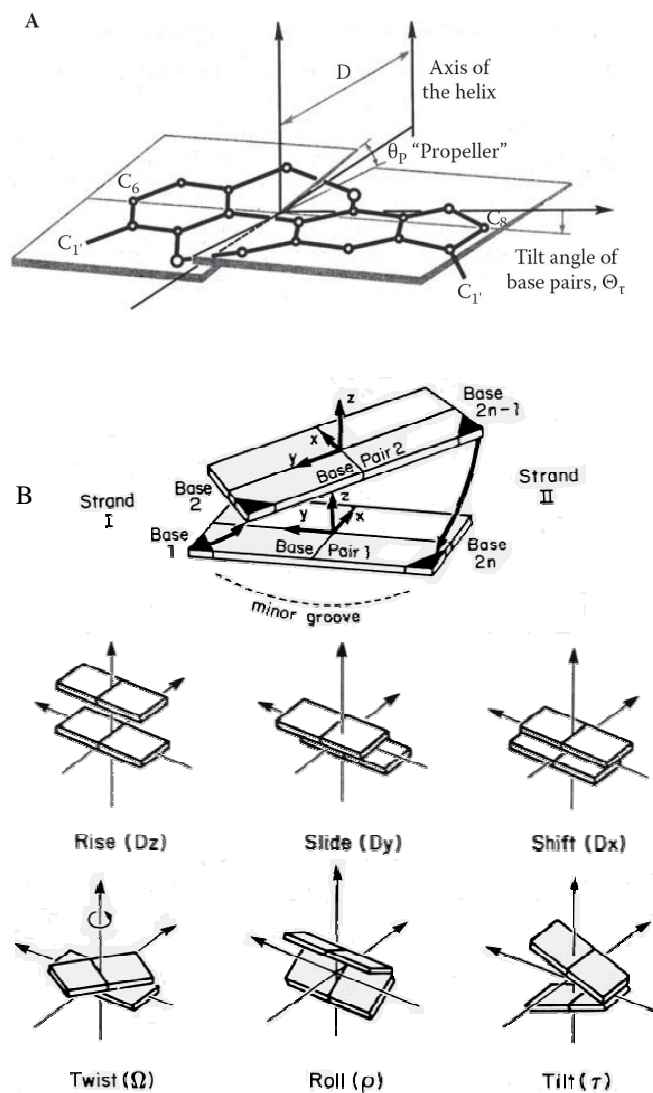


Figure 6. The parameters that determine the orientation of individual nitrogen bases (A) and base pairs (B) in respect to the axis of a linear DNA molecule.

These angles (**Fig. 6**) determine both the local bending of a DNA chain and the total curvature of a DNA molecule. The shape taken by an individual DNA molecule can be analyzed in terms of superposition of thermal fluctuations of the structure and the inner low-energy structure typical of the sequence of nucleobases [31]. Hydrophobic interactions between consecutive bases on the same strand contribute to this winding of the helix, as the bases are brought closer together, enabling a more effective exclusion of water from interaction with the hydrophobic bases. In solution, a DNA molecule exists in a canonical B form, as a rule, although, depending on the base sequence and properties of the solvent, there may be a wide range of DNA structural forms such as the A and Z form.

The structural characteristic of DNA can be studied first, by considering, the specific properties of nitrogen base sequence in a DNA chain. One of these sequences is the called palindromic sequence or palindromic repeat, where palindromic can be understood as a word, phrase or sentence that reads the same from the left to the right and from the right to the left. For a DNA molecule, this term means that both DNA chains contain sequences connected by a twofold symmetry (**Figure 7**). In order to superimpose one repeat on the other, it must be rotated 180° around the horizontal axis and then again about the vertical axis. A mirror repeat of nitrogen bases has a symmetric sequence on each strand. Superimposing one repeat on the other requires only a single 180° rotation about the vertical axis.

Palindromic sequences of DNA can come from alternative structures where bases form pairs in one chain. When only one DNA chain is included in the process, a hairpin structure is formed (**Fig. 7a**). However, when both of the DNA chains take part in the process, the structure is called a cruciform (**Fig. 7b**).

From previous descriptions allows one to make some statements: DNA nitrogen bases have peculiar properties. First, their spatial structure provides the possibility of forming complementary pairs; second, the efficient recognition is only typical of complementary base pairs; and, finally, a stable structure formed of complementary base pairs does not depend much on exterior conditions.

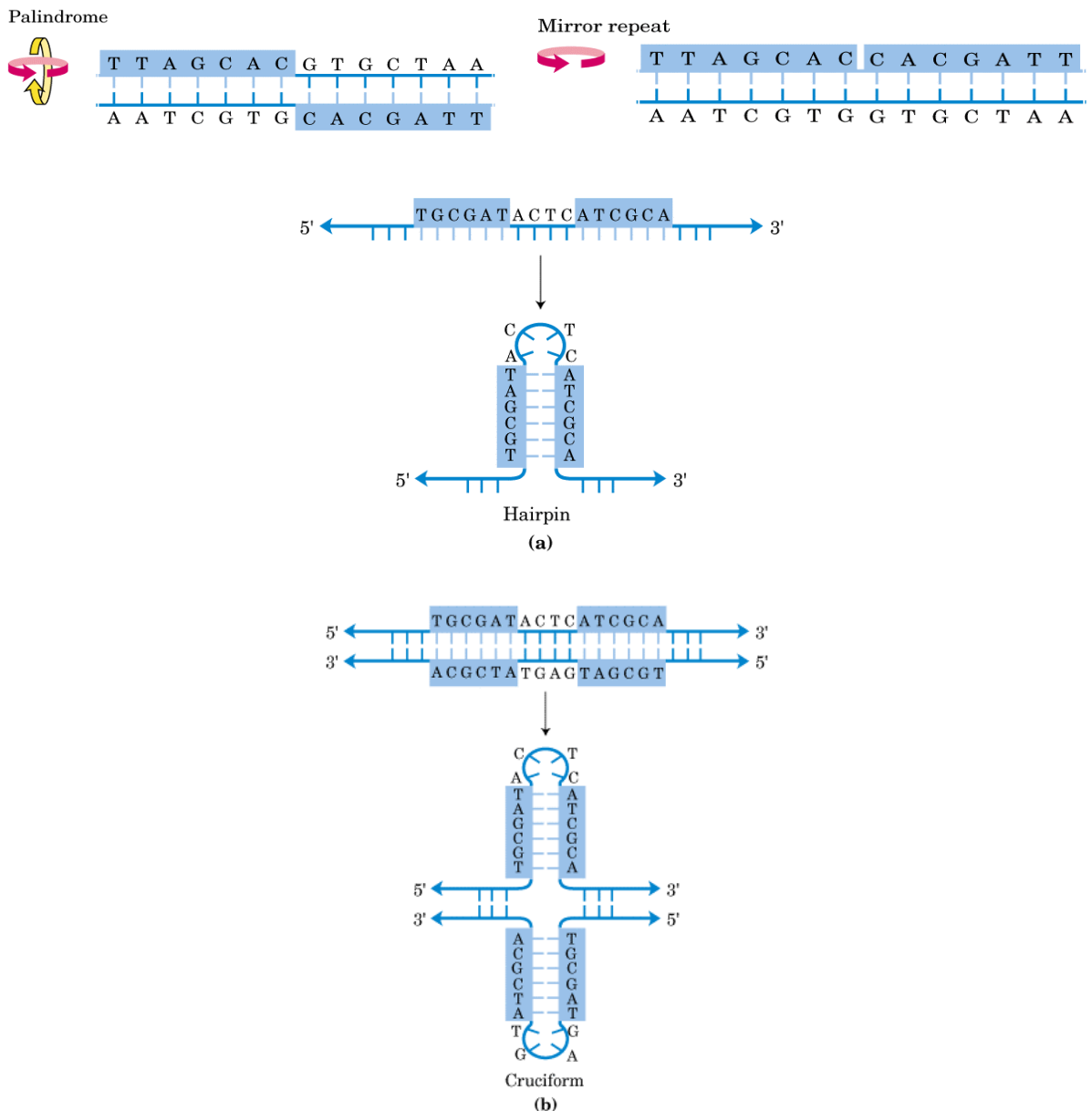


Figure 7. Nitrogen base sequences in DNA strand (repeats) that determine the possible existence of various local structural forms. (a) Formation of a hairpin; (b) formation of a cruciform DNA structure.

An important consequence of the previous base properties is that the formation of complementary Watson–Crick base pairs requires an intact base pair structure. Any displacement of electron or steric structure of base pairs may reduce their ability to form Watson–Crick pairs, and, consequently, different spatial forms of DNA molecules with significantly different properties correspond to different base structures.

From previous descriptions allows one to make some statements: DNA nitrogen bases have peculiar properties. First, their spatial structure provides the possibility of forming complementary pairs; second, the efficient recognition is only typical of

complementary base pairs; and, finally, a stable structure formed of complementary base pairs does not depend much on exterior conditions. An important consequence of the previous base properties is that the formation of complementary Watson–Crick base pairs requires an intact base pair structure. Any displacement of electron or steric structure of base pairs may reduce their ability to form Watson–Crick pairs, and, consequently, different spatial forms of DNA molecules with significantly different properties correspond to different base structures.

2.3 DNA Nucleobases Interactions

2.3.1 Sticky Ends

Double-stranded DNA molecules may have single-stranded fragments at their ends (extensions or “sticky ends”) that can form complementary pairs with other unknown single-stranded DNA fragments (Figure 8 (A)). The most important characteristic of the sticky ends is that they provide the specificity of the interaction between end nucleotide sequences of single-stranded DNAs [17]. A particular distinction of such interaction is

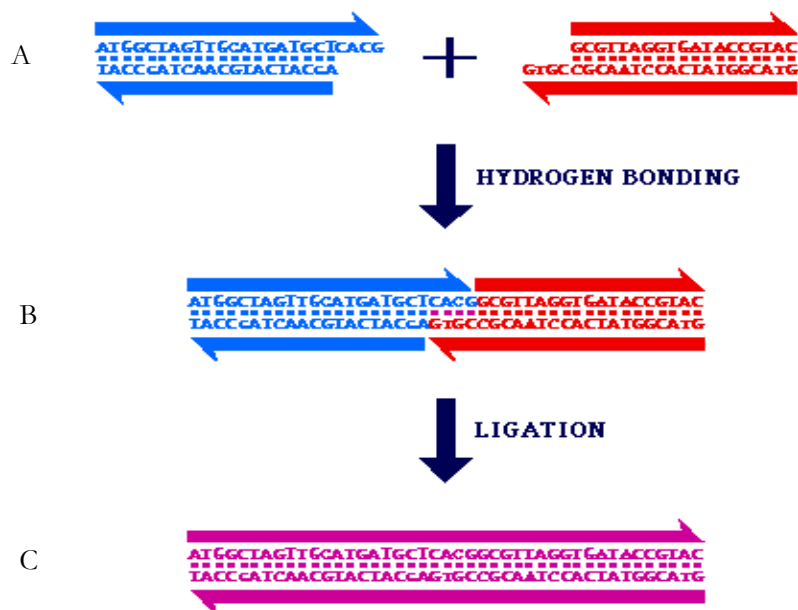


Figure 8. “Sticky ended” cohesion and ligation.

that when the sticky ends overlap, specific hydrogen bonds are formed between single-stranded DNA base pairs. **Figure 8 (B)** represents that under proper conditions, the sticky ends of two DNA molecules recognize and bind to each other specifically by hydrogen bonding to form a single molecular complex. (Predictable affinity and structure are two key features to sticky-ended cohesion that make it important for the application in DNA nanotechnology). The additional treatment of the preformed structure that contains two sugar-phosphate chain breaks by proper enzymes (ligases) promoting the formation of a rigid, helical, a double-stranded DNA complex (B-form DNA) with complementary base pairs (**Fig. 8(C)**). Since the base sequences in the molecules may be known, the example proves that in the case of DNA, intermolecular interactions can be predicted and programmed.

In addition, a more complicated process, namely, the formation of a double-stranded DNA molecule from two single-stranded molecules with complementary base pairs, is known (**Figure 9 (A)**). Here, each interacting unit (oligomer) is an array of four primary nitrogen bases that selectively bind other oligomers in only two possible pairs. In consequence, a strong and specific double-stranded complex is formed between two oligomers. Sometimes a regular structure is obtained, but several incorrect complexes could also be formed (**Fig. 9 (B)**). Single mismatches can be relatively stable. The process of creating a double-stranded molecule from two joining single-stranded complementary DNA chains is called hybridization [32].

The DNA hybridization is a thermodynamically regulated and reversible process. While a double-stranded DNA molecule is separated into two single-stranded chains at the increase in temperature, two complementary single-stranded molecules are joined at the decrease in temperature. Another condition that has a considerable meaning for DNA nanotechnology can be emphasized as: A single-stranded DNA chain construction corresponds to the structure of flexible-chain polymers with most accidental orientation of neighboring nitrogen bases, while the double-stranded DNA molecule is formed as a result of hybridization of rigid molecules, with fixed location of nitrogen bases, respect to the DNA molecule's axis.

In the process of hybridization, two parameters play an important role: the affinity between nitrogen base pairs and the specificity of the interaction between them. For an effective self-assembly, the hybridization of single-stranded DNA molecules must be as high as possible. This means that the formation of base pairs must take place at a maximum efficiency, while the percentage of wrong base pairs has to be minimal. For

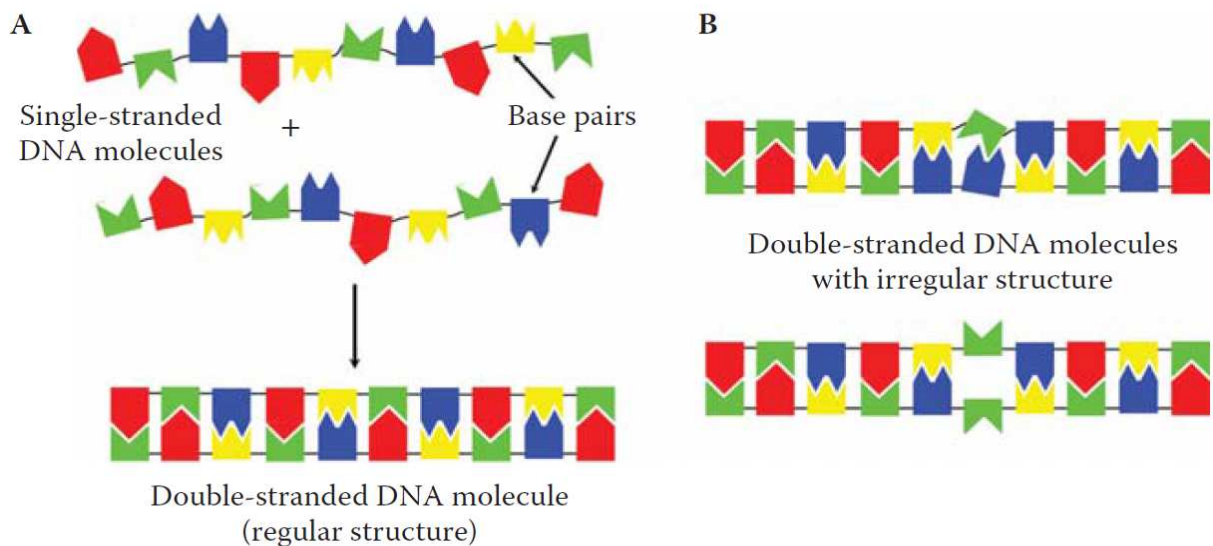


Figure 9. Formation of a double-stranded DNA molecule as a result of the complementary recognition mechanism of nucleation-zipping; A) regular structure, B) irregular structure.

example, the stability of undesirable hybrids measured by the change in the free energy at the formation of complementary pairs has to be minimized, while the stability of the desirable pairs must be maximal. This means that nitrogen bases in the initial DNA chains must be precisely chosen (synthesized), and the experimental conditions for the hybridization must be selected to provide both the affinity and the specificity of the hybridization. The optimal option is to use deliberately designed oligonucleotides that contain sequences of nitrogen bases with a specified structure.

From the previous assessments, it can be concluded that the possibility of using DNA molecules as building blocks, in the case of the hybridization technique of DNA nanostructure formation, is determined by a number of unique properties of these molecules, such as:

1. Nitrogen bases can form specific (complementary) pairs; the complementarity of bases is the fundament in DNA structural nanotechnology.
2. Flexible single-stranded fragments of nucleic acid molecules with a specified base sequence (the sticky ends) hybridize with complementary fragments and form rigid double stranded molecules whose local structure corresponds to the B form. The hybridization is the second fundament in DNA nanotechnology.
3. The predictability of the location of total atoms in the structure of a helical double-stranded molecule relative to its linear axis, as well as the properties of

rigid linear DNA molecules and the nature of intermolecular interactions under different conditions, is the third fundament in DNA nanotechnology.

4. The synthesis of DNA molecules of different sizes and chemical composition in reasonable quantities with the use of modern biochemical methods is the fourth fundament in DNA nanotechnology.

3 Hybridization Techniques of Creating Nanostructures

A fundamental drawback during the creation of DNA nanostructures by the bottom-up approach is that linear DNA molecules cannot form extended two- or three-dimensional (2-D or 3-D) structures with desired requirements under standard solvent properties [33]. This means that the formation of an extended spatial nanostructure with hydrogen bonds between neighboring elements requires the introduction of junction points into the initial DNA structure that would work as the angles in the created construction.

From this context, representing DNA as a branched structure attracts some interest. As shown in Figure 10, there is the hypothetical example of the connection of a four-arm branched DNA molecule (cruciform structure) with sticky ends, (the four sticky ends are labeled as A, B and their complementary fragments as A' and B'). Due to parallelism in the assembly process of four-arm DNA molecules with sticky ends, the hybridization of four such molecules result in formation of a quadrilateral structure (Fig. 10(B)). The formed structure also possesses sticky ends (open valences) on the outside. This means that at the necessary concentration of the four-arm branched DNA molecules in the solution (on the left), this motif could be assembled into a 2-D periodic array (on the right). Under the action of DNA ligase, the splits in sugar-phosphate chains at the sites of sticky ends joining in this structure can be “linked” (eliminated), and rigid double-stranded DNA (B form) ribs, connecting flexible branching points in periodic array, can be formed. The created structure (on the right) has a nanometric size. As the backbone in the square may be from 5 to 20 nm long, this kind of structure can be called a DNA nanostructure. As a result of the self-assembly process, beside the square, an infinite 2-D lattice can be formed. This supposition is based on the presence of sticky ends on the external edges of the structure, which makes possible, the further assembly of a 2-D structure.

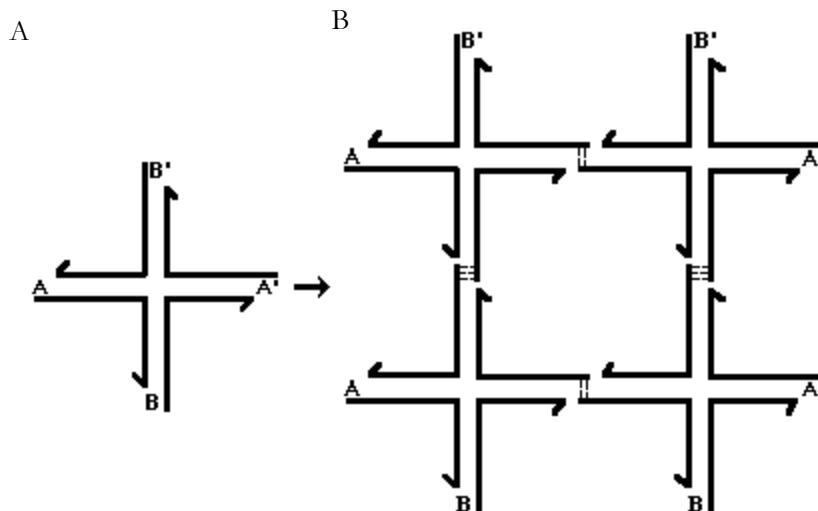


Figure 10. Assembly of a four-arm branched motif and sticky ends (A) to form a two-dimensional lattice (B)

It is probed that the success of the assembly depends on both the stiffness of the DNA segments that form the edges of the square and the stability of junction points on the corners [33]. If any of these components is flexible, the square will not be the desired product, and the formation of a regular structure is highly unlikely. Even if DNA molecules are considered to be flexible, they have a persistent length of about 50 nm at normal solvent properties, which means that locally a double-stranded DNA molecule is much more rigid. Thereby, short DNA molecules with a length equal to two to three helical turns (6–10 nm) can be considered as rigid building blocks.

The objective of the hybridization technique of DNA nanostructure creation is to search for and the synthesis of nitrogen base sequences that provide the formation of the desirable product and make it possible to avoid the formation of intermediate products of the assembly that interact with the final product. In other words, one can analyze the thermodynamic parameters of all of the possible sequences and choose a sequence and hybridization conditions that lead only to the desirable product. To achieve this parameter, there were developed some computer programs, based on the approach called the “minimization of sequence symmetry”, that makes possible to choose the nitrogen base sequences needed for the creation of nanoobjects. Some of these programs are SEQUIN; proposed by Seeman [34]; NANEV from the Turberfield group and some other programs can be found online [35].

The original method proposed by Seeman for the creation of those structures consist on placing the single-stranded DNA molecules into water-salt solution. After that, the solution is heated to 90°C and held at this temperature for 15 minutes, then cool to 65°C (kept for 15 min.), 37°C (kept for 15 min.), to room temperature (22°C, kept for 20 min.), and to 4°C (kept for 20 min.). During the phased cooling, it is considered the difference in melting temperatures of A-T and G-C in base sequences, thereby it contributed to the increase in efficiency of hybridization of the corresponding sequences in single-stranded DNA molecules.

The previous method requires that every element has to be unique. In addition, it is necessary that any element that include a bend does not have its simple Watson–Crick complement anywhere in the sequence. This approach assumes that double helices are the most favorable structures that DNA molecules can generate, and that maximizing double-helix formation will lead to the successful formation of branch points.

Hence, the minimization of the sequence symmetry in individual DNA chains makes it possible to design a single-stranded DNA molecule that will be hybridized in a solution and form a stable branched structure. The success of this approach is based on the concept of the cooperativeness of the DNA double-helix formation as a result of hybridization of zdeliberately synthesized single-stranded molecules with specified base sequences.

The assumption that stable branched structures can be formed from short DNA molecules has led to another assumption, according to which branched nucleic acids can be considered as valence clusters and applied for structural engineering on a nanometric level. Using the high specificity of sticky ends joining catalyzed by ligase, branched structures can be joined in a specified way, forming closed structures. In such structures both edges and angles are nucleic acid double helices. Basically, various spatial shapes, from polyhedrons to periodic lattices and less regular structures may be formed.

3.1 Holliday Junctions

In the way to increase the efficiency of DNA molecule hybridization there was an ongoing search for other DNA structural motifs with higher stiffness. The interest of researchers was attracted to branched DNA molecules formed as intermediate

metabolites in biological processes, namely, the structure known as the Holliday junction [37].

The Holliday junction is the most prominent DNA intermediate in genetic recombination. The principal molecular peculiarity of the recombination is the interaction between two DNA fragments necessary for the formation of a new genetic material that may include segments of both of the molecules. The Holliday structure is the central element in the molecular mechanism of the process.

Figure 11, shows how the Holliday junction is represented during the genetic recombination. At the first stage (A), two homologous DNA molecules with different markers D-F (D'-F') and d-f (d'-f') line up. Then cuts in one strand of both DNA molecules takes place (B). The cut strands cross and join homologous strands to form

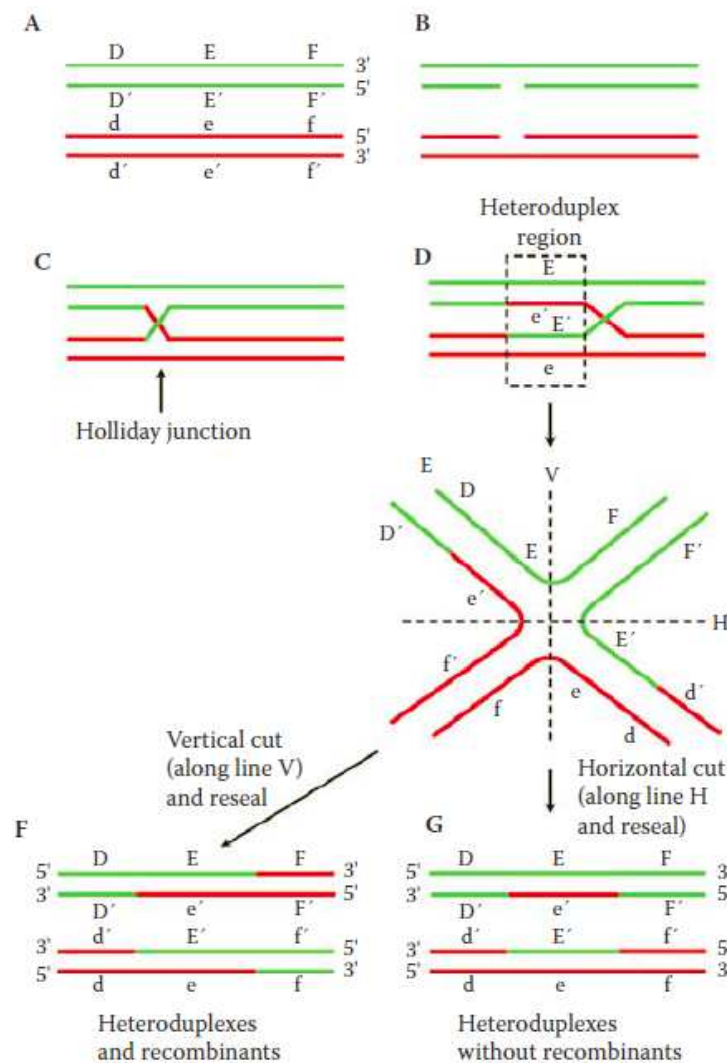


Figure 11. Representation of the Holliday model of DNA crossover

a Holliday structure (or Holliday junction, C). It consists of four strands of DNA that are paired into four double helical arms and wing a junction point. The Holliday junction contains two strand nicked and linked together where the nucleotide sequences of the adjacent strands are joined to form the junction point. The two other DNA strands are not changed and take no direct participation in the recombination process. The strands forming the junction point are called crossover strands, and the two other strands are called the helical strands [37]. The branch point typically is flanked by regions of homologous nitrogen base sequence symmetry. This symmetry modifies the branch point to relocate through an isomerization known as a branch point migration, which includes the change of the initial location of the junction point (D). The area where the strands of DNA molecules are joined is called a heteroduplex region.

Apart of the migration of the junction point, another process can happen, known as the crossover isomerization reaction. In this reaction, the crossover strands and the helical strands change places. Thus, the crossover strands become the helical strands, while the helical strands that were initially intact take the place of the crossover strands. Considering that the Holliday junction is actually a four-arm branched DNA molecule, cutting of the Holliday junction occurs in vertical or horizontal (V and H) direction by enzymes and the further ligase processing of the obtained fragments lead to the formation of products with different properties **Fig. 11(F)** and **11(G)**.

The most important Holliday junction peculiarity especially interesting for nanotechnology is the crossover in DNA strands that is supposed to lead to the increase in the stiffness of the structure. Nevertheless, it has been consider that sequence symmetry destabilizes the location of the junction point so that it can relocate freely. It is clear that the formation of sticky ends in DNA molecules with a fixed junction point may lead to the formation of structures that can hybridize, obtaining more complicated products in comparison to those ones that can be formed from linear DNA. Nonetheless, periodic structures can be obtained from such products. Because the diameter of a DNA molecule is about 2 nm, the assembly of nanometric DNA structures can be formed.

One of the possible variants of formation of a periodic structure using the Holliday junction motif is shown in **Figure 12**. The Holliday junction is shown in **Fig. 12(A)**, where the dyad axis is labeled by a small dot. **Fig. 12(B)** shows a view with the dyad axis vertical. The twisted of both helical domains provide the possibility to form a two-layer structure where each of the layers is formed from the corresponding domains. Although such a structure remains flexible, a more rigid construction can be created by

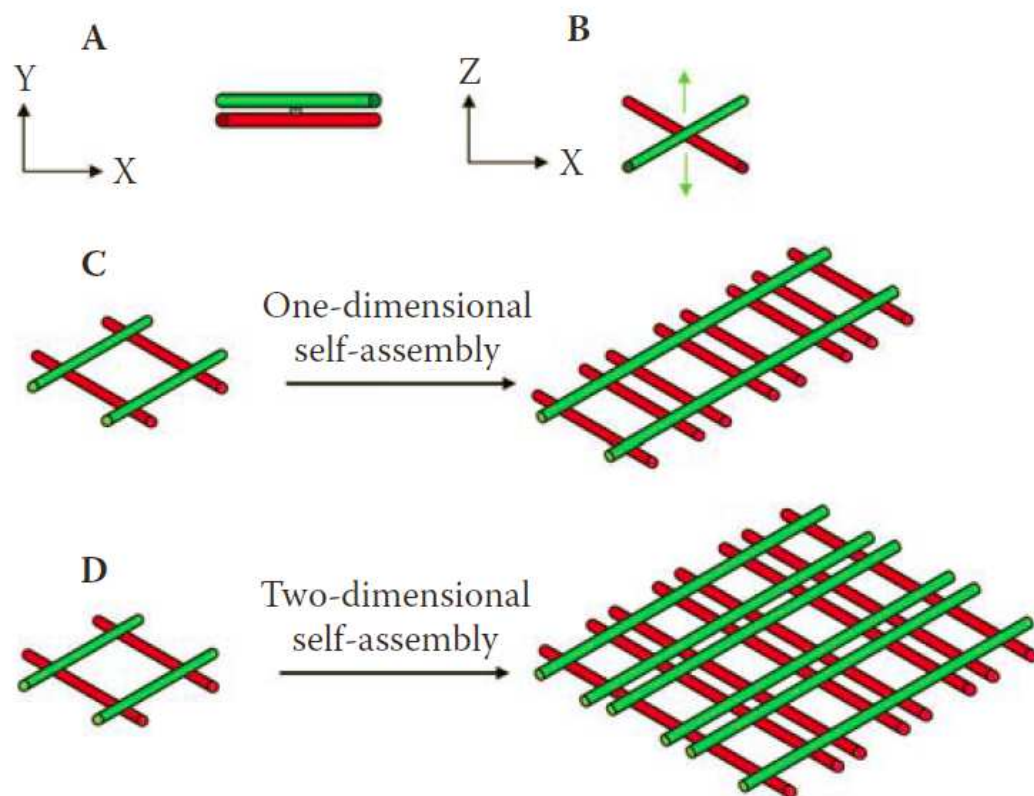


Figure 12. Formation of a periodic structure from branched junctions

joining the four Holliday junctions (**Fig. 12(C,D)**) into a rhombus or a parallelogram [38].

Structures with increased stiffness can be formed from synthetic DNA molecules and used as building blocks for hybridization to form nanostructures. However, studies have shown that the inelasticity of structures like the Holliday structure is insufficient to form nanostructures with high practical yield.

It is known that during meiosis, an intermediate DNA structure with double crossover is formed. This DNA double-crossover molecule contains two crossover links between helical domains. The double-crossed (DX) molecules consist of two double-stranded helices that exchange individual chains in two crossover points. These kinds of molecules are different in the mutual orientation of the helical domains, the continuity of the sugar-phosphate chains, as well as the number of twists of the double helix between the junction points, some of those structures are shown in **Figure 13**.

Besides the double-crossover, other rigid structures, such as DNA molecules with triple crossover points, have been theoretically calculated and synthesized (**Figure 14**). A triple crossover (TX) molecule contains three domains, each of them crossing the neighboring domain twice [39]. **Figure 14(A)** represents the reciprocal exchange

between hairpins. Here, a red hairpin and blue hairpin with zero node between them are presented. Their helix axes are horizontal, and the dyad axis between them is vertical. After reciprocal exchange, the two hairpins have been converted into a single duplex molecule.

From **Figure 14(B)**, it is shown the variety of branched species that can be formed. A single reciprocal exchange between double helices can produce a Holliday junction (HJ) or a four-arm junction. To the right, a DX molecule that is formed as the result of a double exchange is shown. Next to that one, is a triple crossover (TX) molecule that results from two successive double reciprocal exchanges. The HJ, DX, and TX molecules all contain exchanges between strands of opposite polarity. Later, there is a paranemic crossover (PX) molecule, where two double helices exchange strands at every possible point where the helices are contacting. Next to the right of the PX molecule is a JX2 molecule where the two crossovers typical of the PX molecule are absent. The exchanges in the PX and JX2 molecules take place between the strands with the same polarity.

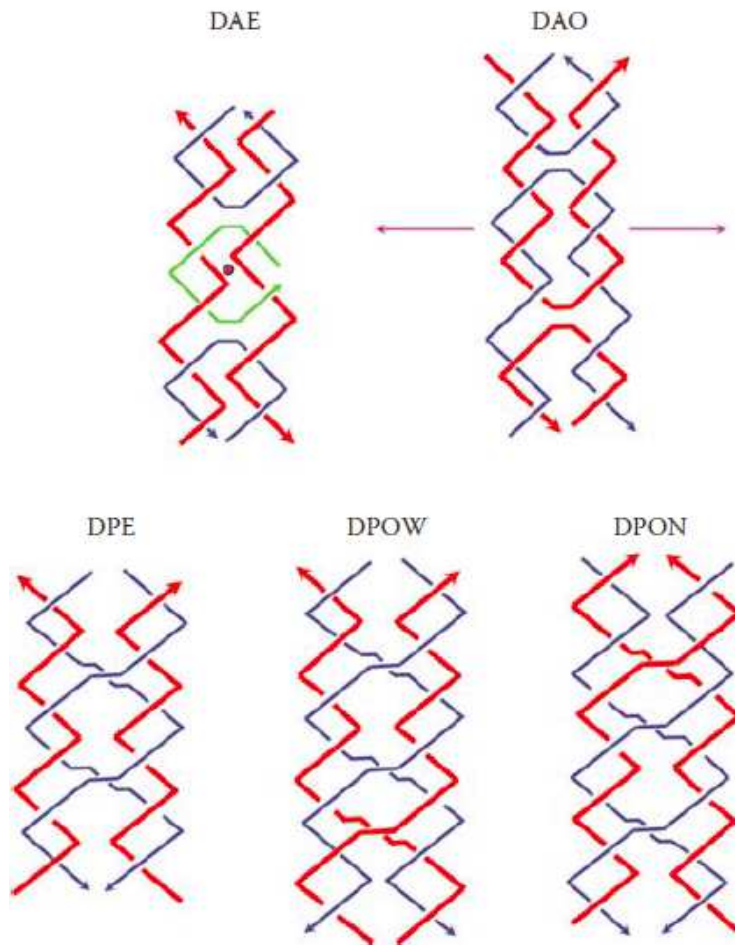


Figure 13. Types of DNA double-crossover strands

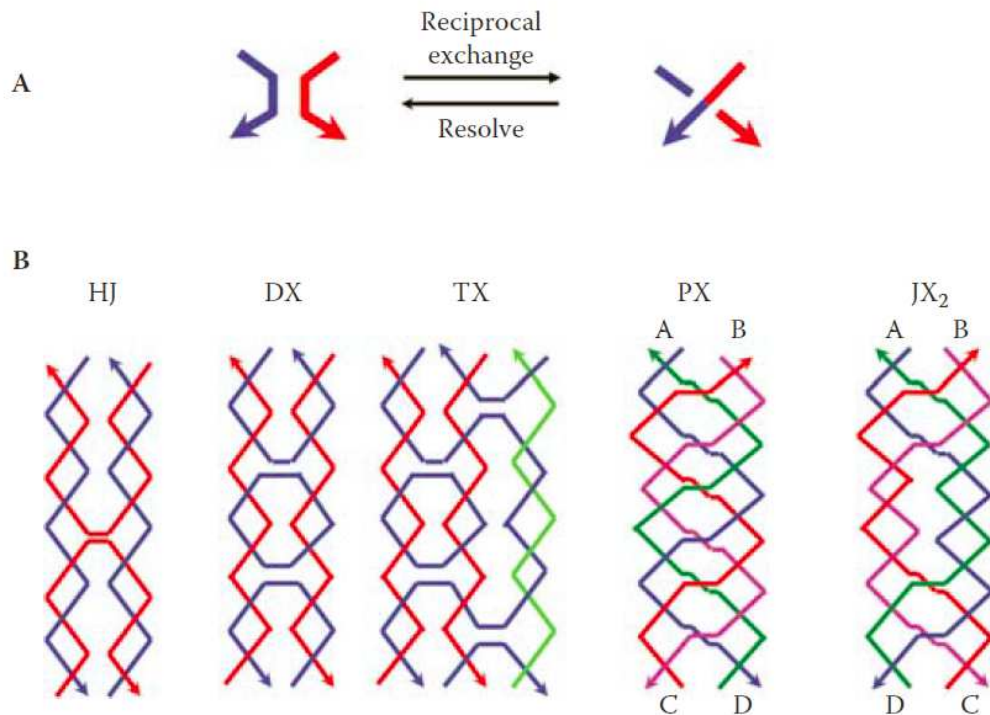


Figure 14. A) The reciprocal exchange process between two DNA hair pins, and B) examples of rigid DNA motifs important in DNA nanoconstruction.

The DNA molecules containing two or more crossover points are called DNA tiles in the literature. DNA tiles can carry single-stranded fragments that hybridize to sticky ends of other DNA tiles and form complementary structures. It should be considered that the continuity of sugar-phosphate chains in the helical domains of DX molecules is important for the process.

DNA tails can be used as building blocks for the hybridization technique of DNA nanostructure formation. Such tiles can be used to hybridize them with other tiles and form a flat 2-D nanostructure (**Figure 15**, here A represents a two-component array and B a four-component array). Extra helical domains, such as DX tiles (tiles B+ and D+) can be introduced into the structure and used as topographic markers (shown as black points) visible in the atomic force microscope (AFM). **Figure 15(A)** shows a structure based in two types of tiles (A and B+). Two helical DX molecules are schematically shown as rectangles with different structures on the ends. These structures represent the sticky ends used for hybridization of DX tiles. To assemble DX tiles into planar 2-D superstructures, the total length of arms (including sticky ends) has to correspond to a certain number of half-turns between the crossover points of adjacent tiles. Black points in the created structure form stripes. **Figure 15(B)** represents a structure consisting of four types of tiles.

Therefore, it is possible to design and produce patterns using DNA components; these patterns contain predictable features, based on the sticky-ended cohesion of individual motifs. In addition to forming arrays from DX molecules, it is also possible to produce periodic arrays from TX molecules. A variety of DNA parallelograms have also been used to produce arrays [40,41], these motifs being produced by combining four HJ like branched junctions. Hence, the structures with crossover DNA molecules are an attractive background for the formation of flat extended 2-D nanostructures.

The methodology of the self-assembly of various 2-D DNA nanostructures includes at the beginning the theoretic calculation and chemical synthesis of single-stranded DNA molecules with specified nucleotide sequences that are joined into tiles for further hybridization. In general, the variety of tiles and branched structures combined with simpler elements, such as sticky ends, helices, and loops, makes it possible to construct a large number of rigid building blocks for DNA nanostructure production.

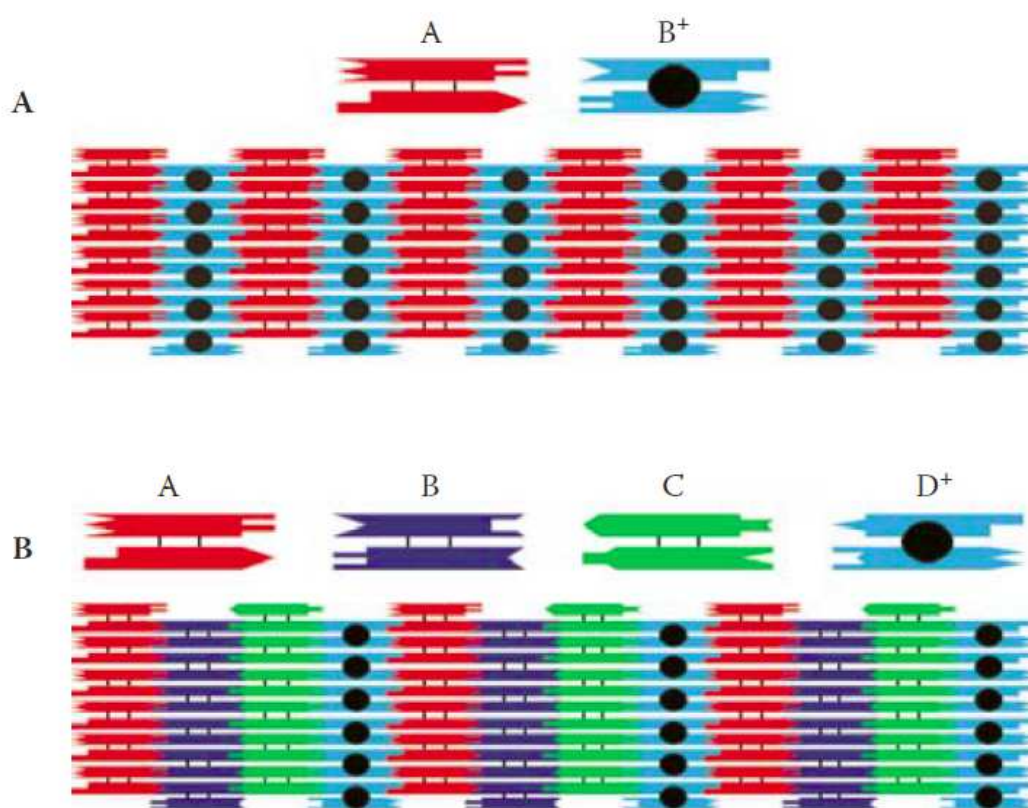


Figure 15. Representation of two variations of flat structures based on DX molecules; A) two types of tiles (A and B⁺); B) four types of tiles (A, B, C and D⁺)

From the previously described DNA fundamentals, it is helpful to summarize some of the key properties that make DNA ideally for nanoscale construction: (1) DNA can be chemically synthesized cheaply using automated synthetic methods that are easy to manipulate to high performance and combinatorial approaches; (2) DNA possesses chemical robustness that provides stability on the architectures, allowing their functionality under a variety of environmental and cellular conditions; (3) double-stranded DNA has uniform and periodic double helical nature irrespective of its primary sequence; (4) it is possible to predict thermal stability of different sequences of DNA; (5) thereby one may program interaction hierarchies into Watson–Crick base pairing of DNA nucleotides and reach site-specific molecular associations within a given architecture; (6) various biochemical and molecular biological methods are available to cut out or link B-DNA duplexes sequence specifically; this allows controlled construction of various DNA sequences and structures; (7) DNA units are modular in nature; and (8) specific sequences of single-stranded DNA can link together to a range of molecules with high specificity and affinities. In consequence, we can use multiple DNA units to construct various complex nanostructures both structurally and functionally [42].

With all those properties, structural DNA nanotechnology can be used to create architectures like (a) Rigid and static DNA architectures, e.g., 1D wires, tubes, 2D sheets, tiles and crystals, 3D polyhedra, DNA crystals, and boxes and (b) dynamic DNA devices, e.g., nanomachines, robots, walkers, and sensors [43-45].

3.2. 3D DNA Polyhedra

The ability to create well-defined, molecularly addressable structures with the capacity to be interfaced with other functional molecules is a highly attractive characteristic for any scaffold with relevance to its applications in bionanotechnology. Thus, a primary advance in this field was the realization of DNA-based structures that could accommodate useful cargo like drug molecules or therapeutic proteins within their cavity. As described before, the first DNA based 3D polyhedron was realized by Seeman and coworkers who formed a noncovalent complex using six strands of DNA that was shown to possess the molecular connectivity of a cube, although with very low synthetic yield [46]. Also, a DNA tetrahedron was created in very high performance using a simple strategy that used four DNA oligonucleotides that self-assembled together in one pot

assembly. This polyhedron was the first to be topologically characterized using AFM, thus providing direct evidence of the formation of polyhedral architectures in solution by DNA [47].

A fundamental progress was the introduction of a new hybridization technique of nanostructure self-assembly called single-stranded DNA origami, presented by Rothemund [30]. Inspired from the same name Japanese paper folding art, Rothemund used term “origami” to describe this new strategy. In brief, DNA origami involves filling the desired shape with a long single stranded scaffold with the help of hundreds of short oligonucleotides, called staple strands, to anchor the scaffold in place (**Figure 16**). Periodic crossovers are widely used along the shape for rigidity, and the distance between successive crossovers is carefully designed to decrease twist. The scaffold sequence does not require a specific design, because the success of DNA origami is ensured by strand displacement reaction, where a longer region of complementarity between the staple and the scaffold stabilizes the staple–scaffold interaction over the scaffold’s secondary structure.

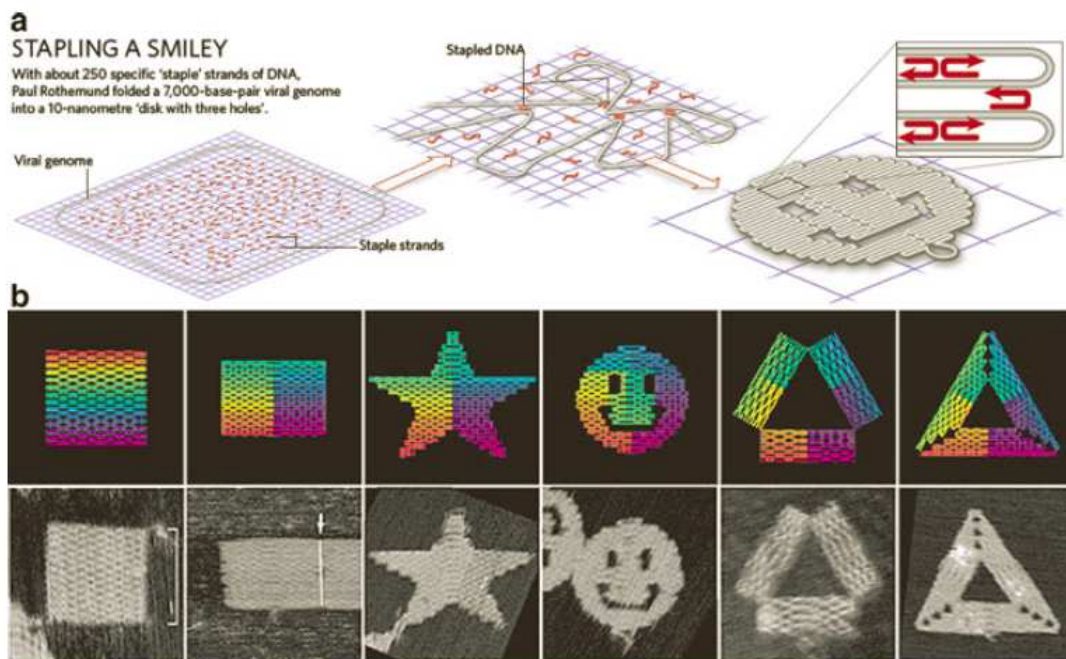


Figure 16. The DNA origami self-assembly technique. (a) The designing principle of origami nanostructure. (b) Some examples of DNA nanostructures obtained by this technique [30, 48]

Subsequently DNA origami was exploited to make 3D polyhedra like icosahedron. The use of origami was further explored to make a cuboidal box using six copies of the genomic DNA of M13 bacteriophage [49], while the controlled opening and delivery of internally attached molecules was achieved using a DNA origami-based 3D robotic device[50].

All the aforementioned techniques relied on the folding of DNA oligonucleotides in 3D space to create polyhedra which, unlike their earlier counterparts, could be created in better yields. An alternative approach was established in 2007, where using small molecules as mimics of DNA junctions, the DNA strands were covalently attached together to form DNA–small molecule junctions, which are stable and prefolded in a defined confirmation. Using these junctions, various DNA polyhedra like cubes, octahedral, and prisms were created [51]. A similar technique was used to create a DNA dodecahedron using small molecule-based DNA 3-way junctions [52]. (**Figure 17**)

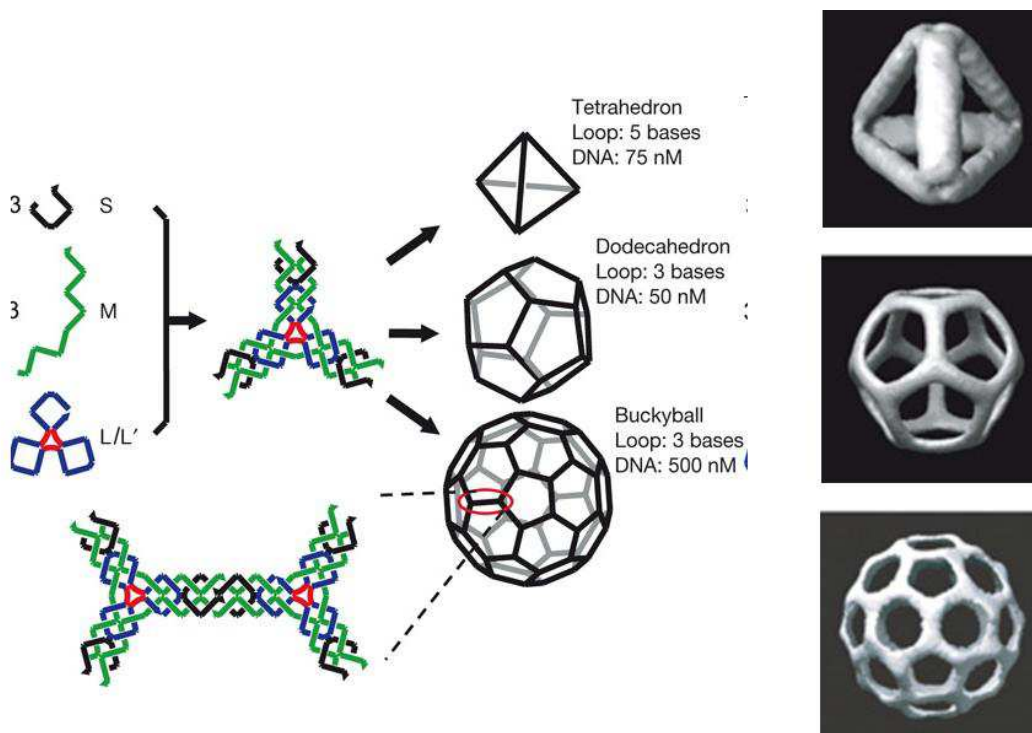


Figure 17. Programmed DNA motifs can be self-assembled into various 3D DNA solid polyhedra like tetrahedron, dodecahedron and high order polyhedra like buckballs [53,54]

3.2.1 Funtionality of DNA Polyhedra

Most polyhedra, constructed and characterized, were postulated to have many applications in areas including drug delivery, biomolecular organization, bioreactors, biosensors, etc. All of these applications lie on two key features of DNA polyhedra: that they could encapsulate molecules like drugs and functional biomolecules within their cavities, and that the DNA could be surface modified with various molecular tags site specifically using standard chemical conjugation procedures.

Some remarkable examples in the use of DNA polyhedra for the encapsulation of molecular cargot. By covalently attaching a protein such as cytochrome C on one arm of a DNA tetrahedron, it was shown to be site specifically positioned on the tetrahedron such as it faced the interior of the polyhedron and occupied the internal cavity of a DNA tetrahedron [55].

Another important aspect of DNA polyhedra is that their surfaces can be modified site specifically with various molecules, nanoparticles, biomolecules, etc. using standard conjugation procedures. This is of particular importance since DNA polyhedra carrying drugs can be surface modified by various targeting moieties, which can carry the host to specific targets in living organisms. With respect to this, folic acid (a well-known marker for cancer cells) conjugated DNA nanotubes were shown to be internalized by cancer cells [56]. Further, a DNA tetrahedron was designed with hairpins outgoing outwards from the edges of the tetrahedron. These hairpins can act as aptamers that recognize and bind various molecules in solution or on the surface of cells [57]

In addition, several studies have shown the ability of different types of nanostructures, especially nanoparticles and nanocapsules, to accumulate inside cells with or without the help of lipid vectors [58-61]. In this context, the progress in developing new nucleic acid nanostructures could be very useful. These can be used in the future as intracellular biosensors or to deliver drugs to the cells, overcoming the known limit that highly charged oligonucleotides have in accumulating into cells. Thereby, the availability of diverse intracellular biosensors may be crucial for cell biology studies and for a fuller understanding of the molecular and metabolic pathways involved in several diseases such as cancer. Moreover, it will be possible to characterize the effect of therapeutics at a single cell level, providing information on time and population variations in cellular response that could make the difference between ineffectiveness, treatment, and toxicity of a drug. The possibility of choosing amongst an

increasing variety of intracellular biosensors will give researchers the chance to stand out on dynamic complex processes.

3.3 Future Directions

It is clear that nucleic acid-based designer architectures have provided a great potential in the development of Nanomedicine. The advantages offered by DNA of control over structure and the site specific addressability of the platform that is generalizable to a variety of molecules are unsurpassed by any other platform. However, there still remain many challenges before DNA can compete with commercially available agents for drug delivery. The key challenges are the ability to increase proportionally synthesis of DNA and RNA per se and encapsulate a wide range of drugs, demonstrate targetability to different tissues within living organisms without off-target delivery and temporal control over release of the encapsulated cargo at the target sites. Taken together, nucleic acid-based architectures offer an extremely powerful tool to develop targetable drug delivery systems for future applications in nanomedicine. Given the reducing rates of DNA synthesis and the increase in efficiency and error free (homogeneous) formation of DNA nanostructures, it is expected that in a near future there are a lot of interesting avenues for this field.

References Part I

- [1] C. P. Poole, F. J. Owens, *Introduction to Nanotechnology*, John Wiley and Sons Inc, Hoboken,N.J., **2003**.
- [2] R. F. Service, *Science* **2002**, 298, 2322.
- [3] The Royal Society, Nanoscience and nanotechnologies: Opportunities and uncertainties. In *Royal Society and Royal Academy of Engineering*, 10, London **2004**.
- [4] <http://www.nano.gov/> [May, **2014**].
- [5] Ratner, M., and D. Ratner. *Nanotechnology: a simple explanation of the next brilliant idea* (Russian ed.). Moscow: Ed. House Williams.,**2004**.
- [6] <http://www.zyvex.com/nanotech/feynman.html> [May, **2014**]
- [7] N. Taniguchi, in *Proc. Intl. Conf. Prod. Eng. Tokyo, Vol. Part II*, Japan Society of Precision Engineering, Tokyo, **1974**.
- [8] Binnig, G., H. Rohrer, Ch. Gerber, and E. Weibel. *Phys. Rev. Lett* **1982**, 49:57–60.
- [9] Binnig, G., and H. Rohrer.. *Scanning tunneling microscopy: From birth to adolescence. Nobel lecture*, December 8, **1986**
- [10] E. K. Drexler, *Engines of Creation: The Coming Era of Nanotechnology*, Bantam Doubleday Dell, **1986**.
- [11] Yevdokimov, Yu. M., M. A. Zakharov, and S. G. Skuridin. Nanotechnology based on nucleic acids. *Herald of the Russian Academy of Sciences* (Russian ed.) 76:112–20. **2006**
- [12] Niemeyer, C. M.. Nanoparticles, proteins, and nucleic acids: Biotechnology meets materials science. *Angew. Chem. Int. Ed.*, 40:4128–58, **2001**.

- [13] Yevdokimov, Yu. M., and V. V. Sytchev. Principles for creating nanoconstructions with nucleic acid molecules as building blocks. *Uspekhi Khimii* (Russian ed.)77:194–206. **2008**
- [14] Seeman, N. C. *J. Theor. Biol.* **1982**, 99:237–47.
- [15] Seeman, N. C. *J. Mol. Biotechnol.* **2007**, 37:246–57
- [16] Seeman NC. *Trends Biochem Sci.* **2005**;30:119–125.
- [17] Seeman NC. *Methods Mol Biol.* **2005**;303:143–166.
- [18] Seeman NC. *Q Rev Biophys.* **2006**;6:1–9.
- [19] Seeman NC.. *Chem Biol* **2003**;10:1151–1159.
- [20] Seeman NC. *Nature* **2003**;421:427–431.
- [21] Roco MC. *Curr Opin Biotechnol.* **2003**;14:337–46.
- [22] Ishijima A and Yanagida T. *Trends Biochem Sci.* **2001** 26: 438–444.
- [23] Misevic GN. *Mol Biotechnol.* **2001**,18: 149–154.
- [24] Whitesides G and Boncheva M. *Proc Natl Acad Sci USA* 99. **2002** 4769–4774.
- [25] Krishnan Y, Simmel FC *Nucleic acid based molecular devices.* *Angew Chem Int Ed* 50(14):3124–3156, **2011**.
- [26] Wilner OI, Willner I. *Chem Rev* **2012**, 112(4):2528–2556
- [27] Adleman LM. *Science* **1994**, 266(5187):1021–1024
- [28] Yurke B, Turberfield AJ, Mills AP, Simmel FC, Neumann JL.. *Nature* **2000**, 406(6796):605–608
- [29] Bunka DHJ, Stockley PG. *Nat Rev Microbiol* **2006**, 4(8):588–596
- [30] Rothmund, P. W. *Nature* **2006**, 440:297–302.
- [31] Saenger, W. *Principles of Nucleic Acid Structure.* New York: Springer-Verlag, **1984**.
- [32] Seeman, N. C.. *Quart. Rev. Biophys.* **2005**, 38:363–71.
- [33] Seeman, N. C.. *Acc. Chem. Res.* **1997**, 30:357–63.

- [34] Seeman, N. C. *J. Biomol. Struct. Dyn* **1990**, 8:573–81.
- [35] Brenneman, A., and A. E. Condon. *J. Theor. Comput. Sci.* **2002**, 287:39–58.
- [36] Holliday, R., *Genet. Res. Camb.* **1964**, 5:282–304.
- [37] Li, X., H. Wang, and N. C. Seeman. *Biochemistry* **1997**, 36:4240–47.
- [38] Murchle, A. I. H., R. M. Clegg, E. von Kitzing, D. R. Duckett, S. Diekmann, and D. M. J. Lilley. *Nature* **1989**, 341:763–66.
- [39] Seeman, N. C. *Nano Lett.* **2001**, 1:22–26.
- [40] C. Mao, W. Sun, N. C. Seeman, *J. Am. Chem. Soc.* **1999**, 121, 5437–5443.
- [41] R. Sha, F. Liu, D. P. Millar, N. C. Seeman, *Chem. Biol.* **2000**, 7, 743–751.
- [42] Modi S, Bhatia D, Simmel FC. *J Phys Chem Lett* **2010**, 1:1994–2005
- [43] Bhatia D, Sharma S, Krishnan Y. *Curr Opin Biotechnol* **2011**, 22:475–484
- [44] Bhatia D, Surana S, Chakraborty. *Nat Commun* **2011**, 2:339
- [45] Krishnan Y, Simmel FC. *Angew Chem Int Ed* **2011**, 50; 3124–3156,
- [46] Chen J, Seeman NC. *Nature* **1991**, 350:631–633
- [47] Goodman RP, Schaap IAT, Tardin CF. *Science* **2005**, 310:1661–1665
- [48] Sanderson K. *Nature* **2010**, 464:158–189
- [49] Andersen ES, Dong M, Nielsen. *Nature* **2009**, 459:73–76
- [50] Douglas SM, Bachelet I, Church GM. *Science* **2012**, 335:831–834
- [51] Aldaye FA, Palmer AL, Sleiman HF. *Science* **2008**, 321:1795–1799
- [52] Zimmermann J, Cebulla MP, Monninghoff S. *Angew Chem Int Ed* **2008**, 47:3626–3630.
- [53] Zhang C, Su M, He Y, Zhao X, Fang PA, Ribbe AE, Jiang W, Mao C. *Proc Natl Acad Sci U S A.* **2008**, 105(31):10665-9.
- [54] He, Y., Ye, T., Su, M., Zhang, C., Ribbe, A. E., Jiang, W. and Mao, C. *Nature* **2008**, 452(7184):198-201.
- [55] Erben CM, Goodman RP, Turberfield AJ. *Angew Chem Int Ed* **2006**, 45:7414–7417
- [56]. Zhao Z, Jacovetty EL, Liu Y. *Angew Chem Int Ed* **2011**, 50:2041–2044
- [57] Lee H, Lytton-Jean AKR, Che Y. *Nat Nanotechnol* **2012**, 7:389–393

- [58] Ko S, Liu H, Chen Y. *Biomacromolecules* **2008**, 9:3039–3043
- [58]. Walsh AS, Yin H, Erben. *ACS Nano* **2011**, 5:5427–5432
- [59] Hamblin GD, Carneiro KM, Fakhoury. *J Am Chem Soc.* **2012**, 134:2888–2891
- [60] Weissleder, K. Kelly, E.Y. Sun, T. Shtatland, L. Josephson, *Nat. Biotechnol.* **2005**, 23:1418–1423.
- [61] J. Panyam, V. Labhasetwar, *Adv. Drug Deliv. Rev.* **2003**, 55:329–347.

PART II

Strategy of Implementations

Strategy of Implementations

The creation of a novel DNA nanostructure usually requires the following steps: (1) Structural modeling: physical and/or graphic models are used to help the design of a new DNA nanostructure; (2) Sequence design: in this step, specific sequences are assigned to all (single-stranded) ssDNA molecules in the model; (3) Experimental synthesis of the DNA nanostructure; and (4) Characterization of the DNA nanostructure. Following this requirements, in this chapter, I describe the methodology used in this thesis for the design, preparation and characterization of our two fluorescent DNA nanostructures. In addition, I present the methodology for the cell culture, the nanostructure delivery to cells, their detection and the preliminary studies for the in vivo biofunctionality of our structures as cellular sensors.

4 Structural Modelling

The inspiration for the design of our particular structures was based on the simplest 3D polyhedral self-assembled DNA nanostructure, the DNA tetrahedron, first proposed by Turberfield and co-workers [1,2]. Basically for the construction, a series of oligonucleotides is required that are assembled in a nanometer-scale 3D tetrahedron whose sides are constituted by double-stranded DNA. In addition, those oligonucleotides can be decorated with fluorophores, making the whole structure fluorescent. Fluorescent tetrahedrons have been also detected inside living cells and even in a full animal [3,4]. Further, the tetrahedra's ability to enter cells has been used to deliver anti-tumor drugs [4,5]. These structures can also be designed for applications such as sensors,

switches, motors, diagnostic markers and targeted therapies inside living cells [6,7]. Recently some researchers have demonstrated the ability for creating specific DNA nanomachines, working as biosensors that can probe the local pH inside a living cell [8]. In addition, those structures could work as diagnostic markers and targeted therapies inside a cell. For example, one can imagine designing nanodevices that first detect the messenger RNA associated with a disease, then release a regulatory DNA strand and subsequently trigger cell death. This proof-of-principle demonstration confirms the great potential of nanodevices based on DNA and other nucleic acids for applications in cell biology and biomedical engineering.

Following the previous idea, we employed the basic design of the Tuberfield group to develop two functional DNA fluorescent nanobiosensors; a pH dependent one that can probe the local pH inside a living cell and a DNA:RNA targeted therapy sensor. In this section I will describe step by step the structural modeling for each nanostructure.

4.1. The pH Dependent Biosensor

4.1.1 The idea

Recently, Krishnan's group demonstrated the first example of an autonomous DNA nanomachine, the I-switch, triggered by protons and functioned as a pH sensor based on the FRET phenomena inside living cells [9,10]. The CT-motif DNA triple helix is a well-documented structure that can be formed from a target duplex with a homopurinic: homopyrimidinic tract and a homopyrimidinic triplex-forming oligonucleotide (TFO), see **Figure 1**. The formation of this type of triplex is critically dependent on the protonation of the imino groups of the TFO cytosines under acidic condition and can therefore be driven dynamically by controlled pH changes.

Based on the dynamic behavior of this transition we designed a particular DNA nanomachine that contains a strand capable of switch between two conformations by means of the pH-driven intramolecular formation and breakdown of a CT-motif DNA triplex helix. We expect to use this nanostructure as an intracellular biosensor with the ability to map spatial and temporal pH changes in live cells.

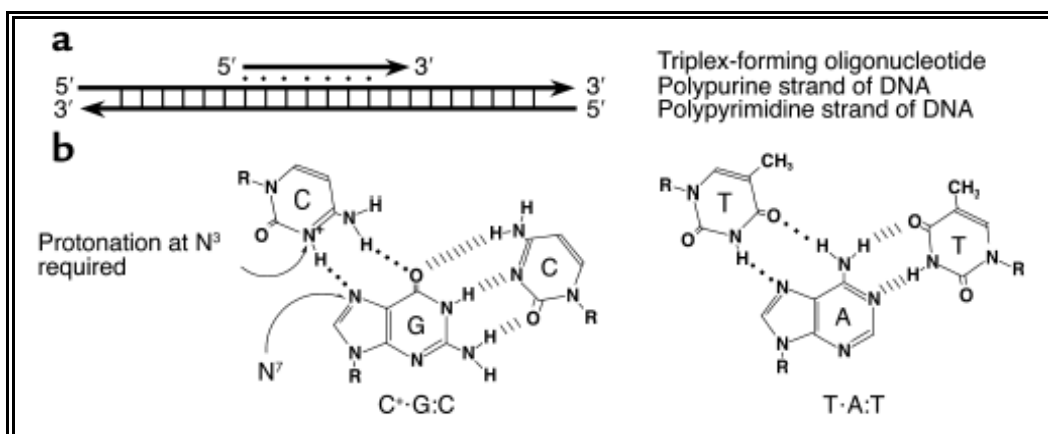


Figure 1. The CT-motif DNA triplex helix formation

4.1.2 The model

For the general design, based on the Turberfield's tetrahedra, our group previously developed a stable fluorescent tetrahedron with the ability to being internalized in live cells with high efficiency (details for the design, synthesis and characterization can be found [11]). In **Figure 2** are shown the 3D model and the oligonucleotide components that form this modified tetrahedron. Following that structure, we introduce some other modifications on the arrangements and the nucleotide sequences, like the insertion of the triplex helix target and TFO, enabling its particular biosensor functionality.

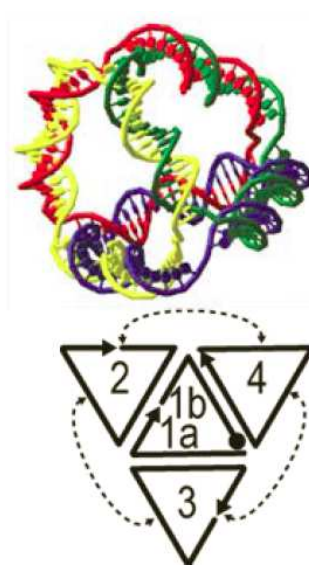


Figure 2. 3D molecular model and scheme of the oligonucleotide components for the fluorescent DNA tetrahedron developed in the group [11]

For the accomplishment and selection of the appropriate new sequences of oligonucleotides, some steps were followed, in order to obtain their assembly. First the size and symmetry of the structure was defined. Then the break point of each oligonucleotide was defined. For applications in live cells, the nanostructures must be stable at least up to 37 °C in physiologic conditions, so it is better to design the oligonucleotides to form double-stranded sections that are stable along their entire length in such conditions. In addition, the presence of specific base sequences has to be included in the design (such as endonuclease restriction sites, tracts of especially high thermal stability, or others). Covering those considerations, we designed a general structure, see **Figure 3**.

In this design, we used 4 oligonucleotides or strands (Str.1, Str.2, REP and Long-strand); each oligo forms one face of the tetrahedron and each weaves with all the others. A common DNA tetrahedron can be made of 20 bp long edges, so each oligonucleotide is slightly longer than 60 nt. Here, the length of each edge has to be commonly an integer number of double-stranded turns, with flexible vertices to avoid the formation of non-equilateral pyramids due to the flexibility of vertices, the only location where unpaired bases are present. To provide thermal stability of all interactions between components, we placed the termini of each oligonucleotide (the end of the narrow) at the vertices of the tetrahedron.

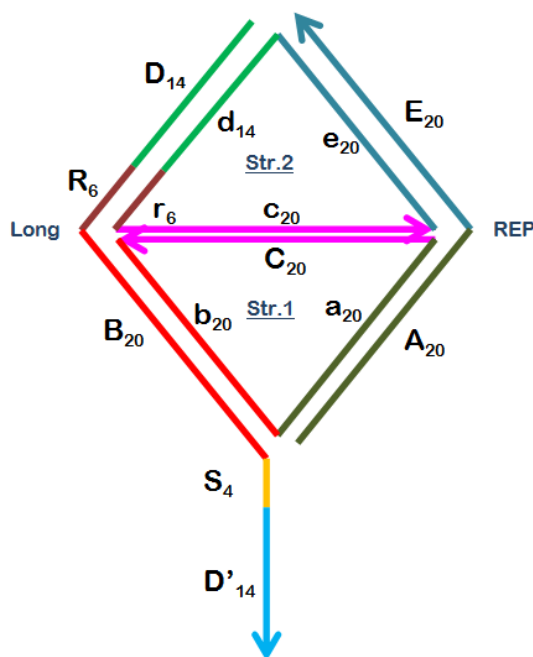


Figure 3. Scheme of the arrangement of the oligonucleotide components for our proposed pH dependent structure

Considering the aforementioned parameters, we describe for each oligonucleotide a series of assembling requirements that must be fulfilled to be part in the structure and provide our desired functionality.

1. Oligonucleotide 1 and 2, that we call **Str.1** and **Str.2** respectively: We design a 62-(nucleotides)-nt for each strand divided in 3 sections of 20-nt each one, in addition to two unpaired bases that must form the vertices. These two structures will thermally assemble with each other by sharing a common edge “C-c” (pink segments in **Fig. 3**) which will fold, one over the other, when conformation of the structure changes. The Str.1-Str.2 termini of both oligonucleotides cannot be internal, this is a low stability breaking point, so the resulting annealing is restricted to the complementary 5' → 3' ending strands (direction of the arrows). The rest of nucleotides are shared with REP and TFO strands as showing in figure. Str.1 and Str.2 are the bedrock oligonucleotides that provides most of the support and stability to the structure.

2. Long oligonucleotide, from this structure we called just **TFO** strand. We must design an oligonucleotide sequence with the ability to generate the CT-motif DNA triplex helix formation, this means, at the end of the long strand is the nucleotide sequence that can latch to the rest of the structure in a triplex helix, leading to a conformational transition. Such TFO tail has cytosines and thymines, so that parallel triple helix can form exploding C-G.C⁺, triplets (**Figure 4**).

In our proposed structure, the TFO oligonucleotide is a long 60-mer divided in 5 segments (the "long" strand in **Fig. 3**). The “B” 20-nt, in red, will form a duplex by normal Watson-Crick interactions with the corresponding complementary “b” 20-nt sequence of the Str.2, also marked in red. In the same conformation, D-d (green) and R-r (brown) also form a duplex. The additional “D’ segment”, represented in blue, will interact with the D segment (green) effect of pH variation through the triplex helix formation. The mechanism is described by the following steps:

a) In a neutral to basic solution (e.g., pH 8.0) after the annealing, the structure is in open state; this means that only normal Watson-Crick, G-C and A-T, duplex base pairs are stable; the tail of the long TFO strand is found in a random-coil conformation, while the rest of it is bound to Str.1 and Str.2.

b) In an acidic solution (e.g., pH 5.0), unpaired cytosines (C) are protonated as C⁺, which can interact with a G-C base-pair through Hoogsteen hydrogen bonding (H-bonding) to form C⁺G-C triplets, so generating a closed structure, **Fig.4**. Notice that in the current design, C⁺G-C triplets are pH sensitive, while TA-T triplets are not

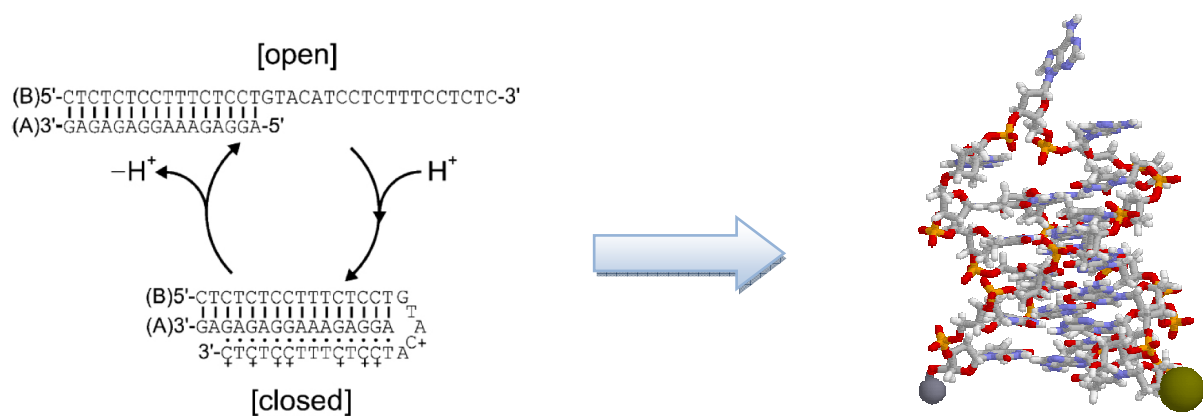


Figure 4. Cytosines protonation for the triplex helix formation [12]

pH sensitive. In our structure, we notice the structural shift when cytosines of the D' subsegment of TFO, in blue, are protonated and have the ability to move freely until they reach their complementary base sequences and forming the C+G-C (H-bonding). In our case, the only possible complementary sequence is found at the "D" segment, in green; thus, the D' TFO section folds back on the duplex, binding parallel to its purine strand in the D major groove and bringing the two opposite termini of the adduct in close proximity, forming the closed state (**Figure 5**). The remaining "S" strand, in yellow, will act as a "hinge" to provide the flexibility to close the structure during the triplex formation.

3. Fluorescent oligonucleotide (**REP**). We introduce two particular fluorophores to develop a DNA fluorescent nanostructure. This is done for several reasons, first to be able to follow, by the use of fluorescence microscopic techniques, the correct introduction of our structure inside live cells; also, we could have an idea about the particular localization of the structure and a possible biosensing response inside the cells. Second, to allow the characterization as a sensor, this means, be able to detect the global transition between the open and the closed state when the pH changes, by the mean of fluorescence spectroscopy, in particular FRET. We chose the CY3 and BODYPY 650/665 (BPY650) organic dyes, which were introduced at the called "rep" oligonucleotide in positions 5' and 3' respectively. In our model, CY3 is placed at the end of the "A" 20-nt, while BPY650 is at the end of the "E" 20-nt (**Fig. 5**). The "rep" strand has the ability to connect by the vertices all the segments in the structure. While the two fluorophores are fluorescent molecules we could visualize them both the open and the closed structure in regards to their respective emissions intensity.



Figure 5. 3D molecular model of our DNA tetrahedron in the shift transition from open (pH 8.0) to closed state (pH 5.0) [model done with NanoEngineer (Nanorex, Inc.)]

For the selection of these two fluorophores we consider the following requirements:

a) About their stabilities; both CY3 and BPY650 have absorptions and emissions properties that are not sensitive to pH changes in the range from pH 5 to pH 10. They are perfectly internalized by cells and remain stable inside.

b) About their position in the "rep" oligonucleotide; were placed them in the site where both dyes, in the closed state, must be in a particular distance apart to allow the phenomena of FRET; in our case, this position was satisfied introducing CY3 at the 5' ending and BPY650 at the 3' ending. The suitable distances for biological macromolecules, called as the Förster distance, at which energy transfer is 50% efficient has to be in the range parameters from 2 to 9 nm. In our case when CY3 and BPY650 are in the closed state -acid conditions-, they are around 2 nm apart each other.

c) About their FRET efficiency; from several research is proved the suitable use of CY3/BPY650 as donor/acceptor pair to generate the FRET phenomena (see section 2.4.2 for more details). This selection was based on their excitation-emission overlap spectrum properties, (**Figure 6**). CY3 is excited by irradiation at wavelength of 530 nm maximum, while its emission is at 560 nm, this value is just enough to create an overlap with the excitation of BPY650 at 640 nm wavelength; in this point, the excited state of CY3 is transferred by non-radiative process to BPY650, inducing its excitation and consequently, to emit a photon at 680 nm which is detected and

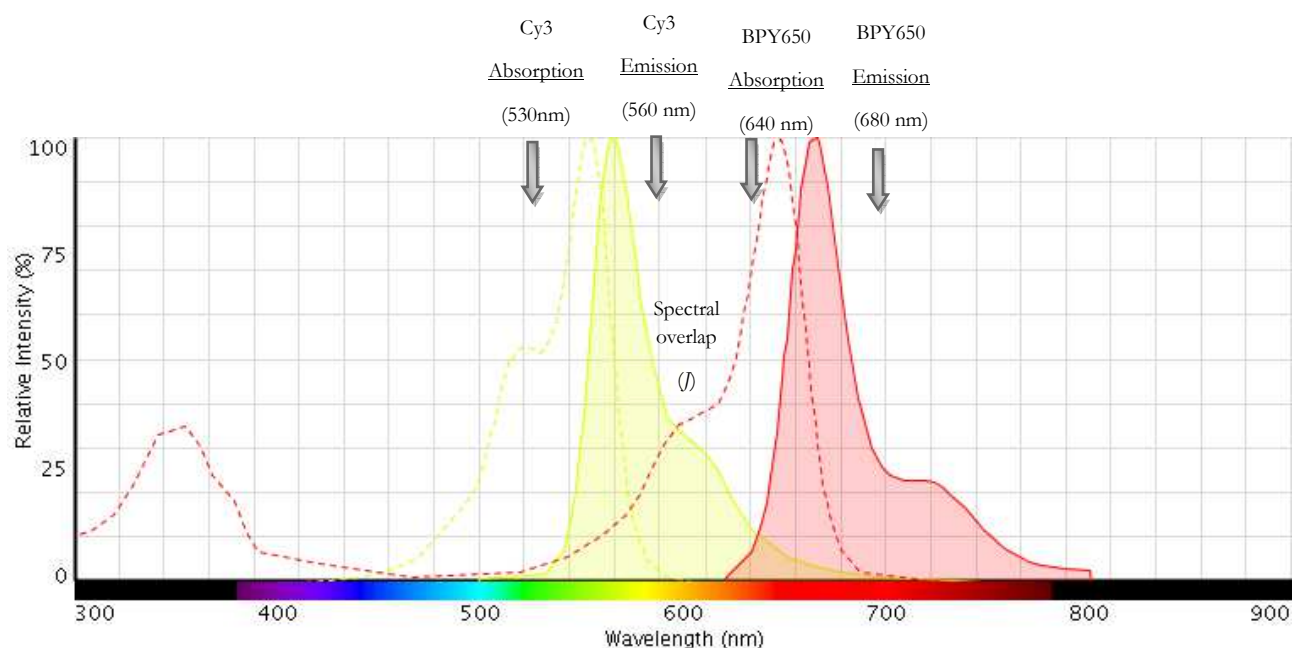


Figure 6. Absorption-Emission and spectral overlap of Cy3/BPY650 fluorophore pairs

measured by the use of a fluorescence spectrometer. Notice that the FRET phenomena will happen just when the two fluorophores are close enough to create the energy transfer, so, when the structure is in the closed state.

Until now, we have designed and described the basic elements to construct our functional pH dependent DNA nanostructure, to avoid confusion we called “TFO”. However for experimental necessities, it is important to have some control structures in the way to corroborate, by comparison, its effective assembly, response and performance. For this purpose, we design two controls; a positive, called post-close (PC) and a negative one, called non TFO (nTFO). The conformation and design of them are described as follow:

1. Positive control (PC). This open structure is represented in **Figure 7a**. In this design we use the same Str.1, Str.2 and REP oligonucleotides in the same conformation and positions as in the “TFO” structure. However the long strand (TFO) oligonucleotide is modified; instead of using 60nt- long term we use 46-nt (now called PC) where the 14 nucleotides of the 5’ end were removed from the original long strand TFO sequence and replaced in the 14-nt, 3’ ending of the PC long strand. The objective for this replacement is that now these D” 14-nt of PC will form a duplex, closing the structure, with the complementary 20-nt of the “d” sequences in

Str.2. The formation of the duplex between PC long strand and Str.2 happens following the same conditions as the normal Watson-Crick base pairing (G-C and A-T); this means, a normal annealing without effect of pH. As a positive control, experimentally, we expect that its electrophoretic mobility in PAGE gel will be different than the normal TFO; also, the structure will remain unchangeable to any pH variation; even, since it is a closed structure, the fluorophore pairs are close each other, that we must notice the FRET effect in all the cases.

2 Negative Control (nTFO), Figure 7b. As the previous one, we maintain Str.1, Str.2 and REP oligonucleotides but in this case, as a comparison to the normal long strand TFO sequence, we completely modify the last D' subsegment 14-nt at the 3' ending position, so they do not represent a triplex-forming oligonucleotide. With this modification, the triplex helix conformation is not formed when the pH changes, this means that the structure will remain always open. As a negative control, experimentally, we expect a different electrophoretic mobility between PC and TFO structures, both in acidic and basic conditions; also, since the structure remains open in any pH environment, fluorophores are apart from each other, leading to the lack of the FRET phenomena.

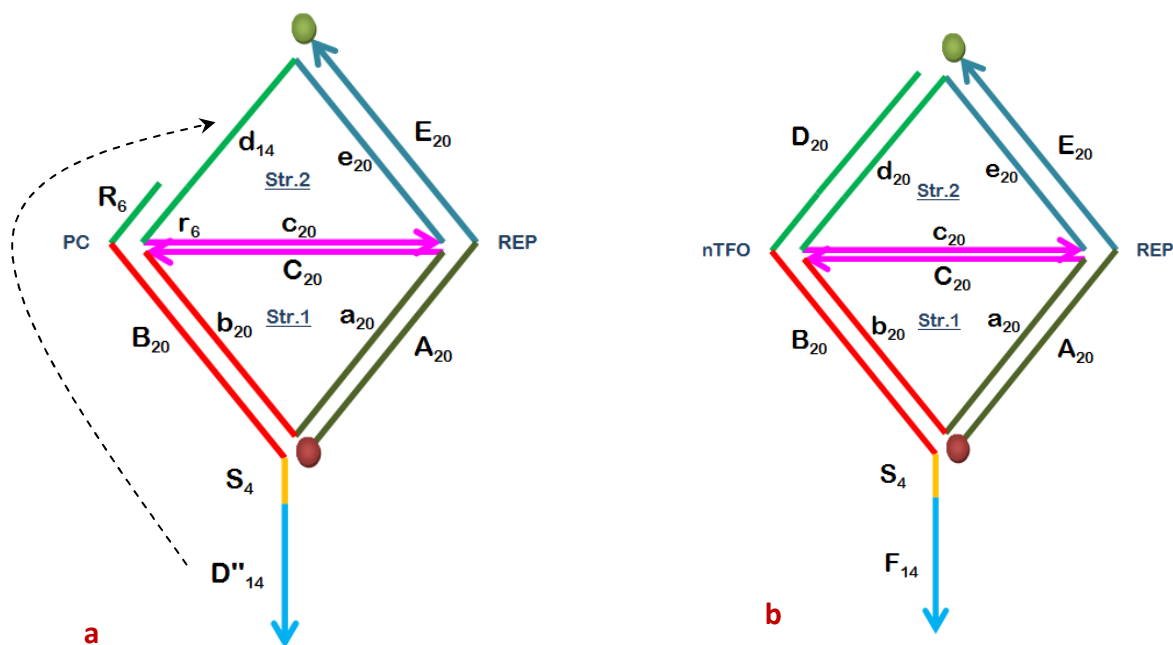


Figure 7. Scheme of the open structure of, a) positive control (PC) and b) negative control (nTFO)

4.2 The Nucleic-Acid Sensitive Nanostructure

4.2.1 The idea

The development of our second nanostructure comes from the anticancer therapeutic agents research context, such as immunotherapy, chemotherapy, and irradiation, that mediate their effects by induction of apoptosis of the cancer cells. It has been proved that there are three major apoptotic pathways originating from three separate subcellular compartments: they have been identified as the death receptor-mediated pathway, the mitochondrial apoptotic pathway, and the endoplasmic reticulum pathway [13]. In the mitochondrial apoptotic pathway, there is a particular family of proteins called Bcl-2 that have been appointed to play an important function to preserve the integrity of the outer mitochondrial membrane by binding to mitochondrial pore channels. [14] Some members of the Bcl-2 family, such as Bcl-2 and Bcl-xL, are potent inhibitors of apoptosis, whereas other family members, such as Bak and Bax, promote apoptosis. During the cellular apoptotic cycle, it was tried out that Bax translocate to mitochondria, changes conformation and inserts into membranes. In response to proapoptotic stimuli, Bax or Bak effect the permeabilization of the outer mitochondrial membrane, allowing proteins in the mitochondrial intermembrane space, such as cytochrome c, to escape into the cytosol where they can induce caspase activation and cell death [15].

On the other hand, staurosporine, is a protein kinase inhibitor, that has been characterized as a strong inducer of apoptosis in many different cell types. One possible mechanism is generally believed that the mitochondrial apoptotic pathway plays a critical role in staurosporine induced apoptosis [16,17]. Some studies found that Bcl-2 family overexpression was ineffective in protecting cells from killing by staurosporine. This means that the Bax expression is induced by the presence of Staurosporine, allowing the activation of members of the caspase family leading to a faster cell death. BAX protein has been reported to be localized in the mitochondria, endoplasmic reticulum membrane and cytoplasm, it is transcribed by the messenger RNA (mRNA) to produce the protein.

From the previous idea, we started with the design of a DNA nanostructure that could evidence the emergence of RNA in the cell, thus, working as a local in situ biosensor for transcription of BAX. We needed a model in which we could identify the transcription of BAX by RNA allowing to the detection of apoptosis in the cell. This

means, we need a BAX sequence present in our structure that has to be complementary to the sequence of the BAX RNA transcript, so to bind it if they come in contact with it. We will use staurosporine to induce the expression of BAX RNA in the cell. A way to detect the binding of our BAX sequence in the structure to the BAX sequence in the cell can be followed by the detection of a signal coming from our structure, for example FRET, done by the presence of the fluorophore pairs in our design.

4.2.2 The model

The design of our second structure was based on the previous TFO model. Here, we maintained the same Str.1 and Str.2 oligonucleotides, to supply the support and stiffness of our structure, as was described before. Also we kept the REP oligonucleotide with its respective Cy3/ BPY650 fluorophore pairs, exactly in the same position as the TFO structure, allowing us the detection inside the live cell and its response by the means of FRET measurement. The only oligonucleotide which has to be modified to provide the functionality as a sensor is the long strand. The deduction of the sequence strand and its conformation was done following the next steps:

The original BAX gene protein sequence was obtained from the literature, and then we proceed with the selection of nucleotides that will be part of our strand in the structure. This selection was done computationally by the use of software like NANEV and NUPACK (see sections 2.2.1-2 for details) where the key parameter for this evaluation was to choose the optimal melting temperature (T_m), which refers to the temperature at which the oligonucleotide, in our strand, is 50% annealed to its exact complement in the transcribed BAX. After a series of calculus and thermodynamic optimization parameters we have determined that a strand of 25 nucleotides divided in two spaced sequences of 10 nt (10nt + 5 gap + 10nt) are enough to find the correct recognition of the BAX transcribed sequence. However, with the aim to experimentally optimize the recognition and satisfying the T_m requirements we have designed two types of segments, one with two tails of 10-nt and other with two tails of 15-nt being part of the ending positions, 3' and 5', in the long strand. Thereby, with the already established oligonucleotides, Str.1, Str.2 and REP we introduce the fourth strand, which we called BAX. Therefore, we have designed two DNA tetrahedrons, that we identify according to the BAX length strand, the TT:BAX10 and TT:BAX15 structures, see **Figure 8**.

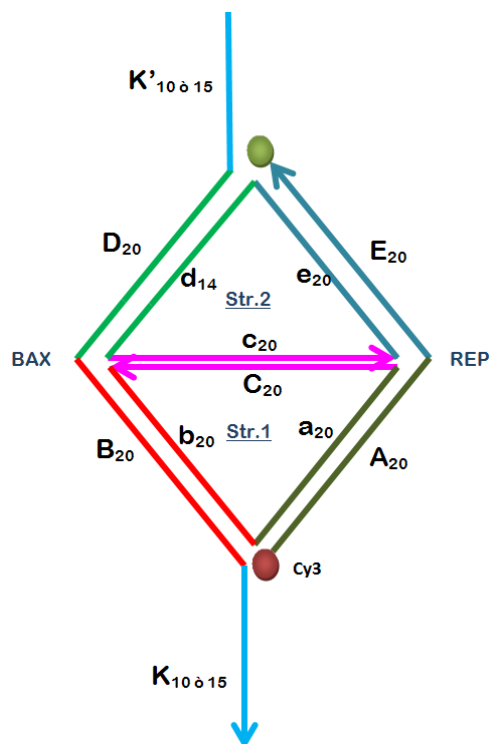


Figure 8. Scheme of the DNA tetrahedron BAX (TT:BAX) design where K could be 10 or 15-nt.

The BAX15 oligonucleotide is a long 71-mer divided in 4 segments (the "long" strand in Fig. 8). The "D" and "B" 20 –nt , in green and red respectively, are assembled with the complementary "d" and "b" strands of the Str.2 and Str.1 respectively; while at the 3' and 5' endings remain the unpaired 15-nt, in light blue. On the other hand, the BAX10 is a long sequence of 61-nt divided also in 4 segments, where "D-d" and "B-b" anneal with the Str.1 and Str.2 as indicated, remaining two 10-nt unpaired at the 3' and 5' endings.

In our design, we have established that both TT:BAX10 and TT:BAX15 must detect the cellular transcriptd BAX:RNA in the course of apoptosis; when this identification happens, our structure must change in conformation, bringing the two ending tails from an open to a closed state; in this shift also the CY3 and BPY650 fluorophores get in proximity leading to the FRET phenomena when Cy3 is excited, **Figure 9**. Thereby, experimentally we need an additional series of targets to simulate the gene recognition and measure the FRET efficiency. We have said that a strand of 25 nucleotides divided in two spaced sequences of 10 nt is suitable to find the correct recognition of the BAX transcript sequence. However, with the aim to test the precise length at which both strands close the structure we use a series of targets of different hybridization lengths (10 or 15) at different gaps (1,3,5).

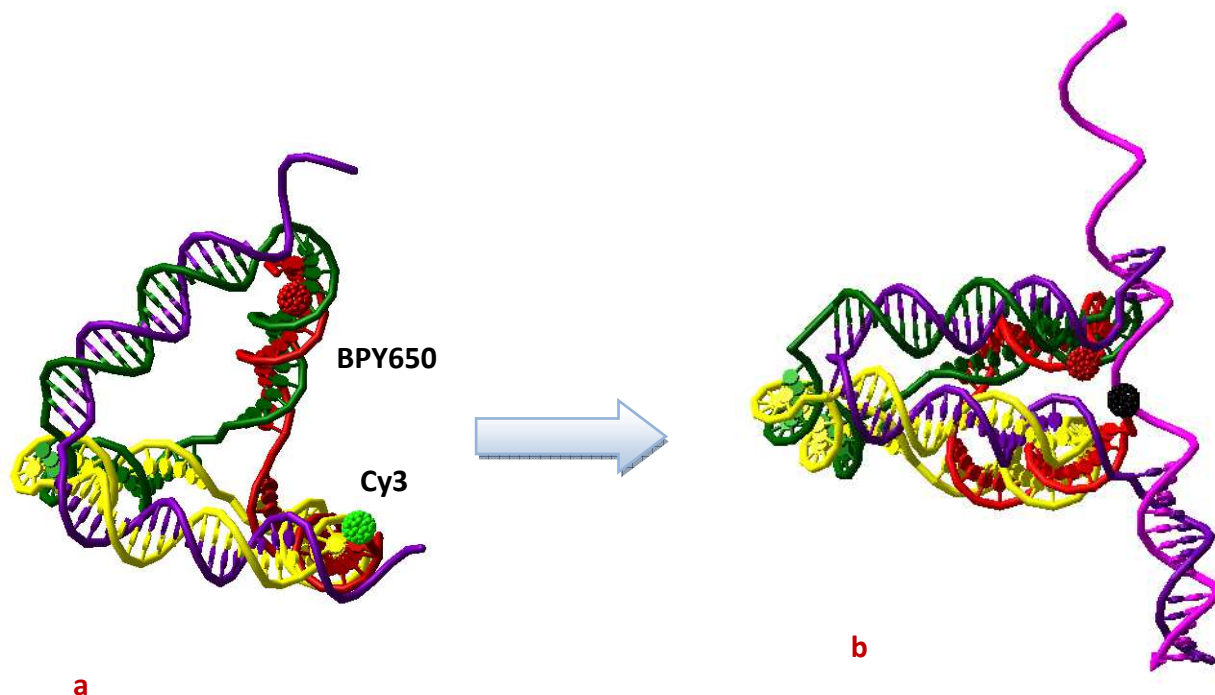


Figure 9. 3D molecular model of a) the DNA tetrahedron BAX targeting sensor, open state and b) targeted to the transcribed BAX:RNA, closed state [models done with NanoEngineer (Nanorex, Inc.)]

The definition of the appropriate targets was done computationally with NANEV and the Vienna RNA package in order to define a target sequence possibly devoid of a stable secondary structure that could interfere with probe-binding. The full list of nucleotide sequences are given in **Table 1**.

5 The Sequence Design

Once we have designed the position and requirements of each oligonucleotide at the corresponding structures, the next step is the deduction of the sequences of (single-stranded) ssDNA molecules in our models. To achieve this aim we used some particular software packages specialized in the design of nucleic-acids based nanostructures. Some of the more commonly used programs are SEQUIN [18], sequence symmetry minimization algorithm; UNIQUIMER[19]; GIDEON [20]; NANEV [21], from the Turberfield group and the online NUPACK [22]. For our structures, we used these last two software packages. A brief description and how we used them are presented in this section:

5.1 NANEV

The interface for NANEV uses subsequences as the building blocks for nanostructures design. A subsequence in the context of the NANEV interface, is understood as the section of a DNA strand designed either to hybridize with a complementary subsequence or remain unpaired in the final construct. To design a nanostructure, first we have to input the connectivity rules of the wanted nanostructure including the number of strands involved, their component sequences, and any desired complementarity rules. The program outputs strands of DNA, that have subsequences that are constrained to be complementary, determining the pattern of hybridization. In other words, the program generates a population of parent strands whose sequences are randomly assigned that obey any specified complementary rules [21].

For our two structures, to generate the parent strands from the specific base sequences for each particular desired oligonucleotide, by the use of the NANEV program, we follow the following general steps:

- a) Introduce parameters, names and number of strands, as described in the model (the pH dependent: Str1, Str2, REP, TFO, PC and nTFO; BAX-RNA: Str1, Str2, REP, BAX10, BAX15).
- b) Introduce the oligonucleotide length (Str1 (62-nt); Str2 (62-nt); REP (41-nt); TFO (60-nt); PC (46-nt); nTFO (60-nt); BAX10 (61-nt); BAX15 (71-nt).
- c) Introduce fixed subsequences that will be maintained in the final design (like the TFO sequence).

Each of these operations was done for every particular structure described previously. In the end of our calculations we obtained a series of base sequences for each desired oligonucleotide (**Tables 1 and 2**).

5.2 NUPACK

NUPACK is focused on the analysis and design of nucleic acid secondary structure for systems involving one or more species of interacting strands. Some notable features include:

- a) Analysis: Thermodynamic analysis of dilute solutions of interacting nucleic acid strands.
- b) Design: Sequence design for complexes of nucleic acid strands intended to adopt a target secondary structure at equilibrium.
- c) Utilities: Evaluation, display, and annotation of equilibrium properties of a complex of nucleic acid strands.

For our purposes, after the full sequences obtained by NANEV for each oligonucleotide, we used the analysis mode of the on-line software NUPACK to corroborate their suitable thermodynamic assembly and stability in a secondary structure at equilibrium. For the calculation we followed the next steps:

- a) Establish the components and conditions of the solution of interest: RNA or DNA (pick DNA), temperature or range of temperatures for melts (37°C), number of strand species (4), for each of our designed structures-, maximum complex size (all ordered complexes with up to this number of strands will be included in the analysis)-only one for each structure-, strand sequences (those obtained by NANEV), strand concentrations (for calculations with maximum complex size greater than one).

Once we fit all the parameters from the previous analysis we use the design mode to corroborate the formation of the secondary structure through the next steps:

- b) Specify design requirements DNA nucleotides: temperature (37°C), number of independent sequence designs (1), target secondary structure – it comes from the evaluation given by the analysis mode-. Target secondary structures that are multi-stranded must be connected.

All those calculations determined a success quantitative hybridization at optimized melting temperatures. It means from these results we corroborate the full list of our sequences nucleotides for the construction of our structures (**Tables 1 and 2**).

Table 1. Series of oligonucleotide base sequences for both nanostructures

Strand	Oligonucleotide sequences for the pH sensor nanostructures				
Str.1	a(20)	b(20)	c(20)		
	TATCGTTGTA CTTACGAGCCA TATTGATTTAGCGGGT CCGA GATCGCTAATGAGGCCAGCG				
Str.2	r(6)	d(14)	e(20)	c(20)	
	TTGCGG TTCTTTTCTTTCTT ACTGTACGGACAGCACCTGGCA CGCTGGCCTCATTAGCGATC				
REP	A(20)		E(20)		
	CY3- GGCTCGTAAGTACAACGATAAGCCAGGTGCTGTCCGTACAG -BPY650				
TFO	D(14)	R(6)	B(20)	S(5)	D'(14)
	AAGAAAAGAAAAGAA CCGCAA A CCGACCCCGCTAAATCAATAGAAA ATTCTTTCTTTTCTT				
PC	r(6)	B(20)	S(5)	D''(14)	
	CCGCAA A CCGACCCCGCTAAATCAATAGAAA AAGAAAGAAAAGAA				
nTFO	D(14)	r(6)	B(20)	S(5)	F(14)
	AAGAAAAGAAAAGAA CCGCAA A CCGACCCCGCTAAATCAATAGAAA TGAAAGAGAGAATA				
Oligonucleotide sequences for the nucleic-acid sensor nanostructures					
Str.1	a(20)	b(20)	c(20)		
	TATCGTTGTA CTTACGAGCCA TATTGATTTAGCGGGT CCGA GATCGCTAATGAGGCCAGCG				
Str.2	r(6)	d(14)	e(20)	c(20)	
	TTGCGG TTCTTTTCTTTCTT ACTGTACGGACAGCACCTGGCA CGCTGGCCTCATTAGCGATC				
REP	A(20)		E(20)		
	CY3- GGCTCGTAAGTACAACGATAAGCCAGGTGCTGTCCGTACAG -BPY650				
BAX10	K(10)	D(20)	B(20)	K'(10)	
	CAGTTCGTCCAAGAAAGAAAAGAACCGCAA A CCGACCCCGCTAAATCAATAGATGCGCTTG				
BAX15	K(15)	D(20)	B(20)	K' (15)	
	CTGTCCAGTTCGTCCAAGAAAGAAAAGAACCGCAA A CCGACCCCGCTAAATCAATAGATGCGCTTGAGACA				

[Colors and letters correspond to the same order as in designs **Fig. 3, 7a -b, 8**. In brackets are the number of base pairs for each sub-strand]

Table 2. Oligonucleotide base sequences for targets, and clip strands

Target	Target nucleotide sequences
15-1-15	TGTCTCAAGCGCATCAGGACGAACTGGACAG
15-3-15	TGTCTCAAGCGCATCAAAGGACGAACTGGACAG
15-5-15	TGTCTCAAGCGCATCAAAAAGGACGAACTGGACAG
10-1-10	CAAGCGCATCAGGACGAACTG
10-3-10	CAAGCGCATCAAAGGACGAACTG
10-5-10	CAAGCGCATCAAAAAGGACGAACTG
8-1-8	AGCGCATCAGGACGAAC
8-3-8	AGCGCATCAAAGGACGAAC
8-5-8	AGCGCATCAAAAAGGACGAAC
Half Trg 15a	TGTCTCAAGCGCATC
Half Trg 15b	GGACGAACTGGACAG
Clip.0-nt	CTTACGAGCCCTGTACGGAC
Clip.2-nt	CTTACGAGCCAACCTGTACGGAC

References Part II

- [1] R.P. Goodman, I.A.T. Schaap, C.F. Tardin, C.M. Erben, R.M. Berry, C.F. Schmidt, A.J. Turberfield, *Science* **2005**, 310.
- [2] R.P. Goodman, R.M. Berry, A.J. Turberfield, *Chem. Commun. (Camb.)* **2004**, 1372–1373.
- [3] K.R. Kim, Y.D. Lee, T. Lee, B.S. Kim, S. Kim, D.R. Ahn, *Biomaterials* **2013**, 34; 5226–5235.
- [4] H. Lee, A.K.R. Lytton-Jean, Y. Chen, K.T., et al., *Nat. Nanotechnol* **2012**,. 7: 389–393.
- [5] K.R. Kim, D.R. Kim, T. Lee, J.Y. Yhee, B.S. Kim, I.C. Kwon, D.R. Ahn, *Chem. Commun.*2013, 49: 2010–2012.
- [6] Alberti, P. & Mergny, J.-L *Proc. Natl Acad. Sci. USA.***2003**, 100:1569–1573.
- [7] Benenson, Y., Gil, B., Ben-Dor, U., Adar, R. & Shapiro, E. *Nature* **2004**, 429:423–428 (2004).
- [8] Modi, S. et al. *Nature Nanotech.***2009**, 4: 325–330.
- [9] Souvik M, Swetha MG, Debanjan G, Gagan DG, SatyajitM, Yamuna K. *Nat Nanotechnol* **2009**, 4:325–330
- [10] Surana S, Bhat JM, Koushika SP, Krishnan Y *Nat Commun* **2011**, 2:340
- [11] Bergamini C., Angelini P., Rhoden K.J., Porcelli A.M., Fato R., Zuccheri G. *Methods* **2014**, 67:185–192
- [12] M. Brucalè, G. Zuccheri, B. Samori, *Trends in Biotechnology* **2006**, 24, 235.
- [13] Debatin KM, Poncet D, Kroemer G. *Oncogene* **2002**, 21:8786–803.
- [14] Shimizu S, Narita M, Tsujimoto Y. *Nature* **1999**, 399:483–7.
- [15] Liu X, Kim CN, Yang J, Jemmerson R, Wang X. *Cell* **1996**, 86:145 –57.
- [16] Tafani M, Minchenko DA, Serroni A, Farber JL. *Cancer Res* **2001**, 61:2459–66.

- [17] Tafani M, Cohn JA, Karpinich NO, et al. *J Biol Chem*, **2002**, 277:49569–76.
- [18] N. C. Seeman, *J Biomol Struct Dyn* **1990**, 8, 573.
- [19] B. Wei, Z. Wang, Y. L. Mi, *Journal of Computational and Theoretical Nanoscience* **2006**, 3.
- [20] J. J. Birac, W. B. Sherman, J. Kopatsch, P. E. Constantinou, N. C. Seeman, *J Mol Graph Model* **2006**.
- [21] Goodman R.P. *Biotechniques* **2005**, 38:548-550.
- [22] <http://www.nupack.org/> [May **2014**]
- [23] Sobey T.L., Simmel F.C., *Methods Mol. Biol.* **2011**, 749:13–32.
- [24] Gorman A., McCarthy J., Finucane D., Reville W., in: T.G. Cotter, S.J. Martin (Eds.), *Techniques in Apoptosis: A User's Guide*, Portland Press, London, 6–7, **1996**.

PART III

Methods for Synthesis and Characterizations

Methods for Synthesis and Characterizations

6 Experimental Synthesis

6.1 Annealing DNA Strands to Self-Assemble DNA nanostructures

As was described in the previous chapter, the formation of hydrogen bonded DNA complex is a self-assembly process. This happens when the DNA strands are mixed at stoichiometric molar ratio in a near-neutral buffer containing divalent cations (usually Mg^{2+}), heated to denature and then gradually cooled to allow the ssDNA molecules to find their correct partners and adopt the most energy-favorable conformation.

The list of oligonucleotides in Tables 1 and 2 were purchased from Eurofin/MWG (Germany), HPLC purified and dissolved in deionized water. The annealing was done following the further general steps.

- a) Addition of stoichiometric amounts of DNA strands into a PCR tube. Addition of $10\times$ TEM/ Mg^{2+} buffer (50 mM Tris, 5 mM EDTA, 20 mM $MgCl_2$, pH 8.0) and distilled H₂O to adjust the final concentration of each DNA strand, usually ranging from 100 nM to 500 nM, we used 500 nM in all the cases.

b) This mixture is then heated on a PCR thermocycler (PCR Sprint, Thermo Electron Corp., Waltham, MA, U.S.A.). Temperature was raised to 95°C for 2 min to melt any possible structure and ensure that no intrastrand secondary structure is still present when the assembly begins. Then, temperature was lowered to 20°C over 20 min (for immediate use or for characterizing the structure of the constructs at 20 or 37 °C).

A more detailed step-by-step guide to assembling DNA nanostructures can be found in [1]

6.2 Non-denaturing PAGE for the Characterization of Self-Assembled DNA Nanostructures

Non-denaturing polyacrylamide gel electrophoresis (PAGE) is an effective assay to characterize the assembly of DNA nanostructures. It works in response to a voltage applied across the gel –done by agarose or polyacrylamide- and DNA-based materials separate according to the relative sizes of their hydrodynamic drag and effective charge. Well-formed DNA nanostructure should migrate as a single distinct band after electrophoresis. Non-denaturing PAGE also provides information regarding the degree of self-assembly formation (stoichiometry), the state of structural integrity, and the percentage functionalization of the DNA structure. In addition, gel electrophoresis benefits from being routine, fast, and cost-effective, the method only requires a few nanograms of material in order to visualize the band.

For our DNA assembled tetrahedrons, the correctness of the stoichiometry and the yield of self-assembly of the structure and substructures were evaluated by non-denaturing PAGE performed in a BioRad Protean II Midi Gel Box with 8% native polyacrylamide in TBE 1X buffer (90 mM Tris, 90 mM boric acid, 2 mM EDTA, pH 8) in most of the cases. However, for particular experiments, the running buffer solution was modified or adjusted according to our requirements; each modification is described through the results section. All the detailed procedure to perform a PAGE that we followed can be found in [1]. The gel was run at constant voltage 180 V (5 V/cm) for 2-3 h depending on the size of the interested DNA complexes. We also run it at controlled temperature; ranging from 20 to 37 °C depending on the complex and particular

requirements. Then, the gel was stained with SybrGold (Invitrogen) and finally documented with a digital camera (Gel Doc 1000, BioRad, Hercules, USA).

7 Characterization of Nanostructures

7.1 Spectroscopic and Optical Microscopy Characterizations

7.1.1 Fluorescence Spectroscopy

Fluorescence has provided remarkable advances in DNA biotechnology. Fluorescence methods are now used for DNA sequencing, detection of DNA hybridization, restriction enzyme fragment analysis, and fluorescence in-situ hybridization (FISH), and to detect polymerase chain reaction products. This technique is generally done in solution and provides a good in vitro reflection of certain key properties when required.

7.1.1.1 Quenching or FRET Interactions

Many dyes and NP materials can act as fluorescence quenchers or FRET acceptors and the ability of DNA to assemble complex nanostructures incorporating these materials has led to elegant “molecular beacon” nanosensors [2-4]. Fluorescence resonance energy transfer (FRET) has become widely used in all applications of fluorescence, including medical diagnostics, DNA analysis, and optical imaging. FRET is an electrodynamic phenomenon that occurs between a donor dye or chromophore that initially absorbs the energy and the acceptor is the chromophore to which the energy is subsequently transferred. The donor molecules typically emit at shorter wavelengths that overlap with the absorption spectrum of the acceptor. Energy transfer occurs without conversion to thermal energy, and without any molecular collision; this is the result of long range dipole–dipole interactions between the donor and acceptor. The theory of energy transfer is based on the concept of a fluorophore as an oscillating dipole, which can exchange energy with another dipole with a similar resonance frequency. The transfer of energy leads to a reduction in the donor’s fluorescence intensity and excited state lifetime, and an increase in the acceptor’s emission intensity.

In terms of vibrational energy levels, the donor is excited from the ground state (S_0) to a higher vibrational level; within picoseconds, the molecule decays to the lowest excited vibrational levels (S_1) and eventually could happen that: a) if there are not FRET conditions, this molecule goes back to the S_0 state and a photon of light is emitted, or b) if FRET conditions are present, the donor's energy in the excited state is transferred to the acceptor molecule, allowing its excitation, in a while this molecule returns to the ground state and emits a photon (**Figure 1**).

Some of the factors that influence the FRET phenomena. The donor and acceptor molecules must be in close proximity to one another (typically 10-100 Å). The fluorescence emission spectrum of the donor must overlap the absorption spectrum of the acceptor (**Figure 6, part II**). The degree to which they overlap is referred to as the spectral overlap integral (J). The donor and acceptor transition dipole orientations must be approximately parallel.

FRET experiments were performed on a LS-50B fluorescence spectrometer (Perkin Elmer, Boston, USA) in a 3 ml quartz cuvette equipped with a magnetic microstirrer and heater to keep a constant temperature- depending of our particular characterization- We followed several methodologies according to the purposes of each structure:

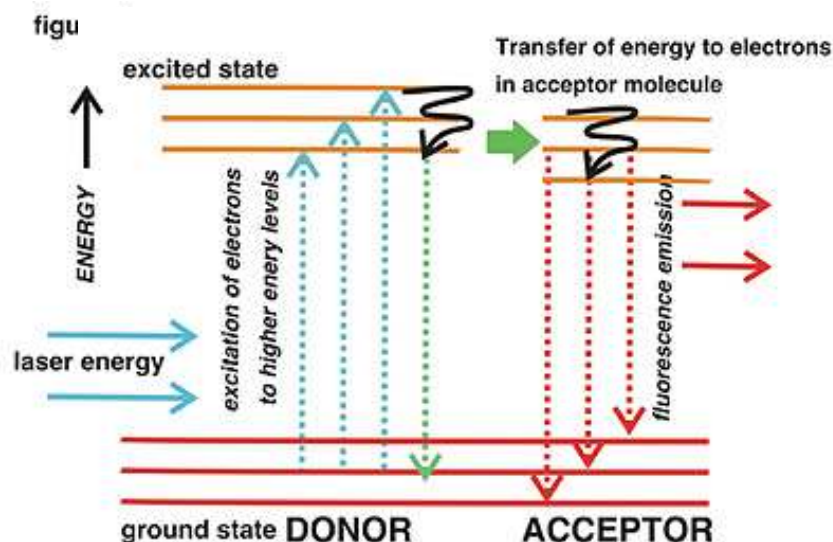


Figure 10. The FRET phenomena process described in vibrational energy levels

- a) The REP strand with their Cy3/BPY650 fluorophore pairs was characterized, taking 10 nM of the oligonucleotide in TEM 1X buffer into a quartz cuvet with magnetic microstirrer at room temperature; direct excitation both donor and acceptor, slit aperture, rate of acquisition were determined. The FRET response was done by the addition, to the REP strand solution [10 nM], of stoichiometric amounts, at interval times, of the “closing reporter” Clip at 0 and 2 nucleotides in aperture (see **Table 2** for their oligonucleotide base sequences).
- b) TT:BAX characterization. To determine its sensing response by the FRET phenomena, we used 20 μ L of the fully assembled nanostructure [50 nM] in 180 μ L of the TEM 1X (in some cases, we also use other buffer solutions – composition is presented in each experiment at the results section-). Some measurements were done at room temperature or at 37°C, according to our particular requirements. Titrations were done by the addition of stoichiometric amounts, at regular times, of the target oligonucleotides in conditions where: a) the length target strands with the same gap were alternated and b) the gap between each target of the same arrays was amended. Determination of the equivalent point was done, following the intensity peak behavior both the CY3 and BPY650 at their maximum emission point.
- c) The pH tetrahedron characterization. To determine its sensing ability we also used 20 μ L of the fully assembled tetrahedron [50 nM] in a buffer solution; for this case, the buffer is a key parameter for its sensing response, we used several types of solution according to our requirements – compositions for each experiment are presented through the result section- Measurements were done both at room temperature or at 37°C. Titrations of each nanostructure were performed by the addition of acidic or basic solutions, of known concentration, to the solution with the tetrahedron; recording the intensity of the maximum emission peak of CY3 at each pH value. The evaluation was done by the design of a repeatedly cyclic titration, from basic to acidic and inversely

7.2 Fluorescence Microscopy

The technique of fluorescence microscopy has become an essential tool in biology and the biomedical sciences, due to attributes that are not readily available in other contrast modes with traditional optical microscopy. The application of an array of fluorochromes has made it possible to identify cells and sub-microscopic cellular components with a high degree of specificity amid non-fluorescing material. Moreover, the fluorescence microscope is capable of revealing the presence of a single molecule. Through the use of multiple fluorescence labeling, different probes can simultaneously identify several target molecules simultaneously. Although the fluorescence microscope cannot provide spatial resolution below the diffraction limit of specific specimen features, the detection of fluorescing molecules below such limits is readily achieved [5].

7.2.1 Imaging Rationale and Image Acquisition

Fluorescent microscopy was used to characterize the fluorescence of cells due to the internalization of the fluorescently-labeled tetrahedra over the intrinsic autofluorescence of live cells. Cellular autofluorescence is normally emitted by internal organelles such as mitochondria or lysosomes due to the presence of autofluorescing molecules like NADPH (phosphates) and flavins. However, it represents an obstacle for the acquisition of the fluorescence tetrahedra. Autofluorescence has a wide band emission spectrum, with some non-negligible emission at long wavelength even if excited at short wavelengths, this should be relatively independent of the emission of an extrinsic fluorophore. For this reason, we recorded the fluorescence emission at the peak wavelength of the oligonucleotide-bound fluorophore twice: when exciting at its correct adsorption peak and off-peak (at lower wavelength) where the excitation of the fluorophore is minimal. Fluorescence from off-peak excitation should only be due to autofluorescence, while one portion of the on-peak fluorescence should be due to autofluorescence and the rest to the oligonucleotide-bound fluorophore (if internalized). In this way, we can compare the on-peak and off-peak fluorescence intensities of individual cells; it could be possible to distinguish fluorophore-related fluorescence from intrinsic autofluorescence. This methodology was implemented previously in our group

[6]. However we have included a series of new measurement parameters according to our particular fluorophore dye pairs properties.

For each field of view, five different micrographs were acquired on a Nikon Eclipse 80i microscope equipped with a monochromatic cooled CCD camera and a mercury lamp, we use the NIS-Elements, version F. 3.0 Imaging Software. Micrographs we acquired with 2X binning in the following five fields of view, with the corresponding filters.

i) Transmitted light. White-light transmission micrographs were obtained using a single exposure time (60ms), in order to delineate its contours, to obtain information on the morphology of cells, their correct adhesion to the substrate and, consequently, their health status.

ii) Off-peak (Autofluorescence) was acquired at an emission wavelength of 488 nm, exciting at 405 nm, using filter at 488 nm (bandwidth 20 nm) for excitation, 530 nm (bandwidth 30 nm) for emission and a 525 nm dichroic mirror.

iii) On-peak (Cy3) was also acquired at an emission wavelength of 488 nm, exciting at 515 nm, using filter at 535 nm (bandwidth 36 nm) for excitation, 590 nm (bandwidth 34 nm) for emission and 525 nm dichroic mirror.

iV) BPY650 fluorescence was acquired using common Cy5 filter set, at an emission wavelength of 647 nm in excitation at 650 nm, using filter at 645 nm (bandwidth 30 nm) for excitation, 660 nm (bandwidth 40 nm) for emission and a 650 nm dichroic mirror (all filters from Omega Optical, Inc.).

Fluorescence micrographs were obtained using a single exposure time of 2 s. Also, to obtain a good quantitative evaluation of the cells' fluorescence, series of micrographs for at least 4 fields of view were acquired for each specimen.

7.2.2 Semiautomatic Analysis of Fluorescence Images

The analysis of our micrographs was based on the evaluation of their fluorescence intensity by turning them into quantifiable data by delimitating the areas, from their pixel intensities, occupied by each cell.

For practical reasons, we chose to write a custom-designed software tool to perform the semiautomatic analysis, using the Matlab software, measuring the fluorescence intensity (pixels) of defined areas in the image and be able to compare with

the other images under the same camera settings for all the filters (off-peak, on-peak Cy3, FRET and Cy5). The individual cell fluorescence data can be used to calculate (and statistically evaluate) each cell's average fluorescence and the standard deviation of the fluorescence of each cell's pixels, allowing to characterize the cellular distribution of fluorescence. The analysis was done through the following steps:

a) We delimited the area of a rectangular section form of 40 by 40 pixels, we use the same delimited are for all the measurements

b) We have taken three different sections in the fluorescent area of each cell and other three sections out of the cells; the background, within the same fixed area (as shown in **Figure 2**)

c) The program automatically does the analysis, the average value of each measurement with their respective standard deviation.

d) Same steps are repeated for the other cells in different field of view for each filter.

e) The quantitative fluorescence data was obtained by removing the fluorescence background to each image

We performed a series of statistically evaluations with the statically integral fluorescence and the standard deviation of the fluorescence data of ach cell to give an idea about the cellular distribution of fluorescence.

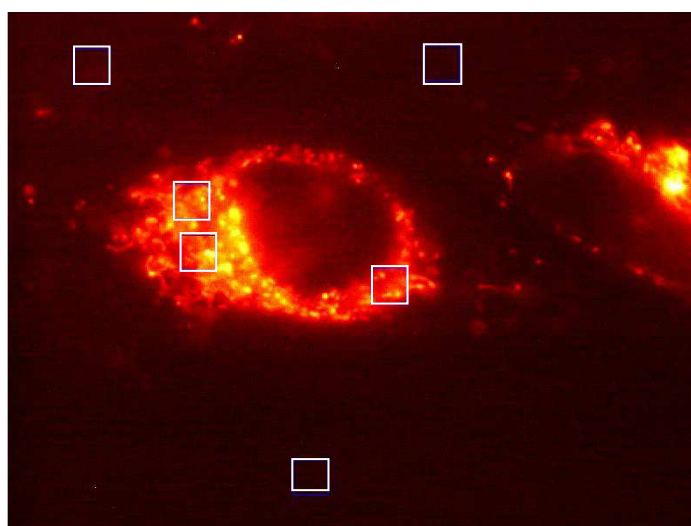


Figure 2. Selection of the fluorescent emission areas; the cells shape (40 by 40 pixels) and the background. [Micrograph of a neuronal cell treated with TT:PC structure].

8 Cell culture and nanostructure delivery to cells

There are two main routes how nanostructured biosensors can be used in live cells either by enabling the cells to synthesize modified proteins and nucleic acids that behave as biosensors, or by inserting in vitro prepared ones into live cells. In our case, we used the latter strategy that can be applied to any non-engineered cell line.

In our experiments to probe the in vivo internalization and delivery of our structures, we have used three different types of live cells; live human cells (HeLa cells), renal human cells (T-769P class) and Human glioma cells line T67 (neuronal). HeLa is a cell type in an immortal cell line extensively used in scientific research; the line is derived from cervical cancer cells; they are very malleable and robust. The T-769P class, are a type of human kidney carcinoma cell line, derived from a primary clear cell adenocarcinoma; the cells are globular with indistinct borders, have a high nucleus to cytoplasm ratio and exhibit both microvilli and desmosomes. Glioma cells (T67) are part of the most common tumors of the central nervous system (CNS) and a frequent cause of death.

Cells were cultured in DMEM high glucose (PAA, DASIT, Milan, Italy) supplemented with 2 mM L-glutamine, 10% (v/v) fetal bovine serum (FBS), 100 U/mL penicillin and 100 lg/mL streptomycin at 37 °C in humidified atmosphere with 5% CO₂ in Petri dishes. Culture medium was changed every 2 days and sub-confluent cells were split with 0.05% trypsin–EDTA solution.

Retained cells were washed with PBS (NaCl 137 mM, KCl 2.7 mM, Na₂HPO₄ 10 mM and KH₂PO₄ 1.8 mM at pH 7.4), separated with 0.05% trypsin–EDTA solution and centrifuged for 3 min at 300 g. The pellet was resuspended in DMEM medium and cells were counted by using trypan blue exclusion method [7]. Quickly, the cell suspension was incubated 0.4% trypan blue solution and the number of viable cells was determined using a hemocytometer. Then, a considerable amount of cells (approximately 5 X 10³) were deposited on custom chambers with glass bottom, in 100 μL of complete DMEM medium and incubated at 37°C in a humidified atmosphere with 5% CO₂. After 24 h, cells were washed with PBS and incubated with 50 μL of the annealed structure (previously dissolved in DMEM without FBS from their concentrated solution). In a typical experiment, we used (a) a blank, untreated cells incubated with DMEM; (b) TT:TFO, cells incubated with 100nM of the fully assembled structure, which contains the

TFO strand; (c) TT:PC, cells incubated with 100 nM of the fully assembled structure; (d) TT:nTFO, cells incubated with 100nM of the structure, that contains the non-TFO sequence; (e) TT:BAX15, cells incubated with 100nM of the structure that contains the BAX15 length sequence strand. Cells were incubated at 37°C in a humidified atmosphere with 5% CO₂ for 6 h. After this time, cells were carefully washed with PBS, later with 50 µL of PBS enriched with calcium and magnesium (NaCl 137 mM, KCl 2.7 mM, Na₂HPO₄ 10 mM, KH₂-PO₄ 1.8 mM, CaCl₂ 1 mM, MgCl₂ 0.5 mM, pH 7.4). Finally, chambers were mounted on the microscope stage for analysis.

References Part III

- [1] Sobey T.L., Simmel F.C., *Methods Mol. Biol.* **2011**, 749:13–32.
- [2] Cady NC. *Methods Mol Biol* **2009**, 544:367–379
- [3] Li Y, Zhou X, Ye D. *Biochem Biophys Res Commun* **2008**, 373:457–461
- [4] Wang K, Tang Z, Yang CJ et al. *Angew Chem Int Ed* **2009**, 48:856–870
- [5] <http://www.microscopyu.com> [May, 2014]
- [6] Bergamini C., Angelini P., Rhoden K.J., Porcelli A.M., Fato R., Zuccheri G. *Methods* **2014**, 67:185–192
- [7] Gorman A., McCarthy J., Finucane D., Reville W., in: T.G. Cotter, S.J. Martin (Eds.), *Techniques in Apoptosis: A User's Guide*, Portland Press, London, 6–7, **1996**.

PART IV

Results and Discussions

Results and Discussions

Through this part, I will describe and discuss the results of our two major DNA nanostructures. The first section describes the characterizations, for each structure, about their self-assembly and sensor responses. The second part, considering both structures simultaneously, includes the characterization about the cell uptake, delivery and localization inside live cells. The third part describes all the structural characterizations when one of the fluorophore pairs was replaced in the structure conformation; it also includes the previous studies for the in vitro functionality characterization of our structures. A practical definition of some abbreviations that I use through the next sections are given as follow:

TT or TET (Tetrahedron); Trg (Target); TT:Trg (the tetrahedron closed by a target); TT:BAX (Tetrahedron that contains either BAX 10 or 15 strand); TT:BAX10 (Tetrahedron that contains exclusively BAX10 length strand); TT:BAX15 (Tetrahedron that contains exclusively BAX15 length strand); BAX:RNA (the transcribed BAX gene by the mRNA inside the cell); TT:TFO, TT:PC and TT:nTFO (the tetrahedrons that contains the long strands TFO, PC and nTFO respectively). BAX15, BAX10, PC, TFO and nTFO (the single oligonucleotide without being part of the assembled structure)

9 The Nucleic-Acid Sensitive DNA Nanostructure

9.1 Characterization of the Self-Assembly DNA Nanostructure

In our first experimental design, to corroborate the effective annealing of the oligonucleotide sequences that shape our nanostructure we performed the PAGE technique. As a first trial, we assembled stoichiometrically (1:1) series of dimers, trimers and the two possible tetrahedrons; the annealing was done with variations between BAX15 and BAX10 strands with their corresponding complementary sequences strands, following the designed model (**Figure 6, Section 4.2.2**). Our assembly conditions were chosen to be similar to the original ones proposed by the Turberfield group [1, 2]. The gel image is shown in **Figure 1**.

By the use of PAGE gel as a qualitative technique, we obtained information about two important parameters, the successful assembly of our strands and the stoichiometry of them. First, following the basic principle of oligonucleotides separations in DNA by their size; larger subsets of the nanostructures display a progressively decreased electrophoretic mobility, due to an increase in dimension and complexity of the various DNA structures, while smaller ones move faster. The slowest band should be the fully assembled tetrahedron.

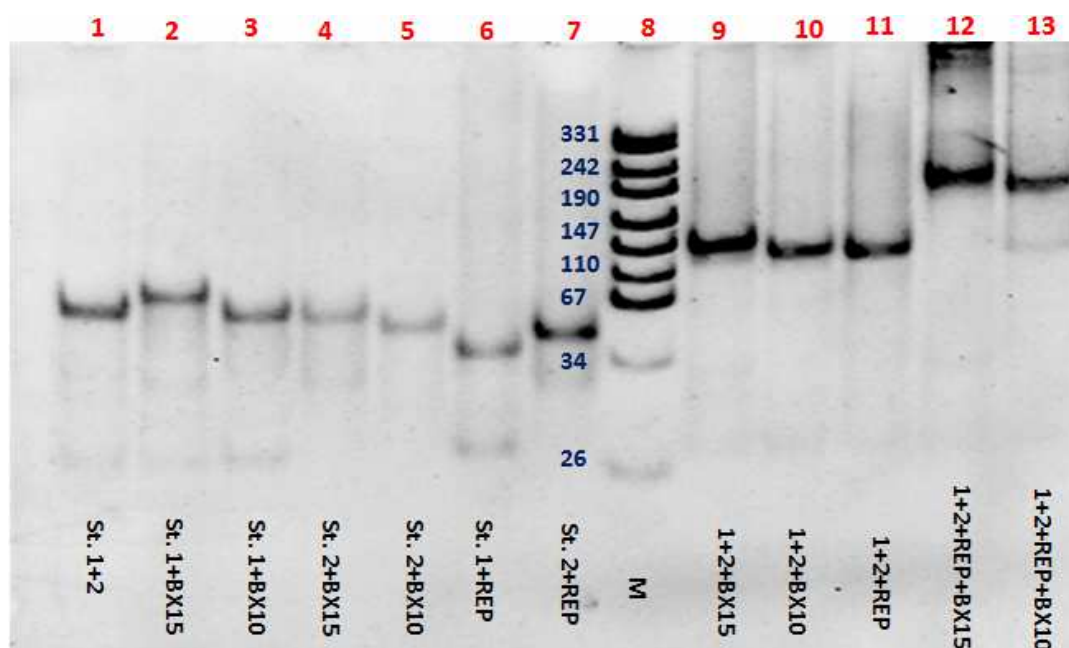


Figure 1. Annealing of dimers, trimers and tetrahedrons [25°C in normal TBE 1X running buffer]

(lanes 12 and 13) while the fastest corresponds to dimers (lanes 1-7) and trimers run at middle velocity (lanes 9-11). In addition, we can corroborate the size (in base pairs) of our DNA fragments by comparison with the bands of the reference ladder (M) -that contains a mixture of DNA fragments of know size- with the bands of our samples; the DNA size of each band in our samples is in correspondence with the size of the bands in the reference ladder. Thus, we confirm the successful assembly of our DNA nanostructure.

In our experiments as others in the literature, we sometimes notice the presence of high molecular-weight smears in the gels run at room temperature or lower [3]. These kinds of aggregates are present in a relatively large amount and migrate much slower than the tetrahedra only where more complex structures were run in room temperature or low temperature gels, especially for the lanes with all tetrahedron components. We interpret the presence of high molecular weight smears as non-specific cross-linking products that form, also possibly due to some imperfect local imbalance in the stoichiometry.

The second evidence that we can obtain from this PAGE image is that our oligonucleotides are not in stoichiometry balance due to the presence of a lightweight band at the bottom of almost all the lanes, thus we can say that they are probably the result of an excess of one or a few oligonucleotides and not due to degradation of the solution.

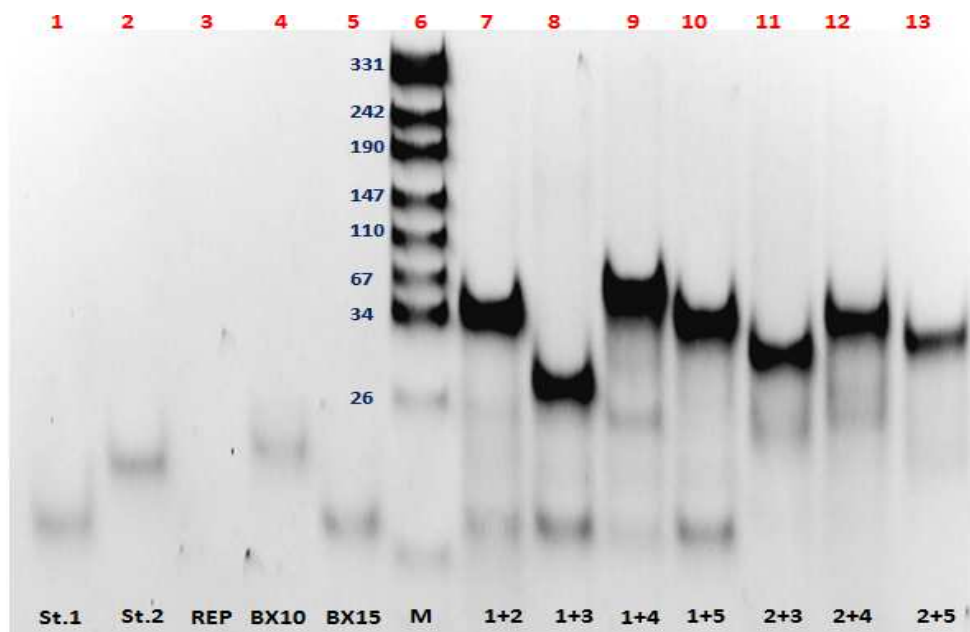


Figure 2. Comparison between monomers and annealed dimers [25°C in normal TBE 1X running buffer]

To find out which oligonucleotide was in excess, we performed another PAGE gel with the same conditions where only monomers and dimers were included. **Figure 2** describe this result.

Monomers (lanes 1-5) and dimers (lanes 7-13), are separated according to their expected electrophoretic mobility. However, the lanes with the dimers that contains Str.1 (lanes 7-10), there is still a remaining band at the bottom which is at the same length that the single Str1 (lane 1), while this band is not present in the dimers from the Str 2. Thereby Str1 is in excess. Notice that even the remaining band from Str1 is not the main (darker) band in each lane, we decided to correct its stoichiometry for the further analysis.

In order to ascertain an accurate stoichiometry, we have reduced 10 and 15% the concentration of Str1 in the same assembly conditions. Comparisons with this modifications are show in **Figure 3**.

With the modification in stoichiometries, it is noticed that decreasing 15% of Str1 in the dimer (lane 8), the remaining of the Str1 is much more lower in comparison with the dimer that contain 10% less of Str.1 (lane 7). From this result, we have decided to take 15% less of concentration of Str1 for the subsequent thermal assemblies.

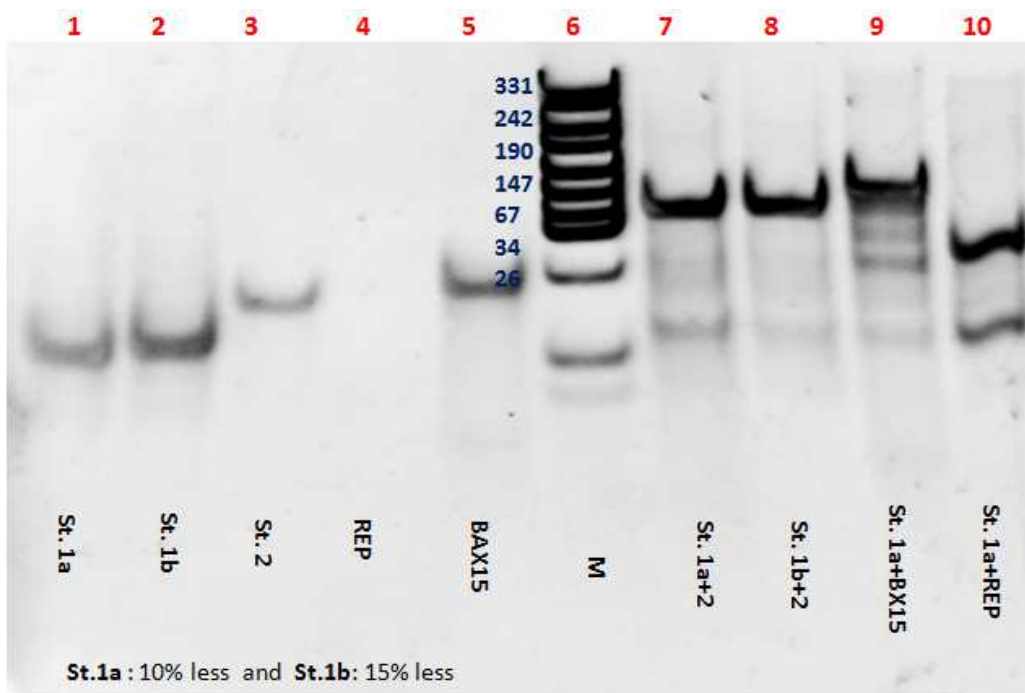


Figure 3. Monomers and dimers for the correction of stoichiometry [Room temperature in normal TBE 1X buffer]

In conclusion, from the PAGE gel technique we have probed the successful assembly of our DNA tetrahedron structure according to our designed model. In addition, it was helpful to identify which oligonucleotide was in excess and through this, the stoichiometry was adjusted.

9.2 Probing the Binding of Targets Sequences to TT:BAX Nanostructures

Following our approach design, we have proposed that to detect part of the functionality of our structure, first we need to be sure about the effective closing of the ending strands that contain the BAX oligonucleotide, for this purpose each target from the **Table 2** must, at least, theoretically attach to our BAX sequence strands in the tetrahedron. To confirm if experimentally this assumption works, we performed the annealing in one step of our four strands that form the structure and the series of targets, in variation both the length of the target and the gap binding to the BAX strand. in this probe BAX15 strand was first considered in the fully assembled structure. Figure below shows such behavior.

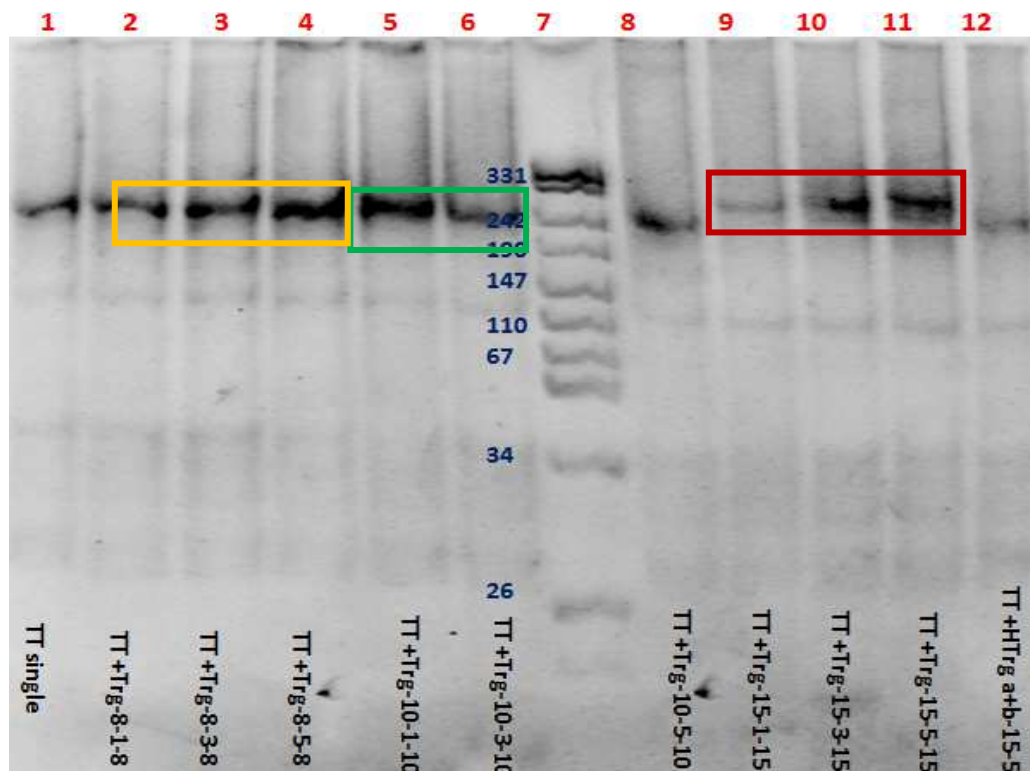


Figure 4. Annealing of TT:BAX15 with all the series of targets [25°C in normal TBE 1X running buffer]

In the first evaluation (**Figure 4**), we can notice some of the following features: a) The assembly of all the structures lead to the formation of the expected tetrahedrons; almost all the bands are of the same length that the single tetrahedron (lane 1); also, we can notice a secondary band in each lane, probably coming from non stable strands at this temperature or due still to stoichiometric parameters that we cannot deduce from this experiment. Nevertheless, the secondary bands in each lane are not relevant whenever the most intense band corresponds to that one from the tetrahedron; b) doing a more detailed comparison in the length of all the tetrahedron bands, it seems like the annealing that contains the series of targets with 15-nt recognition lengths (lanes 9-11) appears to be a little above to the length of the single tetrahedron's band, this means, that from this inspection and at these experimental conditions, the binding of targets with lengths 15 is much more effective with BAX15 strand in the structure and that this behavior is independent from the binding gap to the BAX strand.

The previous result is consistent with what we expected from the 15's targets to BAX15 strand. However, it was also expected that if the length of the BAX target position is longer (15 basepairs), all the targets must be bound to BAX15 at the same conditions. Targets 10's and 8's do not show this tendency in those conditions.

To deduce if also experimental conditions are part of the factors that do not allow the binding of BAX15 with targets 10's and 8's series, we performed new PAGE gels in more controlled conditions. Running the gel at low and high temperatures, increasing the time running gel and modifying the procedure of the annealing with the targets; instead of doing the annealing of tetrahedrons with the targets in one single step, we were adding the corresponding targets to the fully assembled tetrahedron at constant temperature, allowing their incorporation during 30 minutes before running the gel.

Even changing the gel running conditions and the methodology of assembly, it is very difficult to notice by PAGE gel (**Figure 5**) a difference in the electrophoretic mobility between targets 10's and 8's series in comparison with the mobility of targets 15's.

By the use of fluorescence spectroscopy, we performed some quantitative measurements to study the behavior of TT:BAX15 with the 10's and 8's targets. Results and discussions are present in section 3.1.3-i. Fluorescence spectroscopy results show that between TT:BAX15 and the targets 10's, there is an effective formation; while the binding with the targets 8's series is not quantitatively possible.

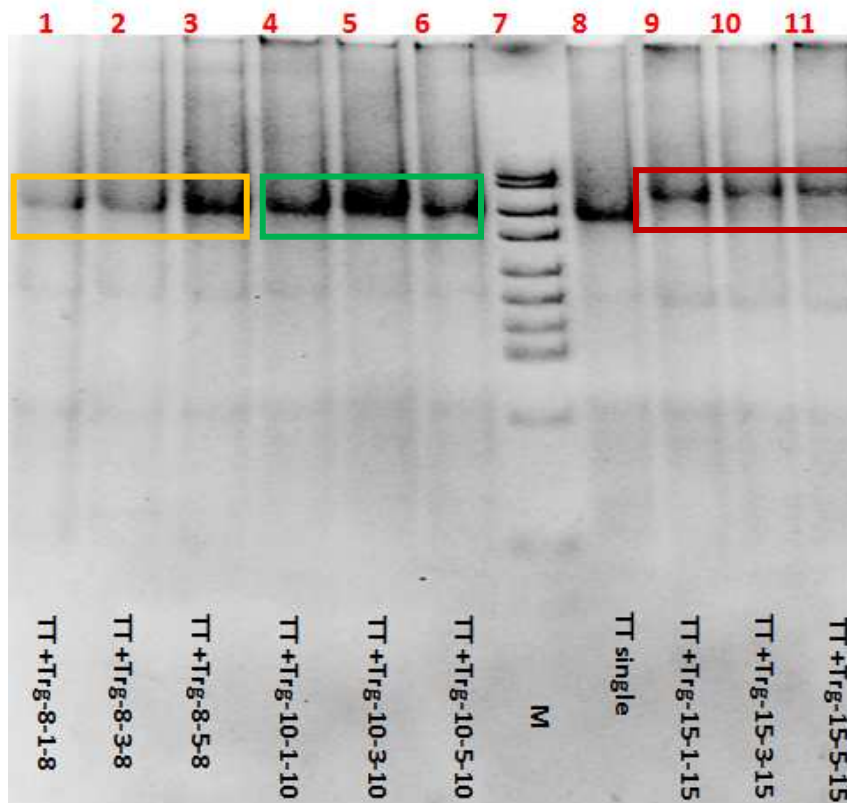


Figure 5. TT:BAX15 with all targets in modified conditions [37°C in normal TBE 1X running buffer]

In order to notice by gel electrophoresis the binding between TT:BAX15 with targets 10's, we performed the annealing with variations in the stoichiometry (1:1/2, 1:1 and 1:2 -TT:BAX15 respect to Trgs-). In addition, since the annealing buffer (TEM) contains certain concentration of Mg^{2+} ions, we also included Mg^{2+} [10 mM] ions in the TBE 1X gel running buffer solution (**Figure 6a**).

After identifying the binding of TT:BAX15 to targets 10's, analogously we performed the same methodology to characterize the binding between TT:BAX10 with targets of series 10's and 15's. The annealing and PAGE gel were done in the same conditions; buffers, temperature and stoichiometries as described above (**Figure 6b**).

Once the amount of Mg^{2+} ions in the running buffer solution was increased, we identified the binding of TT:BAX15 to targets 10's (**Fig. 6a**) (green rectangle). Here, Mg^{2+} ions provide much better stability between bases pairs creating a more stable structure with their corresponding complementary bases sequences of the target, as consequence, their electrophoretic mobility is much more defined. In addition, it is interesting to notice how is the effect over the stoichiometric variations in the 15's target series, showing that there is a clear separation when we use half of the equivalents of target (Trg) 15, the annealing is not

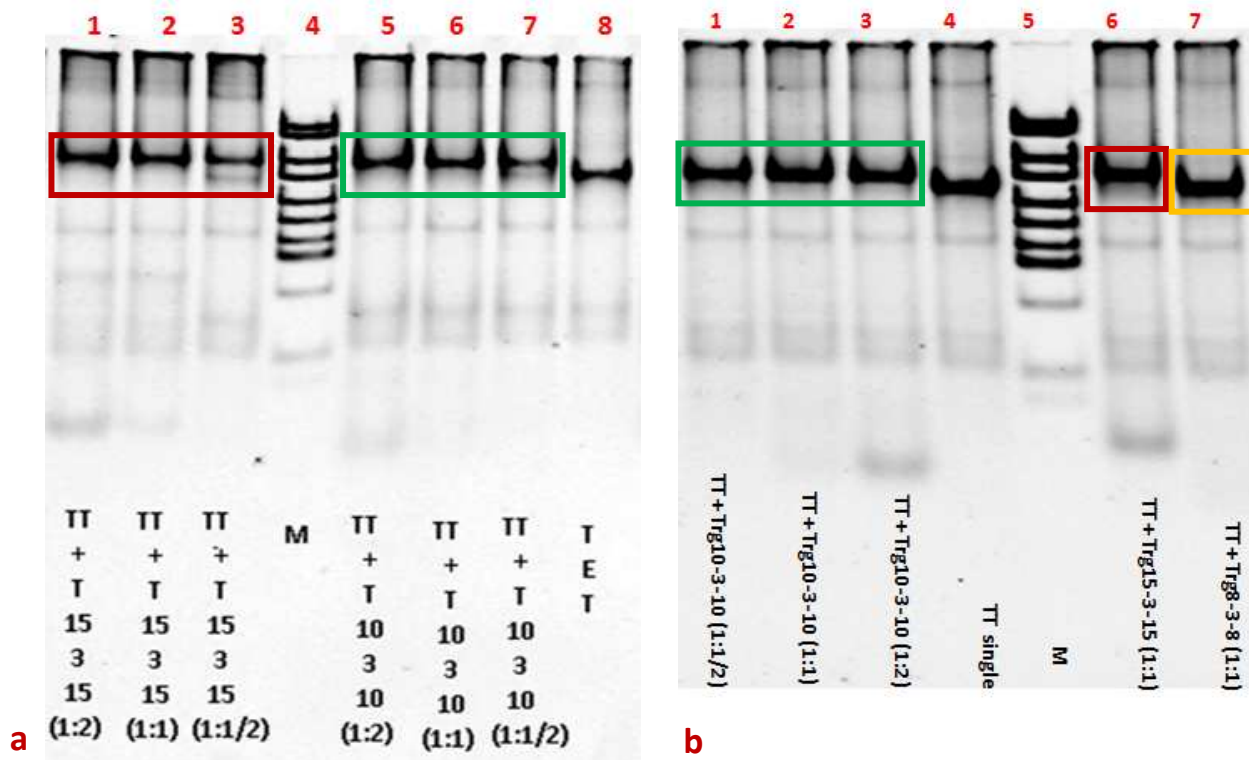


Figure 6. a) Binding of TT:BAX15 to stoichiometric variations of targets 10's and 15's; b) Binding of TT:BAX10 to targets of series 15's, 10's and 8's. Both at [20°C in TBE 1X running buffer enriched with [10 mM] Mg^{2+} ions]

stoichiometric because the band of single tetrahedron (TT) is still present. With (1:1) equivalents we can assert that the annealing is stoichiometric because there are not TT or Trg strand remainders; and at (1:2) we immediately notice the remaining band of the Trg, so is not stoichiometric.

In the replacement of BAX15 to BAX10 strands in the TT structure (**Figure 6b**), after the annealing, we notice that TT:BAX10 is preferential to Trg 10's as we expected, even using half of the amount of Trg 10 seems to provide a quantitative assembly. This behavior could come from some remaining strands after the annealing that facilitate the binding at lower quantities. Target 15 also binds to BAX10 even that at 1:1 ratio we notice the remaining band of the target at the bottom -the 5 bp of each ending-. We also confirm that Trg 8 does not bind to BAX15 neither to BAX10 because it is a very short oligonucleotide.

From this characterization we conclude that TT:BAX15, without Mg^{2+} ions, shows more specificity to Trg 15's while Trg 10's exhibits it at higher Mg^{2+} concentrations. Also TT:BAX10 is more preferential to Trg 10's but also Trg 15's binds.

Thereby the binding is more effective when the target has the same length sequences than the BAX strand has. As suggested in literature, the improvement of affinity of nucleic acid ligand–target binding by the use of high-affinity ligands [4]

9.3 The Functionality of the Nucleic-acid DNA Tetrahedron as a Sensor

As we have described previously, one way to try experimentally the sensing response of our DNA nanostructure, is by the effect of binding each series of targets (8, 10 and 15-nt) with both TT:BAX15 and TT:BAX10 strands, closing the structure, and measuring the response signal by means of fluorescence spectroscopy. The design of each particular experiment is also described in the following sub-sections.

i) Excitation-emission parameters determination of CY3/BPY650 fluorophores and their FRET response in the single REP strand

First we determine the most suitable parameters of direct excitation-emission of both fluorophores in our REP strand for the further use in our experimental purposes, taking the single REP strand [10 nM] “open” state. In addition we probed the FRET responds of this strand by the use of the additional Clip strands, which are exactly the complementary sequences of REP with the difference that one of them has a gap of 2 bp in between while the other does not, this effect was evaluated by the sequential addition of equivalents, at certain time, of the corresponding Clip (see **Table 2** for the sequence)

In **Figure 7a**, we have determined that the highest intensity of CY3 in REP strand is reached when it is excited between 520-540 nm with a 10X10nm aperture slit in the spectrofluorimeter and its highest emission at 570 nm is enough to excite the BPY dye in the region 630-650 nm. We also tried to determine the proper excitation of BPY. However doing the direct excitation over CY3 in the “open” strand we also noticed a signal in the 640-730 nm region which is very strange since we have the open REP strand, which means, the FRET signal should not have to appear; even, this range is very broad to be a signal from BPY emission; this factor did not allow us to perform a correct characterization.

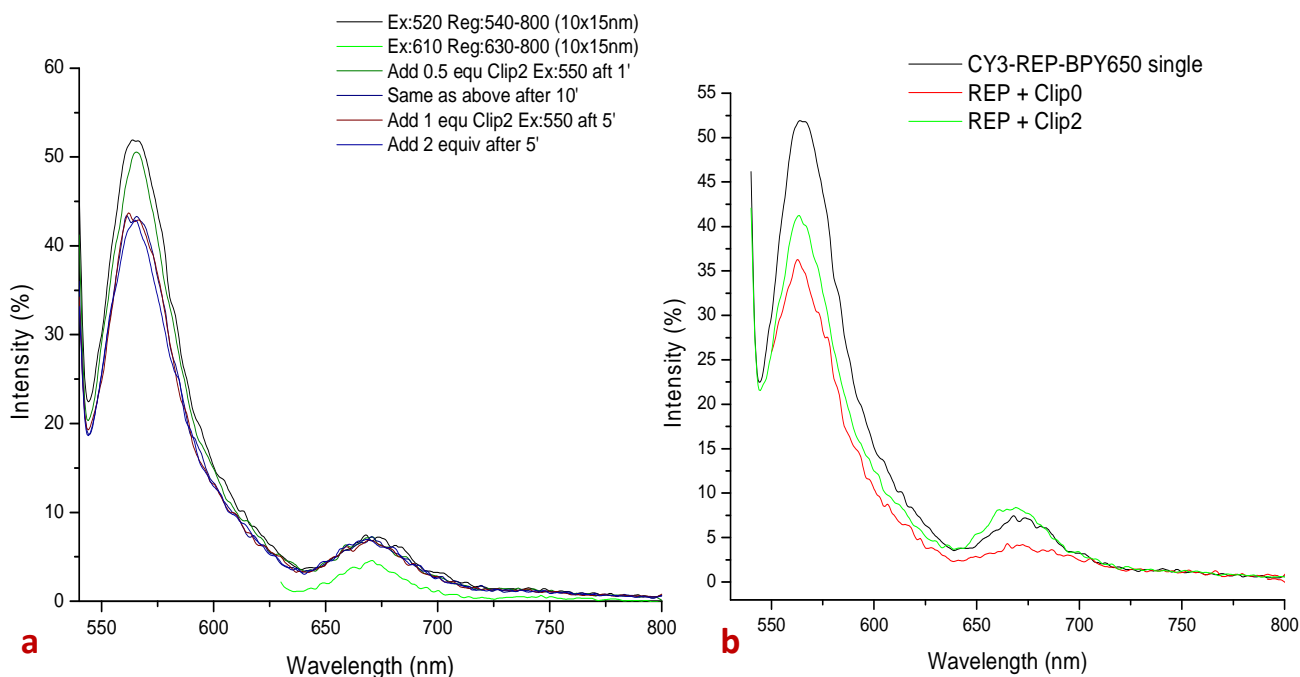


Figure 7. a) The FRET response of the single CY3-REP-BPY650 strand [room temperature in TE buffer]; b) FRET signal behavior of REP strand in the presence of Clips 0 and 2-nt.

With the addition of stoichiometric amounts of the Clips to the open REP strand, the highest CY3 emission peak was decreasing with the addition of more equivalents of the corresponding Clip until reach 1:1 ratio REP:Clip. This indicates that while reaching the 1:1 ratio, the CY3 intensity decreases, it is quenched and the FRET phenomena happens. However, since we have that broad signal in the BPY emission region, we cannot say too much about the FRET response.

Contrasting between the open REP strand and its closed state by 0 and 2 gap Clips (**Figure 7b**), we notice that using Clip0 (the exactly complementary bp of the REP strand) decreases the CY3 emission peak even more that Clip2 does. With these parameters we have a reference as a positive control in our further spectroscopic characterization about the FRET effect.

ii) FRET behavior of the DNA tetrahedron in its open and closed state by the presence of a target

We characterized the fully assembled structure, with the Cy3-REP-BPY650 strand included, first as an “open” structure, later we introduced one of the targets, closing the structure and inducing its FRET response. Here, we took the fully assembled tetrahedron

(TT) [50 nM] which contained the BAX15 strand, measuring its fluorescence emission by the direct excitation of CY3 and BPY at the previously determined parameters. Then we introduced in stoichiometric quantities, at interval times, the target (Trg) 15-5-15. We also probed the negative control FRET behavior in the structure by the use of Half of the target “a” and “b” strands.

It was probed that REP strand with the fluorophore pairs in the assembly does not change its excitation-emission parameters, thus, 540 nm direct excitation for CY3 provides the highest intensity with a 10X10nm slit in the spectrofluorimeter. In addition, the titration of the TT open structure (**Figure 8a**) shows that when the stoichiometric ratio TT:Trg is 1:1, the Cy3 emission intensity is quenched because almost half of its emission peak intensity is decreased; even, this behavior is independent of the interval time between each target addition, thus, the structure is effectively closed and the FRET phenomena must happen; however again for this broad signal in the BPY region, we cannot give any deduction of the intensity of the FRET response. However we assume that it happens.

With the addition of the stoichiometric (1:1) amounts of the called half-strands a and b, which are the complementary base sequences for each one of the 15-nt ending sequences in the BAX15 strand. We notice (**Figure 8b**) that each half target binds complementary to its base sequence and produces a very slight reduction in the CY3 intensity; but no quenching neither the FRET effect occurs; this behavior is consistent from that we expected as a negative control, since all the strands are engaged but the structure remains in the open state.

iii) Titrations of TT:BAX15 with Targets 15 and 10

In order to probe if BAX15 works in suitable conditions both Trg 15 and Trg 10, we titrated the TT:BAX15 fully assembled [25 nM], first with Trg 15-3-15 (gap3) and then with Trg 10-3-10 (gap3) in controlled conditions at 37°C.

The fluorescence spectrum of the titration with Trg 15-3-15 described the same behavior as in **Fig. 8a**; the CY3 emission intensity decreases when a higher amount of target is added to the solution, reaching a saturation point. Looking at the titration curve (**Figure 9**) we could conclude that taking around 0.6 of the equivalents of Trg 15-3-15 is almost fully attached to the BAX15 strand. On the other hand, titration with Trg 10-3-10 shows the same titration curve behavior, there is a gradual decreasing in CY3 emission

intensity, reaching an equivalent point; where most of the Trg is attached to the BAX15 strand, around 0.8 equivalents of the Trg.

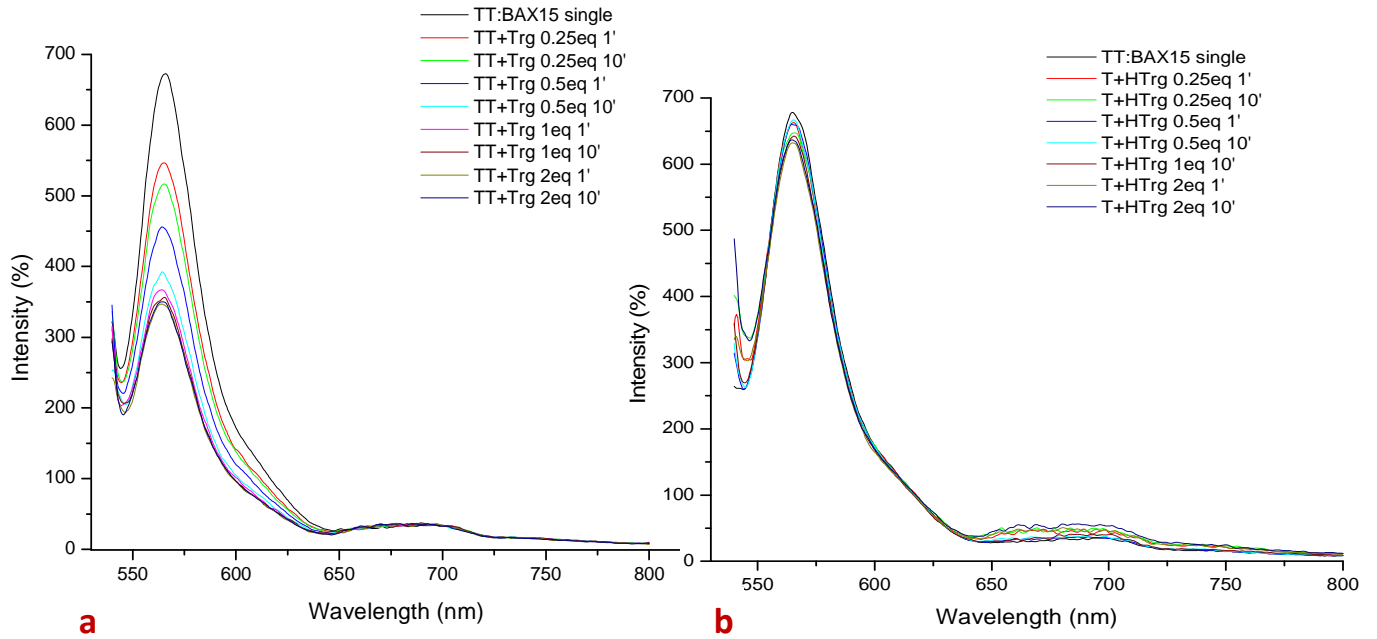


Figure 8. a) Titration of TT:BAX15 with Trg 15-5-15; b) Titration of TT:BAX15 with half of the targets strand [room temperature in TE buffer]

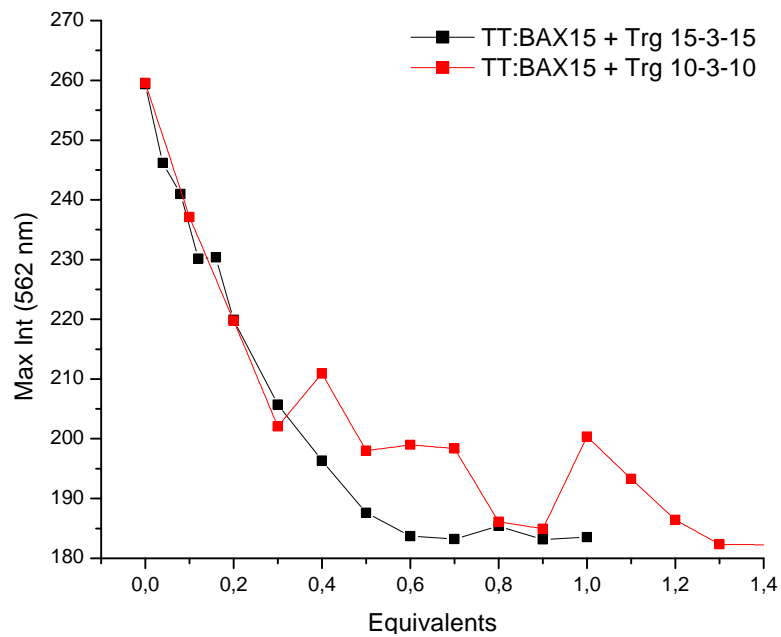


Figure 9. Titration curves of TT:BAX15 with Trg 15-3-15 and Trg 10-3-10 [controlled conditions, 37°C, in TE buffer]

iV) Spectrophotometer correction parameters. Changing from TT:BAX15 to TT:BAX10

The overlap of both titration curves indicates that this behavior is the same with different equivalent points. Thus, it is probed that BAX15 binds both Trg 15 and 10 where there is more specificity to Trg 15. This result also indicates that some conditions in the experimental PAGE gel technique, must be modified in order to detect the evidence of the BAX15 binding to Trg 10 (see discussion 3.1.2).

It was found that the broad band present in the BPY region detected in all the previous measurements was due to the scattering coming from the second stirring magnet used at the bottom of the cuvette, so we used only one and increased the volume in the cuvette up 2 mL.

BAX15 strand in the structure was replaced by BAX10 strand due to a limited amount of the stock solution, thus it was verified that also TT:BAX10 must be assembled to Trg 10-3-10 in the same conditions. Taking the fully assembled TT:BAX10 [50nM] in 2mL of TEM 1X buffer was added the stoichiometric (1:1) Trg 10-3-10.

In the replacement of BAX10 (**Figure 10**), the CY3 emission region shows the same behavior as the BAX15 when only one of equivalent is added but now the broad band in the BPY region is not present as the previous spectra. By the cut-off of the emission signal of BPY we notice, in a very low intensity, the FRET response. In the plot, the green trace shows the emission line when CY3 was excited at 540 nm without the presence of the target, while the blue line shows the emission peak (670nm) of BPY by its direct excitation at 640 nm without the presence of the target. Then, with the presence of the target (closed structure) and doing the excitation over CY3, we notice the energy transfer to BPY by the increasing of its emission intensity at 670 nm (colored lines), reaching almost the same intensity when BPY is directly excited. However we notice a very low intensity in the BPY region in comparison with the CY3 region: We hypothesize that that the detector in our spectrofluorimeter might not be very sensitive in the red wavelength.

v) Titrations of TT:BAX10 with targets 10's series in variation of the gap.

To study the fluorescence behavior of TT:BAX10 bound to the 10's target series when it changes in aperture mismatch (1,3 and 5) we have done the titration with each one target in controlled temperature (37°C), doing measurements each 3 and 10 minutes after the addition of the target. Samples were measured in a buffer solution which contained 140 mM NaCl and 2 mM MgCl₂, to simulate the physiological intracellular ion conditions.

The titration curve describes the same effect over the emission intensity of CY3 by the stoichiometric addition of the target series 10's (**Figure 11a**), we also notice that the binding between BAX10 and the corresponding target seems to be fast, stable and selective, because measuring at different intervals of time, there is no effect over the emission response. Although the intensity in the BPY region is still lower we can sense the FRET response in the same conditions as described before.

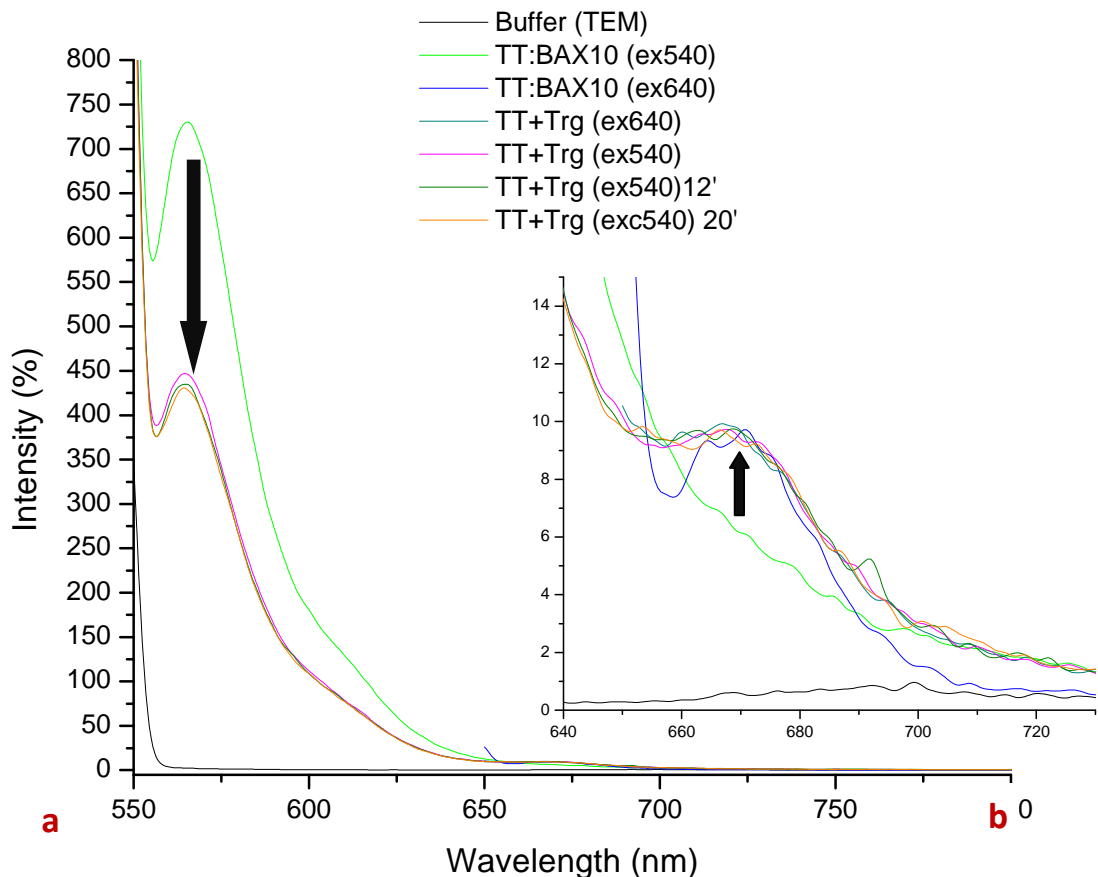


Figure 10. a) The FRET response of the TT:BAX10 by the titration with the target 10-3-10; b) cut-off from the BPY650 emission region. [room temperature, normal TBE buffer]

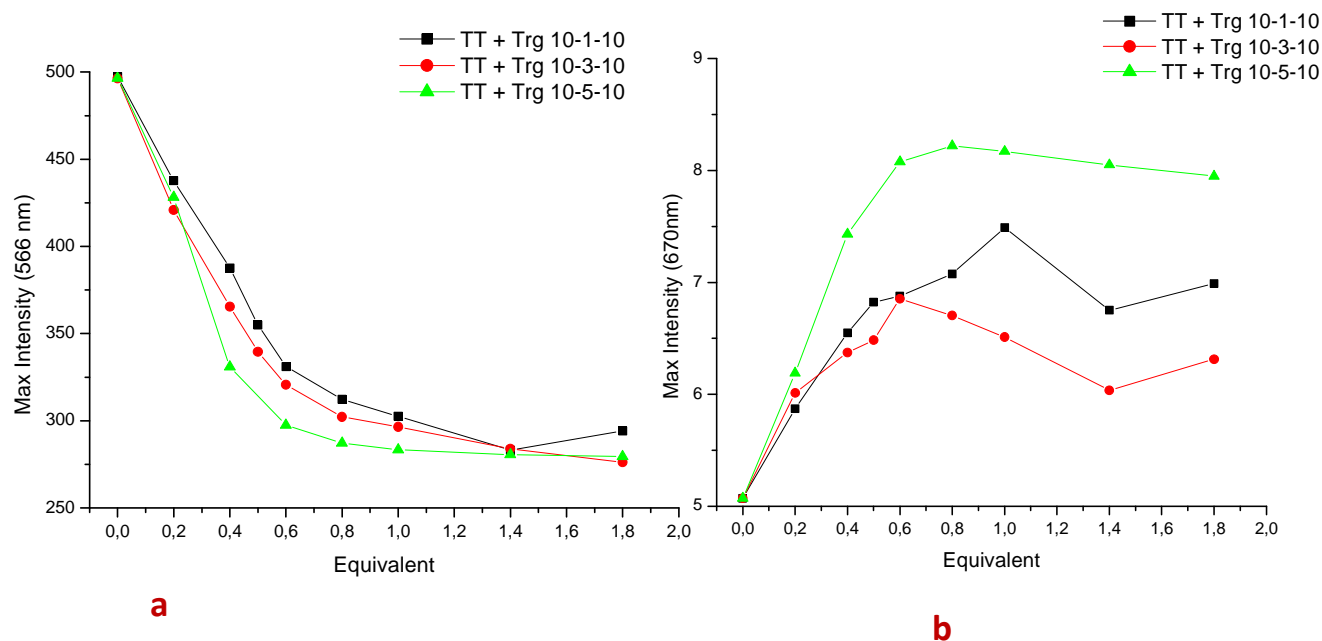


Figure 11. a) Titration curve of TT:BAX10 with targets 10's at different gap binding, emission intensity of the Cy3 region; b) emission intensity of the BPY650 region. [37°C, TBE buffer with 140 mM NaCl and 2 mM MgCl₂]

From the titration curve in the CY3 region emission (**Figure 11a**) we could deduce that the BAX10:Trg's equivalent point is reached around 1:1 stoichiometric ratio. The buffer medium where the measurement is performed does not have any influence over the FRET response. From the behavior when the gap in the target changes we could deduce that Trg 10-5-10, with 5 gap, decreases more effectively the CY3 emission intensity, then Trg 10-3-10 is the next most effective, then Trg 10-1-10 is the least effective. Also, looking at the tendency response from BPY region (**Figure 11b**), -besides its low intensity- it shows that the FRET intensity from Trg 10-5-10 is slightly higher with respect to the other targets. However we could not have a strong evidence from this behavior since the BPY emission intensity is quite low. If confirmed, we could hypothesis that some quenching by contact could take place when the Trg brings the two fluorophores very close and thus acceptor emission could be inhibited, while donor emission could be efficiently quenched.

Thereby, from the behavior of CY3 emission tendency with the 10's series targets we could conclude that; BAX with 10 ending length is much more selective bound to target 10 with a gap of 5 bp; this means that the two 10-nt tails in the BAX10 strand find a better stability when they are broken up apart each other of only few base pairs. Those results also support the theory that high complex-stability of nucleic acid ligand–target binding is achieved by additional topological stabilization via ligand–target

concatenation [4, 5]. This means, the process to pjoin two oligonucleotide sequence strings end-to end (10+gap+10 or 15+gap+15), thus making the target DNA strands locally accessible for Watson–Crick recognition [6, 7]. In addition, the FRET response seems to happens more efficiently when both fluorophores are at 5 bp distance each other.

10 The pH Dependent DNA Tetrahedron

10.1 Self-Assembly and Characterizations of Nanostructures

In our first experimental design, to corroborate the effective annealing of the oligonucleotide sequences (Str1, Str2, REP and long strand -TFO, PC and nTFO) that shape our first designed nanostructures (**Figures 2** and **6** in part II), for this purpose, we performed the PAGE technique. As a first trial, we assembled in stoichiometry quantities a series of dimers, trimers and the three different designed tetrahedrons (TFO, PC and nTFO), **Figure 12**. In a separate gel we also compare the electrophoretic migration between monomers and dimers

In **Figure 12** dimers, trimers and the tetrahedron assemblies are shown, according to the preferential conditions that we designed at the beginning. Here we can notice immediately that the separation in the PAGE gel is related with the mobility parameters that we expected. Assembled dimers (lanes 1-6) run faster according to their low molecular weight; lanes 1-5 are expected to describe almost the same electrophoretic mobility due their almost similar length but probably different conformation, dimer in lane 6 runs the fastest since the PC strand is of low molecular-weight. Trimers (lanes 8-10) describe the same mobility; they are higher in molecular weight than dimers but lower than tetrahedrons. Our desired DNA tetrahedron nanostructures (lanes 11-13) run slower that dimers and trimers, showing a strong band due their high molecular-weight.

Even though that we notice some secondary bands in each lane, coming probably from the excess of one strand; however, they are much less stronger than the principal ones, thus we confirm that the main product corresponds to our predicted assembly design. For this case, we assume a fully assembled structure where the remaining strands are not so important for our purposes, thus we followed this stoichiometric annealing for the further analysis.

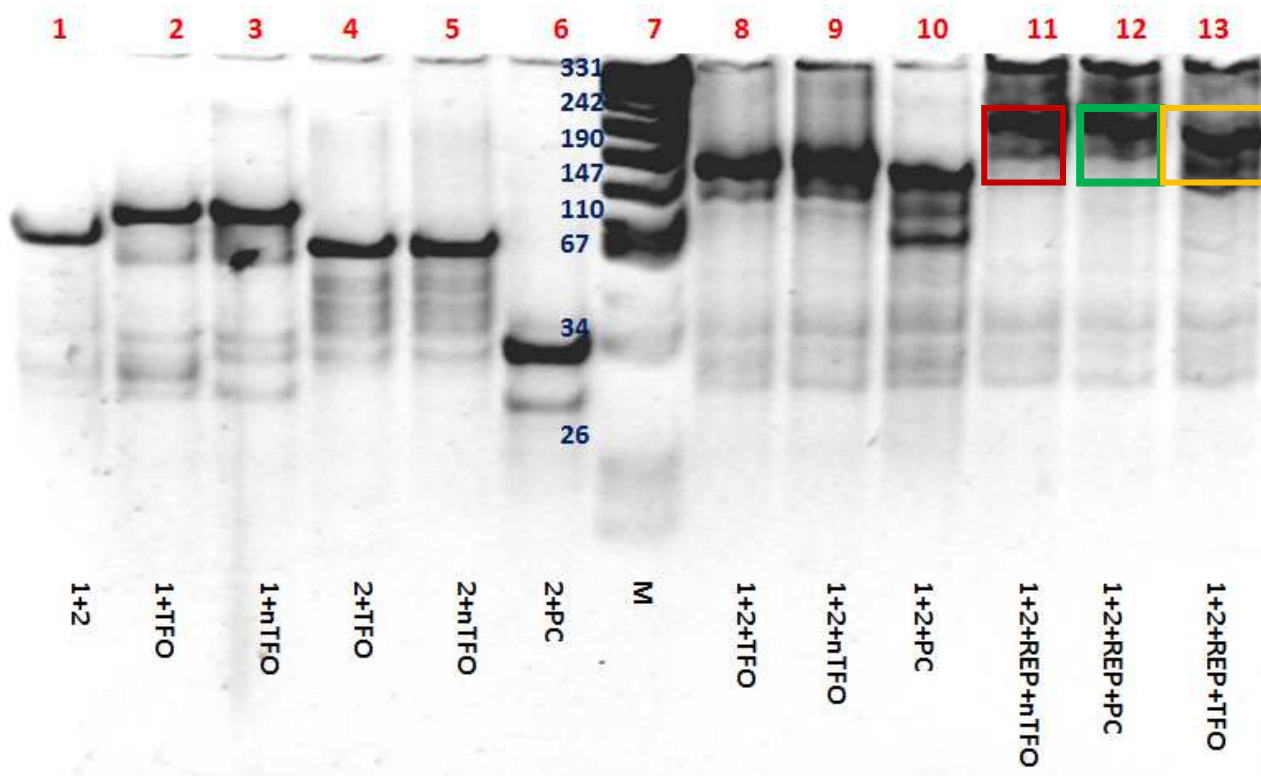


Figure 12. Dimers, trimers and tetrahedrons of their thermal self-assembly strands [20°C in TBE 1X running buffer]

10.2 Probing the Triple Helix Formation

The characterization of the triplex formation was previously studied and reported in our group, which was not part of this thesis. In this report, it was shown that the dynamic formation of the cytosine-thymine motif triplex by the use of two synthetic DNA oligonucleotides and characterizing the transition from the open to the close state by the use of circular dichroism (CD) spectroscopy, UV spectroscopy and electrophoretic mobility shift assay (EMSA) [8, 9]. The shift between open and closed conformation was determined with pH titrations by UV spectroscopy finding that a sharp variation happens between pH 6.0-7.0, while the open state remains stable at pH 8.0. They also used basic (pH 9.0) and acidic (pH 5.0) running buffers conditions for the PAGE gel characterization [10].

Based on the previous information, our first goal was to characterize by PAGE technique the triplex helix formation in our DNA tetrahedron design (TFO), taking as a references the positive and negative controls (PC and nTFO).

The running buffer solution in which we perform the PAGE gel has to be accurately chosen to achieve the triple helix formation in TFO; this means, at acidic conditions it must form while in basic conditions does not. Based on this principle, we were trying different running buffer solutions like TAE 1X or TBE 1X buffer solutions in acidic and basic conditions. Nevertheless, results showed that either the gel was too brittle or not evidence at all of the triplex formation was shown (results not shown in this section).

After some attempts, we found the proper running buffer conditions to notice the first evidence of the triplex helix formation in our structure, considering also the conditions previously described in our group [10]. Thus, the running buffer was prepared using 20 mM acetate, 20 mM MgCl₂ and 50 mM NaCl at pH 5.0. After the thermodynamic assembly of our structures (the triplex helix, the positive and negative controls), we added a small amount of the same running buffer solution at pH 5.0 to each one of the PCR tubes containing the annealed solution; waiting 40 minutes at controlled temperature before introduce them into the electrophoretic slits. The first probe was done at 20°C in this running buffer at pH 5.0; the second one was done with the same running buffer solution in acidic conditions, same procedure at 37°C while the third probe was done also at 37°C with the same buffer at pH 8.0 within the same sample preparation procedure.

According to our model design for these three structures, we could have an idea about the electrophoretic mobility range that we expect for each structure in acidic conditions. TFO structure will form the triplex helix; so, being closed as we designed, it depicts a compact and thicker structure (225 bp) which will describe much more free mobility through the polyacrilamide gel, thus, we expected that it will run faster than PC and nTFO structures. PC structure being closed anytime is lightweight (211 bp) than TFO but probably less compact, thus they could run almost the same length, but must run faster than nTFO. Since nTFO is open all the time, it will find more migration difficulty through the polyacrilamide gel; even though that this has the same molecular weight than TFO (225 bp), it will run slower than TFO and PC.

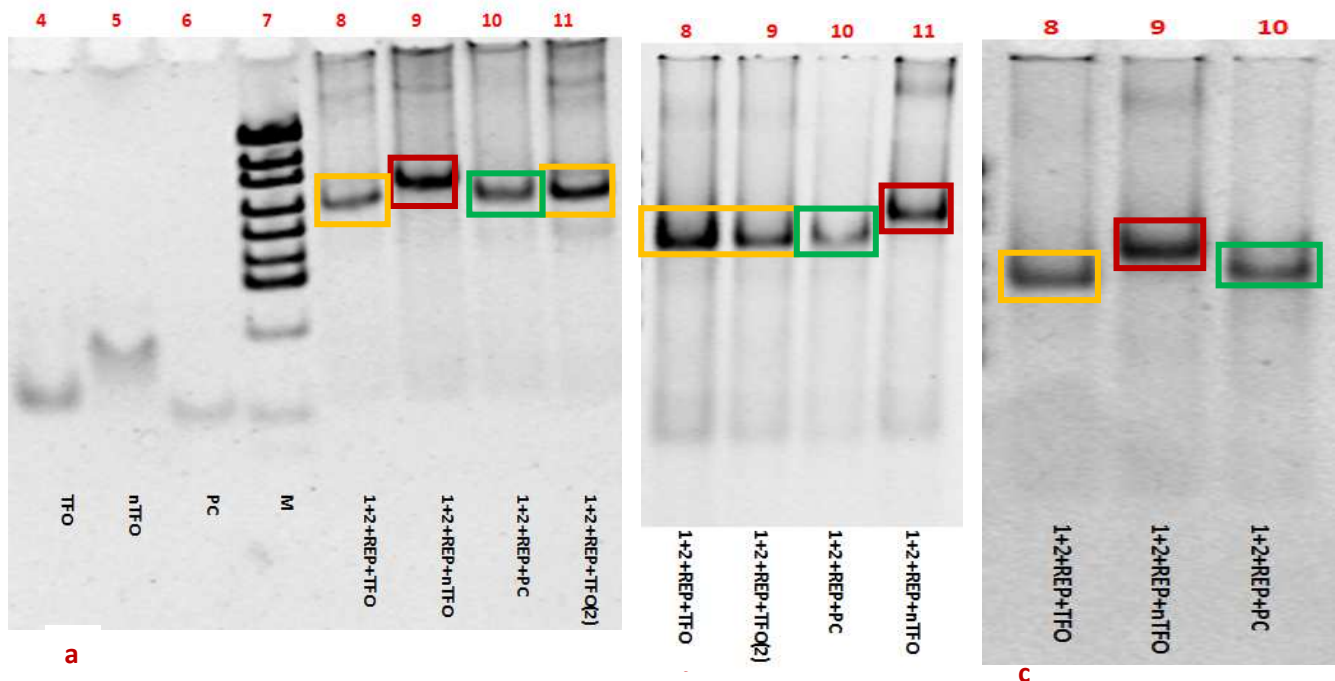


Figure 13. The triple helix formation at different running buffer conditions, a) 20°C at pH 5.0; b) 37°C at pH 8.0 and c) 37°C at pH 5.0 same buffer solution [20 mM sodium acetate, 20 mM MgCl₂ and 50 mM NaCl]

On the other hand, in basic conditions, TFO structure will be open, PC structure closed and nTFO open, thus, from the previous deduction, we could expect that the fastest band will be PC while TFO and nTFO will have the same mobility.

Thereby we establish our expected migration criterions in acidic and basic conditions between the three structures. At pH 5.0; TFO \geq PC > nTFO, while at pH 8.0; PC > TFO = nTFO.

In acidic conditions at 20°C with this running buffer solution (Figure 13a) the fully assembled structures show a single strong band, the tetrahedron structure is formed. However their mobility is described different. The TFO (lane 8 and 11) and PC structures (lane 10) describe almost the same behavior while nTFO structure (lane 10) runs slower. This behavior is consistent with our expected mobility migration. Thus, we can state the successful triple helix formation by the TFO structure in the aforementioned running buffer solution.

The acidic PAGE gel, run at 37°C in the same conditions (Figure 13b) shows the almost the same electrophoretic mobility between TFO and PC structures (lanes 8-10) where PC (green square) seems a bit slower than TFO, difficult to determine by eye inspection. This result is consistent with the previous one and confirms the triplex helix

formation by TFO which is also stable at higher temperatures; advantageous for its *in vivo* applications in live cells. On the other hand, the strongest band in nTFO (lane 11) is slower than TFO and PC as we expected. However at the beginning of the lane, it describes a high molecular-weight smear band that could be interpreted as non-specific cross-linking products, formed possibly due to some imperfect local imbalance in the stoichiometry.

When we change the pH of the running buffer at basic conditions (pH 8.0) at 37°C stable temperature, we notice (**Figure 13c**) that the TFO and PC structures describe almost the same mobility (lanes 8 and 10) while nTFO is the slowest one (lane 9). This behavior is not consistent for that one that we expected; TFO and nTFO must run the same because they are in the open state. With this behavior it seems that TFO is again in the closed state. This result is interpreted by the excess of Mg^{2+} ions concentration in the running buffer solution. It is well known that magnesium cations stabilize nucleic acid duplexes and facilitate their folding into secondary and tertiary structures, which are biologically active. The total magnesium concentrations in various cells range from 5 to 30 mM; however, free Mg^{2+} concentrations are tightly controlled between 0.4 and 1.2 mM. Thus, we assume that at higher Mg^{2+} concentration the TFO could also adopt part of the triplex helix state, less stable than the Hoogsteen pair, and being a bit more compact than the unfolded nTFO.

To understand the previous TFO mobility behavior, we reduced the concentration of Mg^{2+} ions to 10 mM in our previous described running buffer solution. We performed again the PAGE characterization, doing first in acidic conditions and at 37°C controlled temperature within the same procedure.

With the reduction of Mg^{2+} ions concentration in the running buffer solution (**Figure 14**), we notice a better separation between each structure, and also they separate clearly according to our expected mobility parameter at acidic conditions. TFO (lane 8) structure runs faster than PC and than nTFO structures (lanes 9 and 10 respectively). Thus, we use this Mg^{2+} ions concentration in the buffer solution for our further characterization analysis.

We have probed that our designed TFO structure responds effectively to the pH of the running buffer solution, showing the transition from open to closed structure as we expected. Also we determine that the presence of Mg^{2+} ion in the running buffer solution is a key parameter to notice the mobility separation between nTFO and PC structures

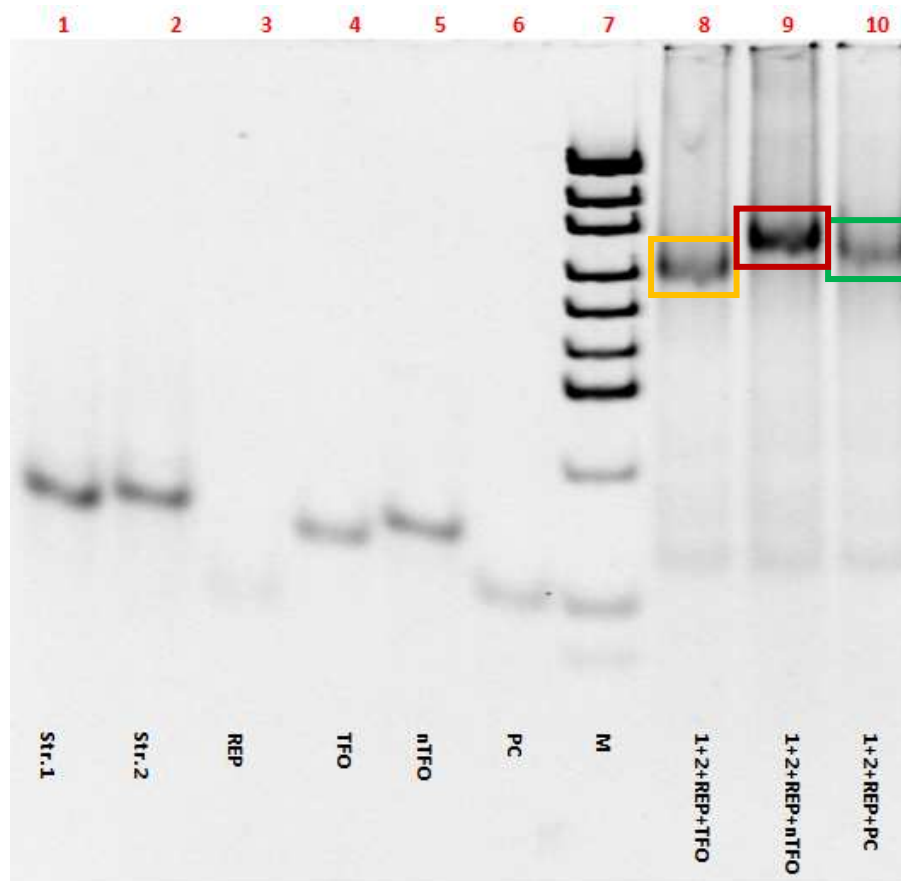


Figure 14. Electrophoretic mobility of the triple helix at 37°C in acidic modified buffer [20 mM sodium acetate, 10 mM MgCl₂ and 50 mM NaCl]

10.3 Probing the Sense Response to pH Changes

After we had the evidence of the triplex helix formation by TFO structure in acidic conditions, the subsequent step was the characterization of its response by a quantitative method, fluorescence spectroscopy. For this purpose, we take advantage of the CY3/BPY650 fluorophore pairs contained in the REP strand, as we described in our model. The aim with the use of fluorescence spectroscopy is determine the FRET response from the fluorophore pairs when they are in close proximity with each other when the TFO structure change conformation by the pH variation [11]. As we described previously, we expected that the TFO structure in acidic conditions will form the triple helix, being in closed state, so, the FRET signal must be much more intense; while, in the open state (basic pH) we should not notice the FRET response or at least to notice weaker. In the PC structure we expect to notice the FRET response at basic and acidic

conditions since the fluorophore pairs are in close proximity all the time. The negative control (nTFO structure) must not show any FRET response since it does not manifest any response to pH changes and remains open. Thus, a suitable technique to determine this sense response is by the use of the fluorescence FRET titration technique, where the pH variations in the solution were detected by the fluorescence intensity signal emitted by the DNA nanostructure.

In our first experimental determination, the FRET response in the TFO structure was measured when the pH of the sample was repeatedly cycled between 5.0 and 8.0 with controlled additions of concentrated HCl and NaOH. However in this first probe we notice that HCl and NaOH are too strong that destroyed our structures -results not shown-.

As a second trial, it was included an acidic and basic buffer with each annealed solutions; tris solution for the basic one (pH 9.0) and sodium acetate for the acidic (pH 5.0). However we could not notice any FRET behavior due to the pH instability -results not shown-.

Then, we use the same buffer solutions for the annealed structure as above at lower concentrations; sodium acetate [10 mM] and tris [10 mM]. Titrations were done with tris [2 mM] solution at pH=9.0 and sodium acetate [2 mM] and [0.5 mM] solutions at pH=4.3. Fluorescence measurements done first at room temperature and the at 37°C, controlled conditions .

From **Figure 15**, in red, we notice the behavior of PC structure which since the beginning describe a constant behavior which remains stable along the repeatedly cyclic titration; this behavior is consistent with our expected fluorescence response. This means, PC in the closed state will describe the highest FRET phenomena, thus, the emission intensity of CY3 (565 nm) will remain lower due the energy transfer to BPY650.

In blue nTFO structure is described, this represents almost a constant behavior from acid to basic pH along the titration, describing a slightly tendency to decrease its CY3 emission intensity at basic pH which does not return to their original point after the cycle. We interpret this effect due to the free mobility of the open nTFO, this means the fully assembled structure has two ending pairs which can move freely and possibly adopt a conformation at extreme pH that place the two fluorophores in a position that creates a low energy transfer when CY3 is directly excited.

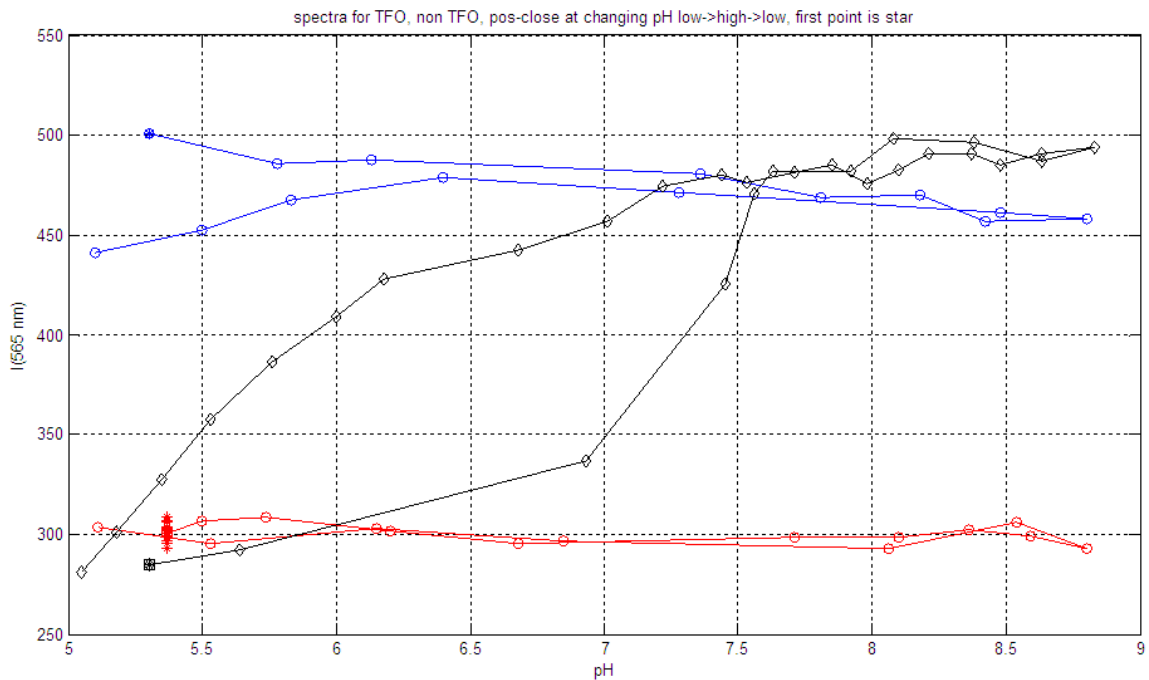


Figure 15. Titration curve for TFO (black), PC (red) and nTFO (blue) structures ranging from acidic to basic pH in repeated cycle [Buffers 10 mM sodium acetate and 10 mM tris at room temperature].

In dark color, the TFO structure is described in its repeatedly cyclic titration. At acidic conditions, closed structure (folded), depict a low CY3 emission intensity due the effective high-FRET effect, which is similar to the PC structure. As we expected, while increasing the pH the structure unfolds gradually; losing the triplex formation, specially between pH 6 to 7 the shift is more evident, reaching the same CY3 emission intensity than the nTFO structure, the open state; higher CY3 emission intensity; low-FRET effect. The cyclic behavior is also shown when pH comes back to acidic even if this does not represent the same path. The slight gradual reduction observed in the overall fluorescence intensity over the cycles is due to, and quantitatively correlates with, the dilution of the construct solution upon acid or base addition [12]. From the cyclic drift we could deduce; a) the unfolded conformation, is more preferable than the folded one and b) the triple helix is marginally stable at room temperature.

In **Figure 16** is only shown the behavior of titration of TFO structure, starting at basic conditions (red dot) in the first cycle describes: a) at higher intensity of CY3 emission it changes its conformation between pH 6-7; b) going from acid to basic at lower intensity it opens easily remaining in this state almost all the first cycle; during the second cycle, the intensity is also constant and the open structure is dominant until it

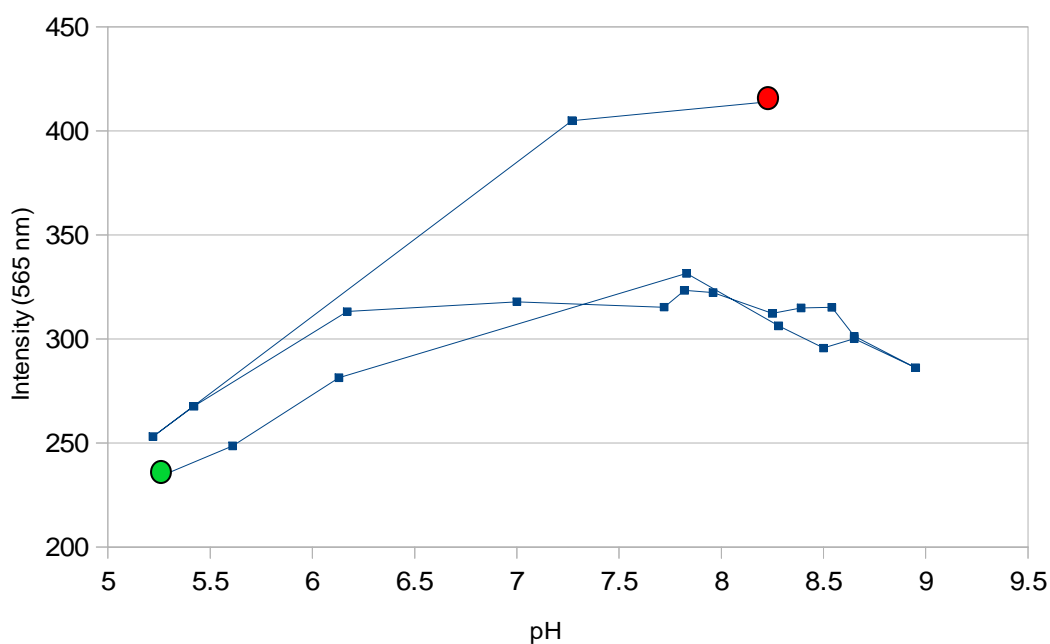


Figure 16. Cyclic titration curve of the TT:TFO structure from basic (beginning -red dot) to acidic pH (ending -green dot) [sodium acetate-tris buffer solution at 37°C]

closes decreasing even more the CY3 emission intensity. Thus from this behavior, at 37°C the unfolded (open) structure is also preferred, decreasing the CY3 emission intensity when folds.

One of the main goals for this structure is to probe its biosensing functionality in live cells, this means, to characterize them at physiological conditions. Reports point out that in cellular environment there could be up to 2 mM of Mg^{2+} ions and around 140 mM of Na^+ ions concentrations. Based on this relation, we performed the spectrophotometric titrations. To achieve them we used sodium acetate [0.2 and 0.05 M] solution at pH=4.3 and tris solution [0.2 and 0.05 M] at pH=10. We carried out this titration at 37°C constant temperature.

Figure 17 describes the behavior spectra, by regions, during the titration of the TFO structure in physiological buffer conditions. The CY3 emission intensity decreases when pH is changing from basic to acid, the structure is changing to the closed state, fluorophore pairs are closer, the FRET response is more effective and the emission intensity is decreased (**Figure 17a**). The BPY region shows the evidence of the FRET response over the TFO structure (**Figure 17b**); while pH is changing from basic to acid, the emission intensity of BPY is increasing. In the titration the nTFO does not change the BPY emission intensity (**Figure 17c**); the structure remains open all the time. In the

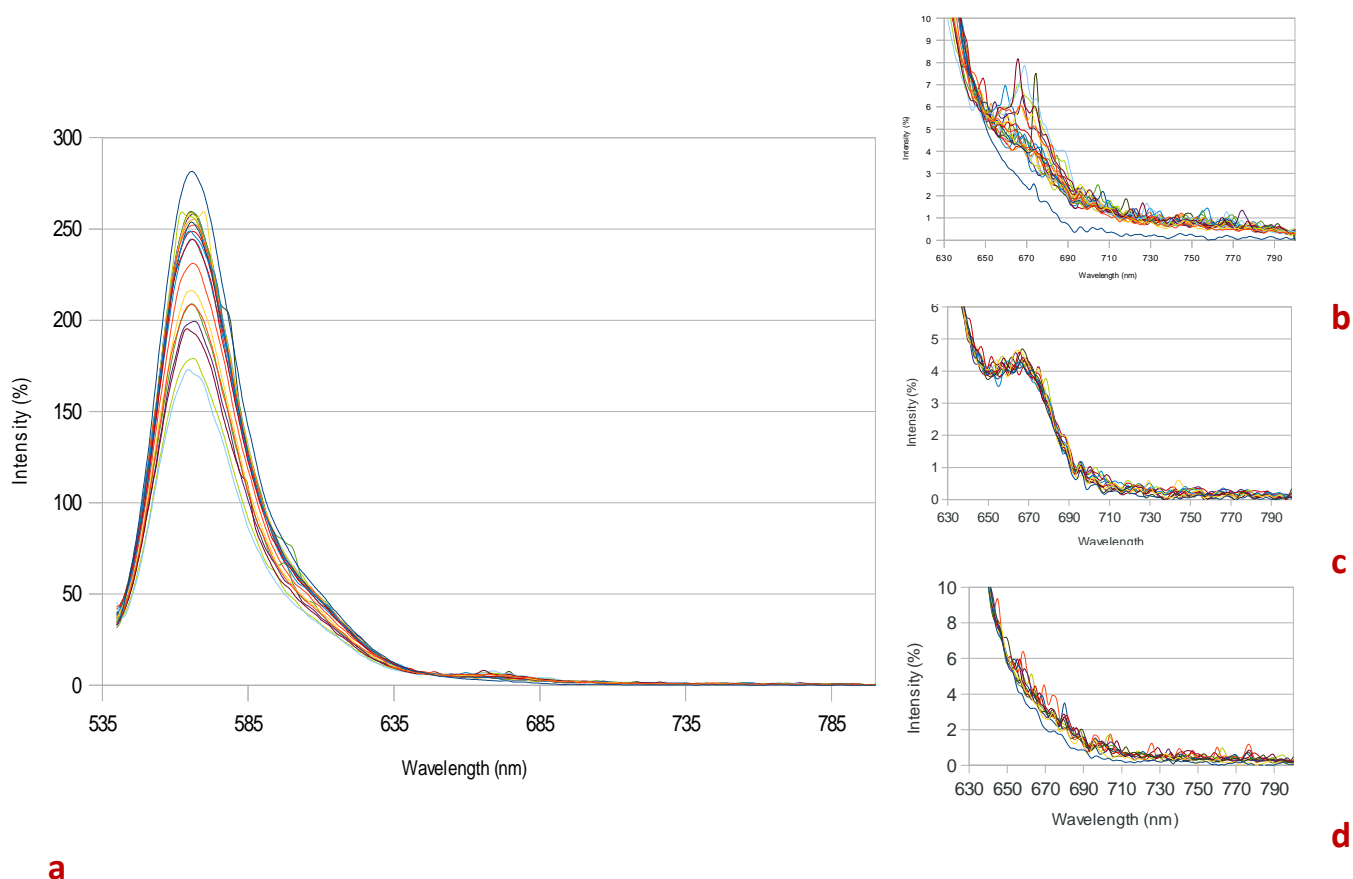


Figure 17. Spectra of the TFO structure titration at different pH values; a) behavior of the Cy3 emission intensity; b) FRET behavior of the BPY region in the titration of TFO; c) FRET behavior of the BPY region in the titration of nTFO structure; d) FRET behavior in the titration of PC structure. [37°C in buffer with Mg^{2+} [2 mM] and Na^+ [140 mM]]

titration PC is not affected along the titration (**Figure 17d**); the structure is always closed, and the FRET effect is always present.

From **Figure 18**, the titration at physiological conditions, we corroborate the behavior of our three designed structures in their pH responses. As in Figure 15, the PC structure keeps constant the CY3 emission intensity while the nTFO's remains also almost constant both behaviors are independent of the buffer solution where the measurement is done. The TFO structure shows the same behavior as the previous analysis, where the unfolded structure seems to be preferred and also noticed that during each cycle the emission intensity of CY3 is reduced even more. In this conditions, the emission intensities from the TFO structure in the open state, do not reach the intensity from nTFO structure; it seems that at higher temperatures the TFO structure is not completely open and still there is some fluorophore interactions. On the other hand, we notice the intersection point with the emission intensities from PC structure, so at pH=5.5

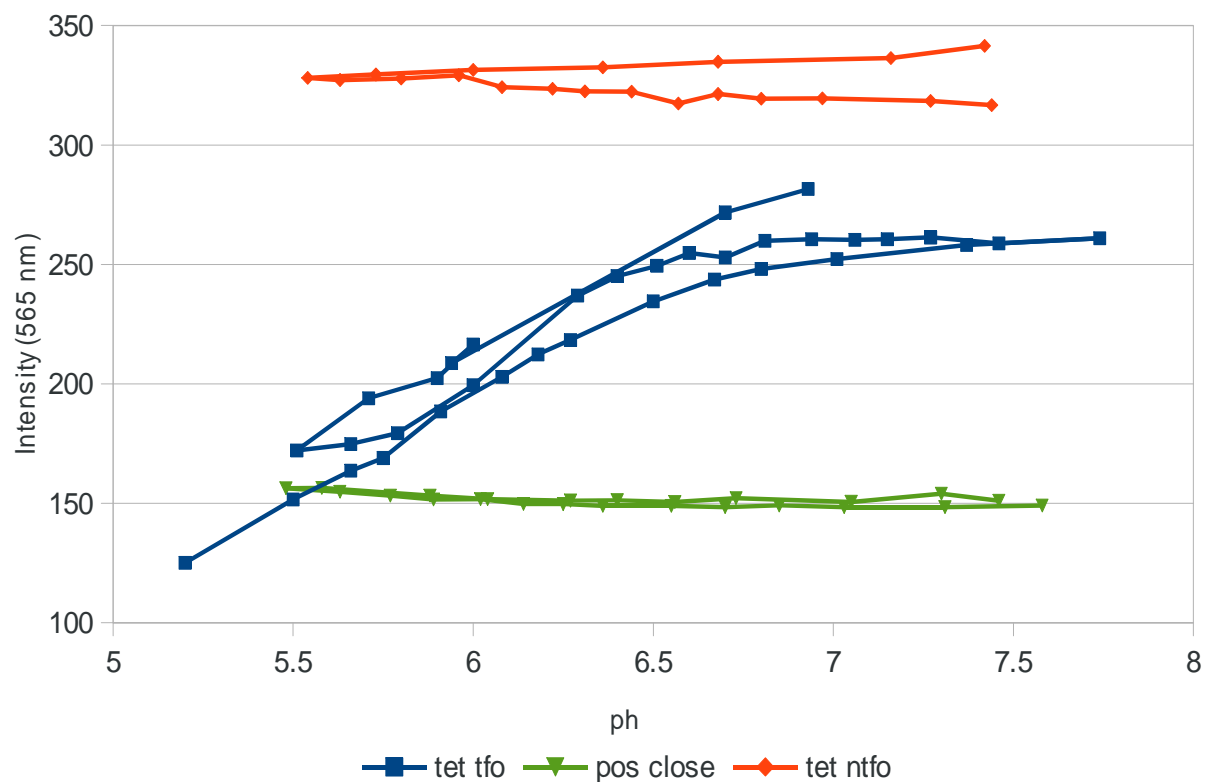


Figure 18. Cycled titration curve of PC(green), nTFO (red) and TFO (blue) at physiological buffer conditions. [37°C in buffer with Mg²⁺ [2 mM] and Na⁺ [140 mM]]

the TFO structure is completely folded; the fluorophores are in their closest state and the intensity over Cy3 is decreased.

In conclusion, by the use of FRET technique, we have probed the effective sensing of the TFO structure and its response at pH variations as we expected in different medium buffers solutions. It shows a constant cycle reproducibility. Kinetically, the unfolded structure is preferred. We have also probed its effective functionality even at physiological conditions.

11 Cell Uptake

Based on publications of other research groups in the field, it was shown that DNA tetrahedron nanostructures have been probed to successfully internalized in live cultured human cells with or without the aid of transfecting agents [13-15]. Additionally, it was also recently reported that tetrahedral DNA nanostructures do not elicit a significant immune response in live cells or a full animal [16]. Even more detailed investigations proposed a rapidly internalization by a caveolin-dependent pathway; also, after endocytosis, the nanostructures were transported to lysosomes in a highly ordered, microtubule-dependent [17] If this is true, we could take advantage of the physiological conditions between the organelles and our nanostructure.

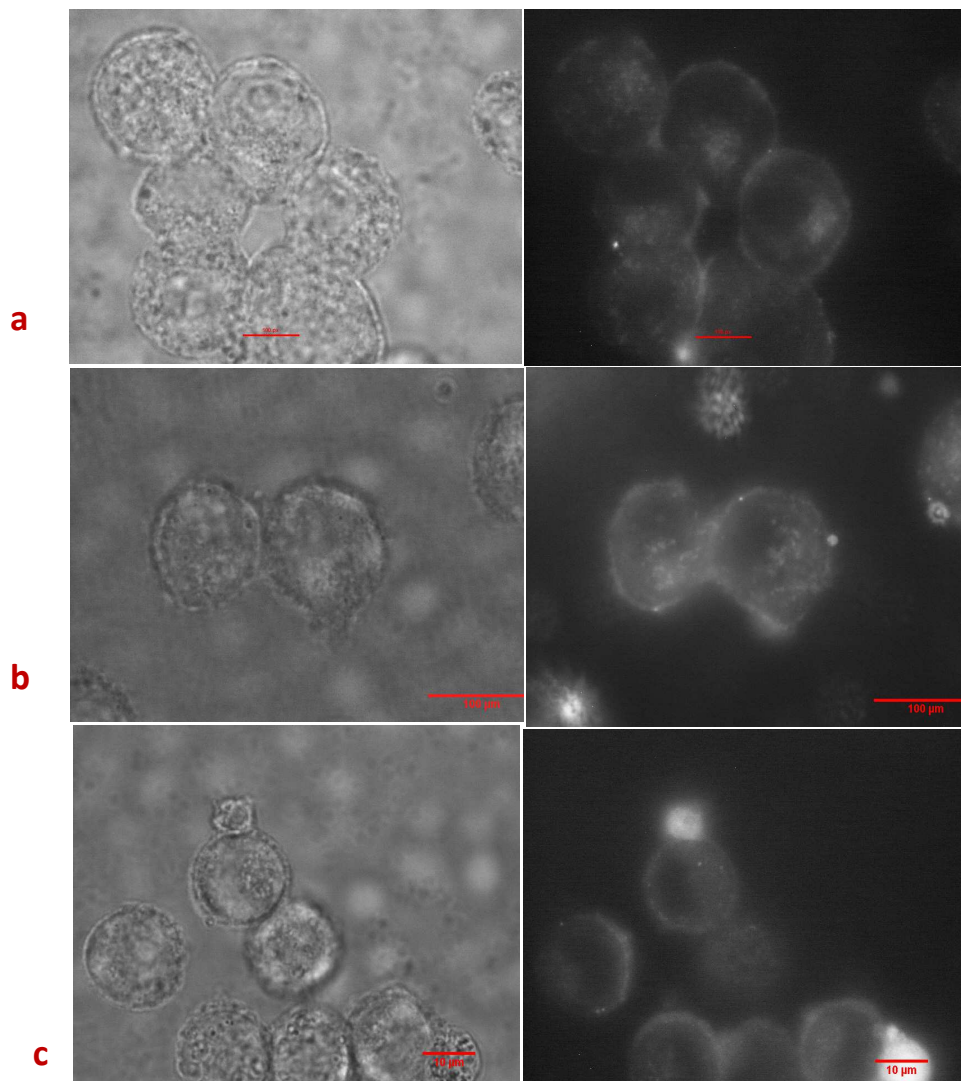
From that point of view, one of the objectives was also to determine by microscopic and quantitative techniques, a) the successful internalization of our designed structures; b) the internal localization inside the cell; c) the biosensing response from the cells about the particular effect produced by our DNA nanostructures. From here, I present the results from both structures in the same context, since we were doing all the microscopic characterization and statistical analysis simultaneously following the same methodology, highlighting the particular results for each case.

11.1 The DNA nanostructures internalization by the cells

First, we examine the evolution of the internalization of one of our assembled structures by the cells in normal conditions, following the protocol for cell culture and nanostructure delivery described in Section 2.5. To achieve this, we used the cultivated human HeLa cell types, treated with 100 nM of our TT:nTFO nanostructure. The evolution was followed at certain incubation times (2, 6 and 8 hours), monitoring the internalization by the signal detection of CY3 emission intensity using fluorescence microscopy.

The set of micrographs in **Figure 19** in white-light (exposure time 60 ms) show the morphology and health status of HeLa cells during the treatment with the structure in time. The internalization is shown as: (a) After 2 h of incubation the structure seems to start to internalize, due to the fact that CY3 emission intensity is brighter at the membrane; b) after 6 h of incubation, emission of CY3 is also coming in low intensity

dots from the membrane but also some bright points are localized at the cell center, from this point of view is not possible to state their particular localization; and c) after 8 h the internalization is better due the higher emission intensity from the CY3 fluorophore in form of “dots” but the signal is more diffused and also for the white-light image, cells start suffering morphological damage. Thereby an ideal incubation time for doing the microscopy analysis is after 6 hours. With this probe we also confirm that HeLa cells successfully internalize our nanostructures.



--- 10 µm ---

Figure 19. Micrographs showing the internalization of TT:PC [100 nM] in HeLa live cells, following at: a) 2 , b) 6 and c) 8 hours incubations

11.2 The internal localization inside the cells

The study for the internalization was based on the fluorescence parameters from the excitation-emission fluorophore pairs. White-light, fluorescence with 380 nm excitation filter (off-peak), Cy3 fluorescence with 560 nm excitation filter (on-peak) and Cy5 fluorescence with 600 nm excitation filter.

HeLa cell line was used at the beginning of the characterization showing some drawbacks in the analysis; due to their morphology. Technically, when cells present a spherical morphology it is difficult to focus only over one stratus, leading to a strange emission detection intensity that also comes from the surrounding stratus, too diffused or sometimes not detected at all. Moreover, a serial experiments were done to detect the emission intensity over the BPY650 fluorophore region, resulting in poor or almost not signal (data not shown here). As a result, we changed the type of cells.

Renal human cells (T-769P) were used in substitution of HeLa cells where the first one exhibit better morphological cellular distribution; they have a flat shape where the internal organelles are better distinguished, this provides better microscopic focalization; these cells are also bigger, which supposedly will facilitate the internalization. So, as a second step we used this cellular line within the same culture and delivery methodology treated with TT:PC [100 nM] and BAX:15 [100 nM]

Using white-light we can distinguish the morphology, stability and healthy status of renal cells without the treatment of any structure, blank (**Fig. 20A**); after the treatment with the TT:PC structure (**Fig. 20E**) and after the treatment with the TT:BAX:15 structure (**Fig. 20I**). From the blank almost any fluorescence signal is showing up with the use of the diverse series of filters (**Figs. 20 B,C,D**).

Taking the renal cells after 6h of incubation with the TT:PC structure [100 nM] it shows that in principle, the off-peak filter (**Fig. 20F**) shows a diffuse but distinguishable cell autofluorescence; normally this effect is emitted by internal organelles such as mitochondria or lysosomes due to the presence of autofluorescing molecules like NADPH (phosphates) and flavins. However the cell off-peak represents an interference signal for the deduction of the fluorescence in situ coming from the fluorophores, thus, we also have to quantify this value to be consequently subtracted in our statistical evaluations.

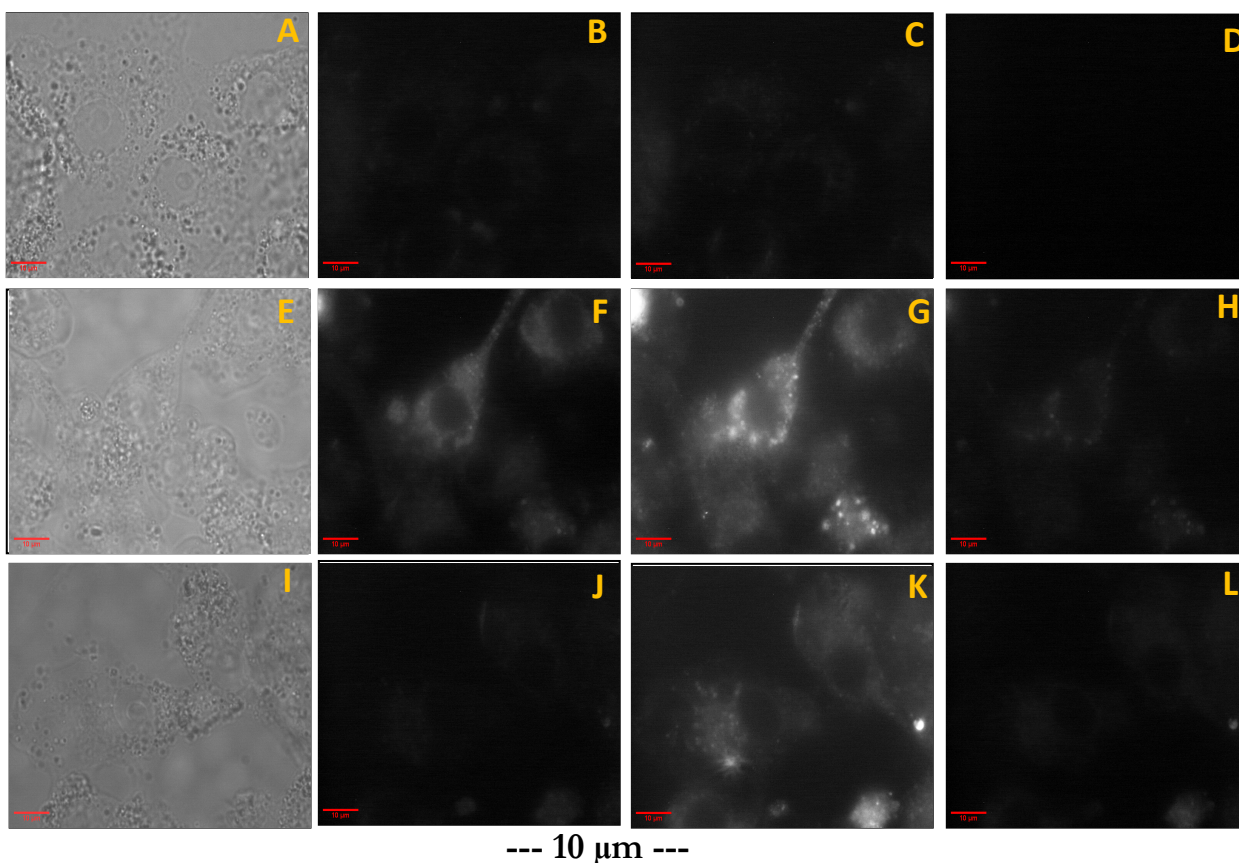


Figure 20. Examples of micrographs of HeLa cells treated with the fluorescent structures TT:PC and TT:BAX15. Panels A, E, I (first column) in white-light; panels B, F, J (second column) with off-peak excitation; panels C, G, K (third column) with on-peak excitation. Where A,B,C and D correspond to the blank; E, F, G and H correspond to cells treated with TT:PC [100 nM], while I, J, K and L correspond to cells treated with TT:BAX15 [100 nM]. [100X, gain 4.8X, exposure time: 2s]

The on-peak (CY3) filter (**Fig. 20G**) shows a perfect well-defined internalization of the structure, where Cy3 fluorophore seems to be distributed in the cytosol, and also showing the form of very brilliant dots, probably, vesicles that from this perspective we cannot provide the exactly localization. It is also noticeable that the BPY emission is shown in very low intensity (**Fig. 20H**), this is also represented in the cytoplasmic region, it also shows a kind of dotted distribution; those dots that are brighter in CY3 are also brighter in BPY.

Renal cells treated with the fluorescent TT:BAX15 structure (**Fig. 20 I, J, K and L**) show almost the same behavior intensity emission for each filter as the TT:PC structure, where the off-peak emission (**Fig. 20J**) is in low intensity; the on-peak emission (**Fig. 20K**) is also of lower intensity but a detailed view shows also a distribution inside the cells with a diffused dotted form; from the BPY (**Fig. 20L**) a very low emission is obtained, difficult to give a probable internal distribution.

In conclusion, using HeLa and renal cells we have determined the effective internalization of our fluorescent DNA nanostructures, it seems that they are well distributed in the cytoplasmic region with a particular brilliant spot form, like in vesicles; it appears that they are not bound to any particular cellular compartment. However from the previous results it was not possible to conclude about the specific localizations, also the phenomena of photobleaching occurs after few seconds of exposure, which does not allow a perfect image definition, the image is diffused, thus from these results was not able to perform static analysis. In addition, at the time of this analysis, the microscope was not equipped with the FRET filter set, that was acquired during the course of my work, so by this technique, we still do not have evidence about the FRET emission from our nanostructures.

We attribute those effects probably due to the low efficiency of these fluorophore pairs which suppressed from some factors that could be from the medium or even coming from their arrangement in the structure.

12 Re-design of the Nanostructures with the Cy3/Cy5 Fluorophore pairs

From the above results we have detected a low emission from the BPY650 fluorophore in the FRET emission and even when was directly excited. We suppose that in addition to the low emission intensity of the BPY650 dye, it could also come from the low sensitivity over the red wavelength detection sensitivity that is characteristic of CCD cameras. However, a more detailed investigation has to be done to find the optimized parameters to improve their fluorescence response. A strategy to overcome the drawbacks from the BPY650 dye was the substitution for the CY5 organic dye. The CY5 fluorophore has the same working emission-excitation parameters as the BPY650. Also, the CY3/CY5 is a well known fluorophore pairs probed effectively in several DNA nanostructures design [18, 19]

Within the fluorophore replacement, we also have changed some of the sequences in the Str.1, Str.2 and REP oligonucleotides to provide them better stability. The oligonucleotide conformation and distribution remained unchanged, shaping the same designed structures. We also purchased the CY3-REP oligonucleotide to corroborate the

Table 1. Sequence strands of the new purchased oligonucleotides.

Stran	Sequence (5' ---->3')
Str. 1b	TATCGTTGTACTTACGAGC/ATATTGATTAGCGGGTCCGAGATCGCTAATGAGGCCAGCG
Str. 2b	TTGCGGTTCTTTTCTTTCTTA/ATGTACGGACAGCACCTGGCACGCTGGCCTCATTAGCGATC
CY3-REP-CY5	CY3-TGCTCGTAAGTACAACGATAAGCCAGGTGCTGTCCGTACAT-CY5
CY3-REP	CY3-GGCTCGTAAGTACAACGATAAGCCAGGTGCTGTCCGTACAG

Str.1b, Str.2b and CY3-REP were purchased from Eurofin/MWG while CY3-REP-CY5 from the Sigma Aldrich

single function of CY3 in the fully assembled tetrahedron. In the following table are shown the new oligonucleotide sequences.

12.1 PAGE gel characterizations

With this new oligonucleotide sequences, first we corroborate their correct thermal self-assembly with the PAGE gel technique, proceeding within the same experimental conditions that we found from the previous characterization results.

Characterizing the self-assembly of the pH dependent DNA nanostructure in the same conditions as established from the previous structure (**Fig. 21**) compares between the assembly using both the CY3-REP strand and the CY3-REP-CY5 strand, showing any difference in electrophoretic mobility. In addition, we distinguish both in acidic and basic conditions the expected electrophoretic mobility for each DNA nanostructure (TFO, nTFO and PC) that were discussed before. Thus we confirm the successful self-assembly with the modified oligonucleotides, we also verified that the reproducible characterization with the established buffer solutions and both Cy3-REP and Cy3-REP-Cy5 are perfectly annealed in the full structure.

On the other hand, we also have done the self-assembly of the TT:BAX10 nanostructure, including the new oligonucleotides; assembled individually with Cy3-REP and other with Cy3-REP-Cy5 in the fully structure. We characterized both the open and closed (with target 10-5-10) structures, running the gel at 37°C and at physiological conditions.

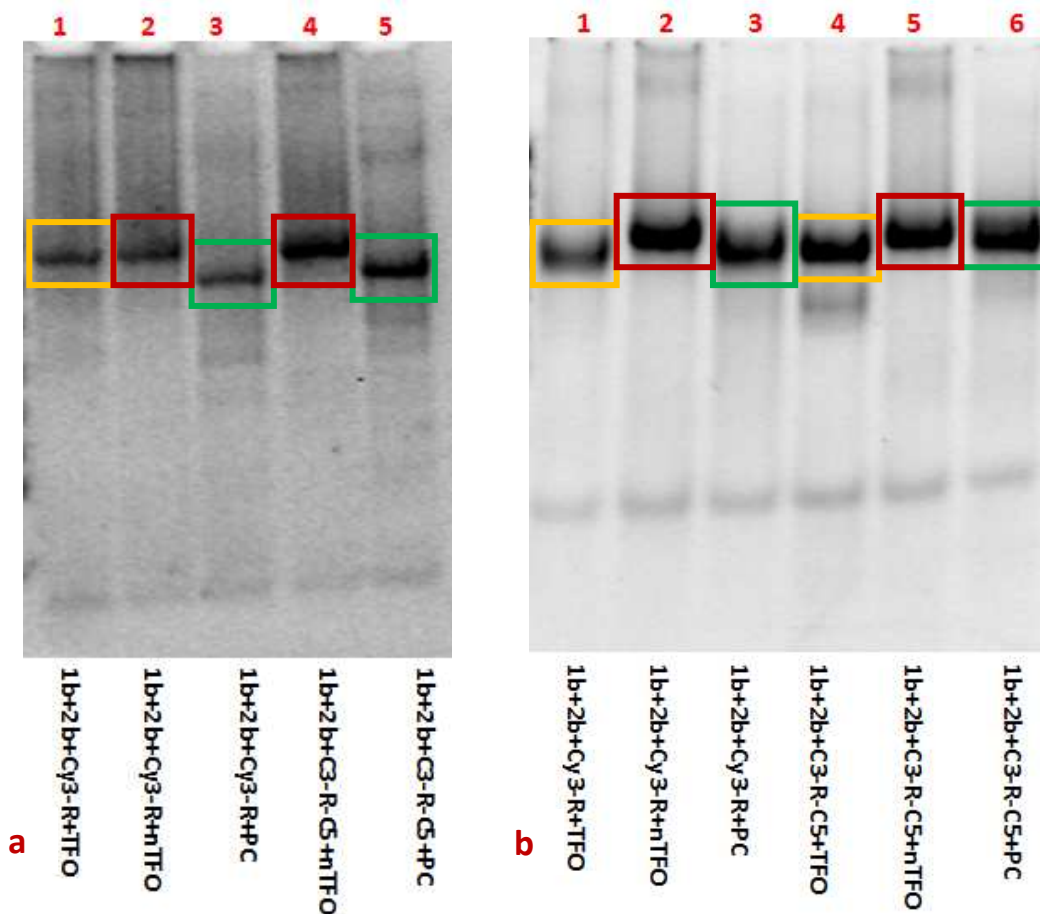


Figure 21. Characterization of the self-assembly of the new purchased oligonucleotides and fluorophores; a) TBE running buffer, pH 8.0 at 37°C; b) Sodium acetate [20 mM], MgCl₂ [10 mM] and NaCl [50 mM] running buffer, pH 5.6 at 37°C.

The self-assembly of the TT:BAX10 nanostructure was also confirmed by the well defined electrophoretic migration between monomers, dimers, trimers and the desired tetrahedrons with their correspondence variations with Cy3-REP and Cy3-REP-Cy5 oligonucleotides (**Fig.22**). In addition, we verified the correct binding of the TT:BAX10 to the Trg 10-5-10 (lanes 12 and 13) at physiological conditions. Thus, with this new oligonucleotides, we have confirmed their successful self-assembly formation and stability of the TT:BAX10 nanostructure and also the closed nanostructure, by the presence of a target, at physiological conditions.

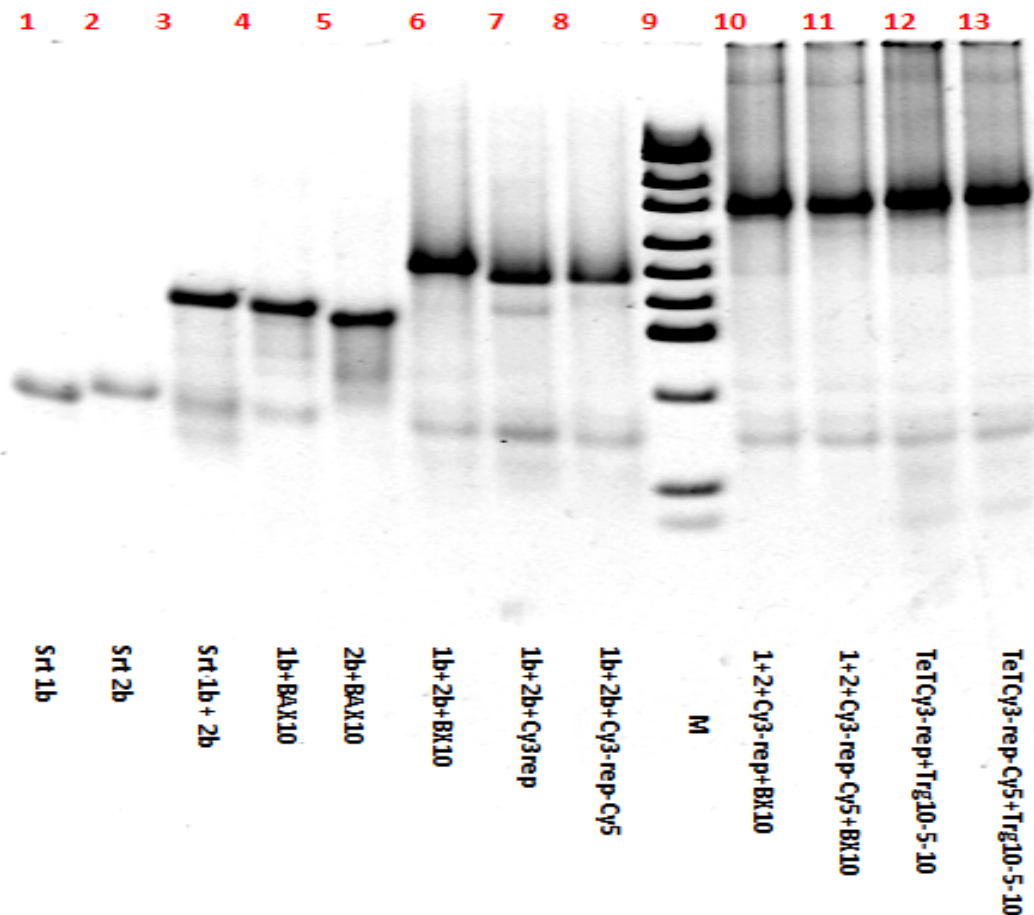


Figure 22. PAGE gel of the self-assembly with the new purchased oligonucleotides and fluorophores modification in the TT:BAX10 structure; comparisons between monomers, dimers, trimers and open and closed tetrahedrons [37°C in TBE 1X buffer with 120 mM NaCl and 10 mM MgCl₂]

12.2 Fluorescence spectroscopy characterizations

Fluorescence characterizations were done both; a) the blank, detecting the CY3 emission coming from the single CY3-REP oligonucleotide, in its open and closed state; b) probe the FRET efficiency of the fluorophore pairs when the CY3-REP-CY5 is included in the structure and when it is closed by the use of a target.

The CY3-REP single strand describes a well defined emission peak of high intensity at 565 nm when it is excited at 540 nm. The quenching of CY3 emission intensity is perfectly shown after the addition of the Clip.3b which closes the strand (**Fig. 23a**). When the CY3-REP-CY5 is included in the fully assembled TT:BAX10 nanostructure, in

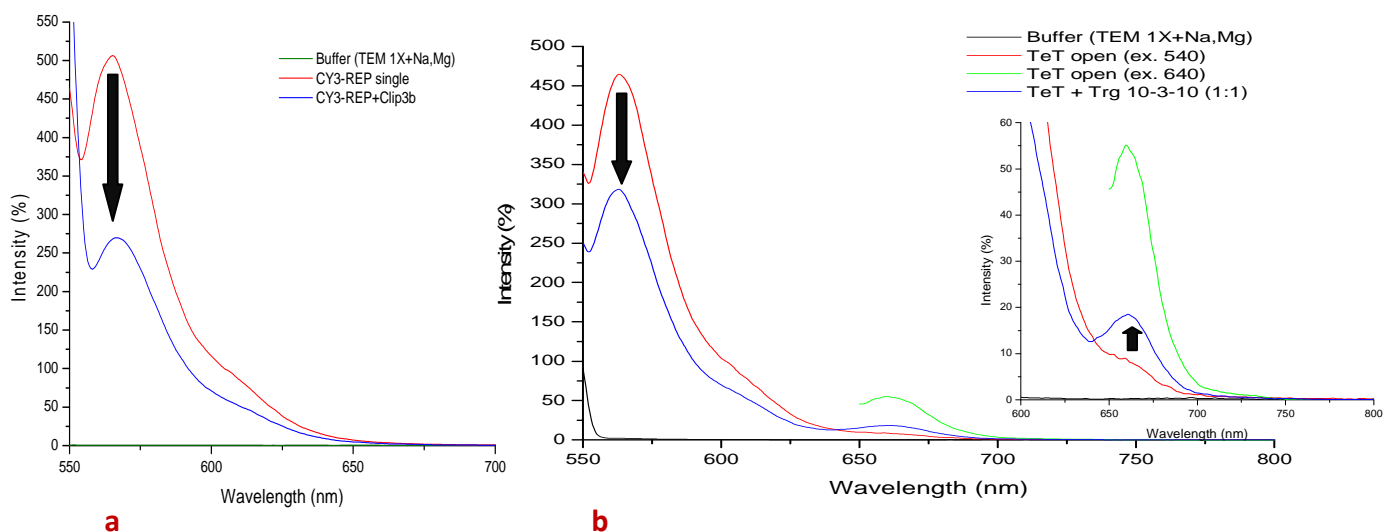


Figure 23. a) Emission spectra of single CY3-REP strand in its open and closed state -with Clip.3b (1:1); b) spectra of TT:BAX10 where Cy3-REP-Cy5 strand is included in its open and closed state -with Trg 10-3-10 (1:1). [Conditions, room temperature in TEM 1X buffer enriched with 120 mM NaCl and 10 mM MgCl₂].

the open state, the CY3 emission peak is well described (**Fig.23b**); while, doing the direct excitation of CY5 at 640 nm, its emission peak is present with a very low intensity. Then when the Trg 10-3-10 was included (1:1) to close the structure, the FRET effect is noticed (cut-off of the b spectrum) but also, its Cy5 emission intensity is low. The Cy3/Cy5 fluorophore pair seems to perform a better FRET performance in comparison with the Cy3/BPY650 pair, even if its FRET emission intensity is still low detected by the spectrofluorimeter.

12.3 Fluorescence microscopy characterization. The cell uptake

At the microscopy characterizations done in the first part, the FRET response between Cy3/BPY650 was not detected due to the absence of the proper filter set. However to characterize the nanostructures with the new Cy3/Cy5 fluorophore pairs, the FRET filter set was integrated to the fluorescence microscope. In an additional step, we also have carried out the characterization of such filter, allowing to determine its optimal FRET emission intensity by the suppression of the direct Cy3 emission over the FRET intensity (see Appendix section for results).

It was noticed that renal cells were suitable to characterize the nanostructure delivery with some improvements in comparison to the HeLa cells. However, the type of cells for this section was also changed; glioblastoma cells (T-67 line) were chosen because they show a higher internal morphology with better definition of their cellular compartments, thus we could notice the possible preferable internal localization of the structures. Additionally, T67 cells are also smaller than renal cells, so that full cells can be displayed in the field of view.

Glioblastoma cells were treated, in the same conditions as renal and HeLa cells, with the corresponding fully assembled structure; TT:PC, TT:nTFO, TT:TFO and TT:BAX15. For the static analysis, a set of structures were assembled containing the CY3-REP strand and the second one containing the CY3-REP-CY5 strand. Fluorescence microscopy visualizations were done after 6 hours of incubation.

The series of images showed in **Figure 24**, provides the characterization of the TT:PC structure with the assembly that contains CY3-REP and the one with the CY3-REP-CY5. In the white-light column is presented the morphology and conditions of the glioblastoma cells; the nucleus and membrane are well defined. The blank in exposure with the series of filters does not show any coming signal, thus we have an optimal qualitative reference. The structure with contains only Cy3-REP strand show the expected behavior; a very normal low off-peak (cellular autofluorescence); any FRET emission, it is expected due Cy5 is not present; a noticeable on-peak emission coming from the direct excitation of CY3 and any distinguishable signal from the Cy5 filter, there is not present. The structure which contains the Cy3-REP-Cy5 strand shows the normal off-peak, very low intensity; the FRET response is detected in low intensity, higher than the off-peak; the on-peak is perfectly well detected in higher intensity respect to the previous structure and the Cy5 is also detected but in a very low intensity.

From the Cy3-rep and Cy3-rep-Cy5 behaviors it is evident that the FRET phenomena is detected when both fluorophores are present, even that the intensity is low. As we expected, the on-peak is the most intense in each raw where the structure with only Cy3-rep shows a more brilliant spots, while the one with Cy3-rep-Cy5 describes, besides the dotted form, a type of "branched" diffused signals spread on the cytoplasm. In addition it appears that the presents of Cy5 in the rep strand increases the Cy3 emission when it is excited. The direct excitation over Cy5 is not detected with an exposure time of 2 seconds, while exciting at 10 seconds we notice some signal intensity; unfortunately the background is also coming out.

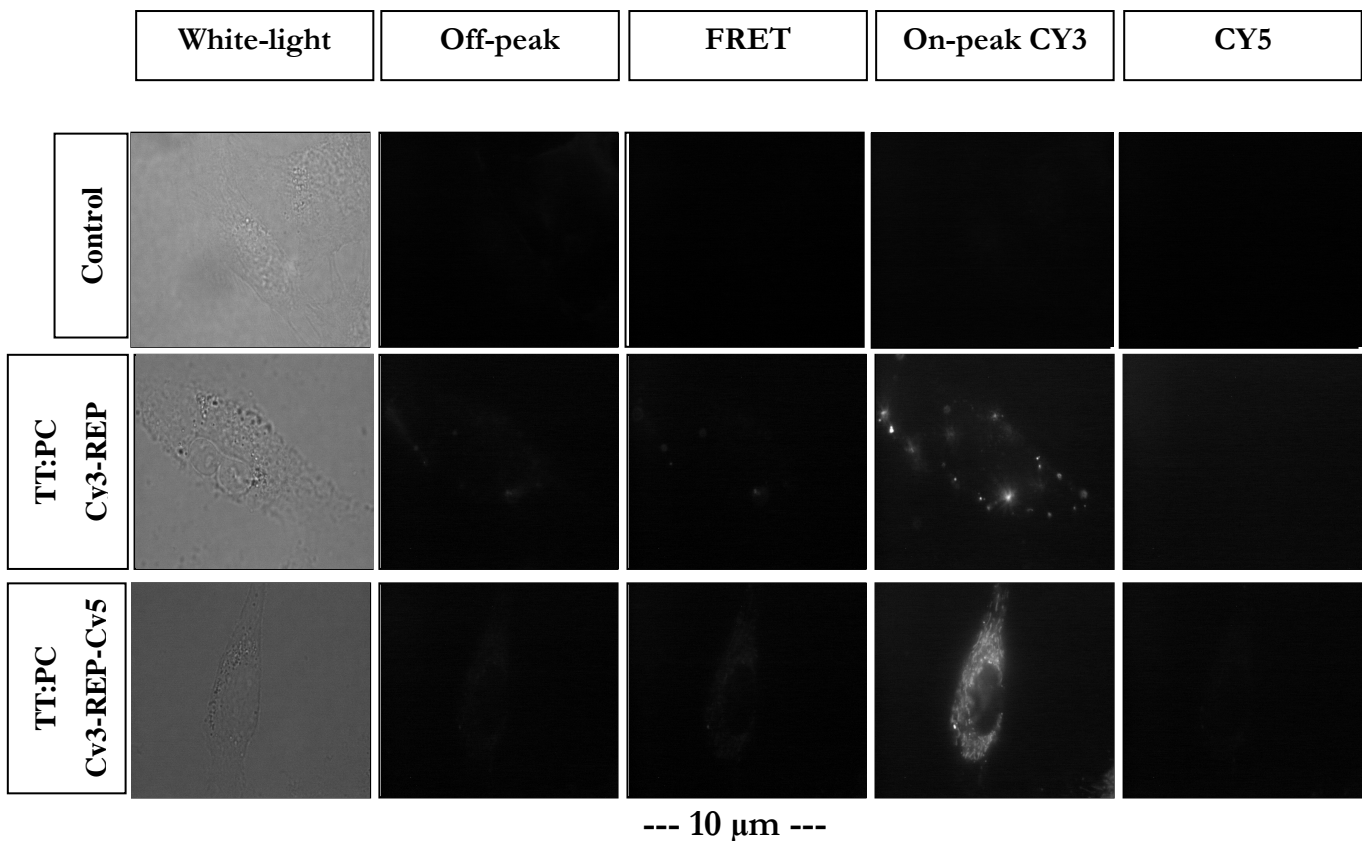


Figure 24. Examples of micrographs of glioblastoma cells treated with the fluorescent nanostructure TT:PC [100nM] after 6 h of incubation. Comparisons between the white-light, off-peak, FRET, on-peak (Cy3) and Cy5 filters for the two types of TT:PC structure, one containing the Cy3-REP strand and the other containing the Cy3-REP-Cy5 strand. [100 X, gain 4.8 X, exposure time: 2s].

A more detailed inspection of the micrographs from the on-peak filter over TT:PC (Cy3-rep) and TT:PC (Cy3-rep-Cy5), suggest that once the TT:PC structure is internalized, it appears from TT:PC (Cy3-rep) micrograph they are bound to some cellular compartments in form of vesicles which are spread in the cytoplasm, where they are more brilliant, we attributed this localization to lysosomes. On the other hand TT:PC (Cy3-rep-Cy5) micrograph, besides the dotted form, fluorophores are also bound to some tubular or branched organelle, diffused in the cytoplasm or in the perinuclear region which could be either mitochondria or the Golgi apparatus, even though localized in the central portion of the cells.

An overlay of the Cy3 donor emission fluorescence with the Cy5 acceptor FRET emission fluorescence micrographs, also shows the localization of high-FRET states in point-like organelles identifiable as lysosomes (**Figure 25**). Thereby we point out that the pH sensor tends to localize more preferential in lysosomes

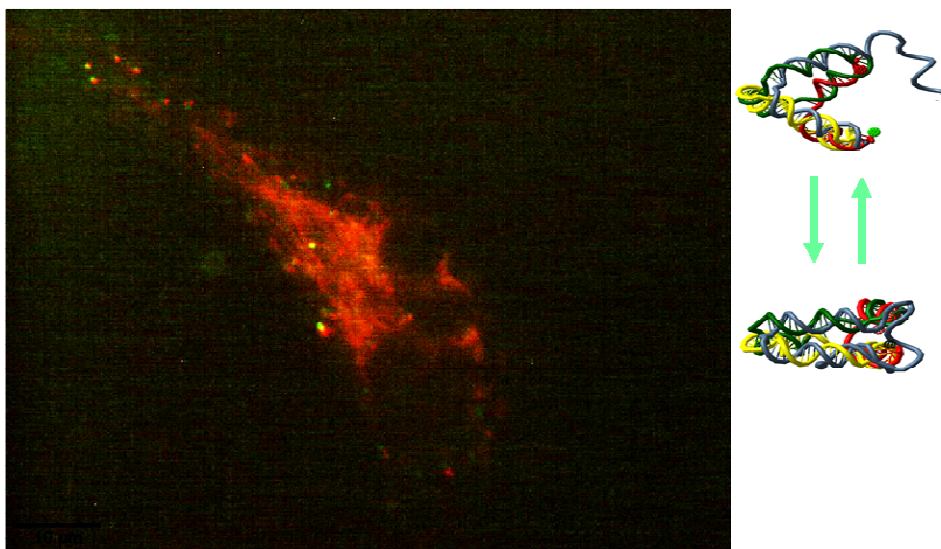


Figure 25. Overlay of the fluorescence signal of the donor dye represented in red with the signal from the FRET channel, represented in green. Localization of the green signal (or perfect overlay of signals that shows as yellow) reports on the localization of high-FRET states in point-like organelles identifiable as lysosomes.

Following the same procedure, the TT:BAX15 structure with the fluorophore variants (Cy3-REP and Cy3-REP-Cy5) were also treated with the human cultured glioblastoma line cells, after 6 hours incubation we performed the fluorescence microscopy characterization with the same series of set filters.

Micrographs are shown in **Figure 26**, blank showing almost any signal coming out besides the cell autofluorescence, as was described before. The structure which contains the Cy3-REP strand, also shows a similar behavior like the TT:PC structure, while in this case, we also notice the branched distribution around the nucleus and also very small point-like organelles; this follows almost the same internal localization. When the two fluorophores are present, the FRET signal is noticed, again in very low intensity; looking at the Cy3 emission filter, this is more brilliant than the one with only Cy3-REP strand, thus we confirm that when the CY5 is present, the CY3 emission intensity is also higher, very likely due to more efficient internalization. The morphological distribution also shows the cytoplasmatic distribution in a kind of spherical and tubular or branched compartments.

It seems that both TT:PC and TT:BAX15 nanostructures show almost the same internal distributions, both seem to be preferentially localized in the lysosomes and mitochondria or Golgi's apparatus. However, we still do not have a strong evidence to

confirm such hypothesis. For that case, experimentally, we have to compare the internal localization with a reference, this means, to deliver a specific lead molecule going to the lysosomes and to the mitochondria. This can be allowed by the use of the Lyso-TrackerRed dye for lysosomes and the Rhodamine Green for mitochondria. Lyso TrackerREd is an orange-red-fluorescent dye with excitation/emission of 647/668 nm, it is well used for labeling and tracking acidic organelles in live cells. On the other hand, Rhodamine Green shows a strong fluorescent emission at 530 nm when excited at 500 nm. Both organic dyes have been probed to enter the live cells efficiently, in virtue of being hydrophobic.

Additionally, the human glioblastoma cells were treated separately with Lyso-TrackerRed [50 nM] and Rhodamine Green [200 mM] dyes, incubated at 37°C and in humidity conditions for 20 minutes and then characterized by fluorescence microscopy, following the same filter sequences, as previous described.

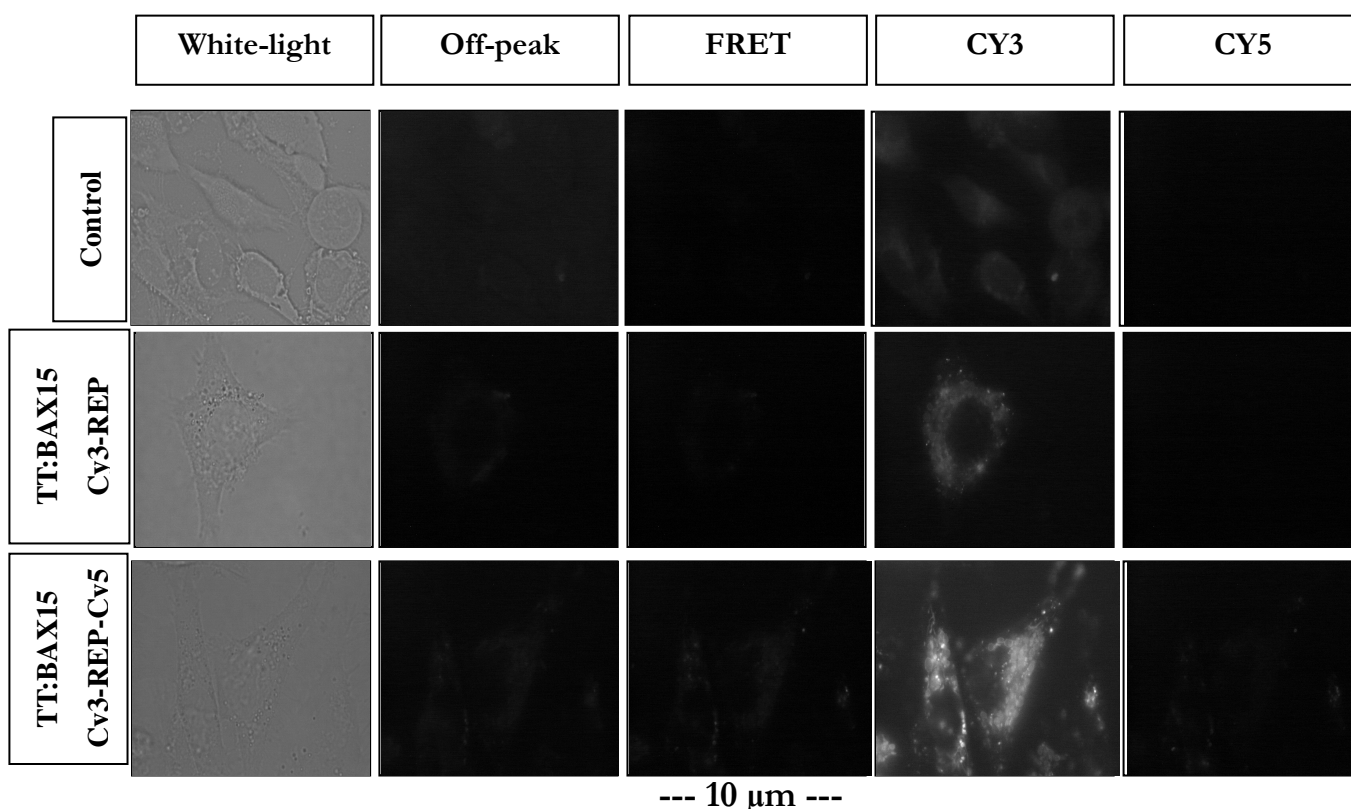


Figure 26. Examples of micrographs of human glioblastoma cells treated with the fluorescent structure TT:BAX15 [100 nM] after 6 h of incubation. Comparisons between the white-light, off-peak, FRET, on-peak (Cy3) and Cy5 filters for the two types of TT:BAX15 structure, one containing the Cv3-REP strand and the second containing the Cv3-REP-Cv5 strand. [100X, gain 4.8 X, exposure time: 2s].

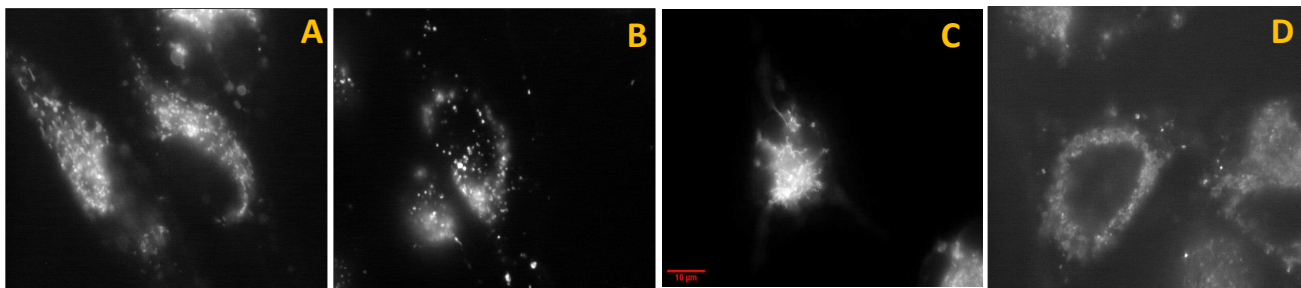


Figure 27. Micrographs of the on-peak (Cy3 filter) of human glioblastoma cells treated with: A) the TT:PC structure with (CY3-REP-CY5) after 6 h of incubation; B) Lyso-TrakerRed after 20 min incubation; C) Rhodamine Green after 20 min incubation and D) The TT:BAX15 structure with (Cy3-REP-Cy5) after 6 h incubation.

As a comparison, in **Figure 27**, are represented the results of treatment of the same type of glioblastoma cells with the free Lyso-TrakerRed and Rhodamine Green dyes. Lyso-Traker (B) displays a defined distribution, like if in vesicles. We presumably realize that due to the positively charged of our DNA nanostructure, it will preferentially localize at the negatively charged lysosome organelle, it is also seen from the like-dotted brilliant points exhibited by our both fluorescent nanostructures (micrographs A and D), thus we assume that part of the two nanostructures are localized in the lysosome compartments; corroborating in this way the results presented in [17]. On the other hand, Rhodamine green, due its negative charge, accumulates and localizes preferentially at the mitochondria; contrasting with our micrographs (A and D) with the one with Rhodamine (C), we have obtained a similar type internal distribution, a type of tubular branched arrange, more preferential around the nucleus, which we assume could be both mitochondria or Golgi's apparatus. Thereby we also presume that part of our structures are localized at mitochondria or Golgi.

Some important considerations to determine the specific intracellular localization upon uptake of our structures are that on the cell line, on the treatment conditions, on the cell state and possibly also on the type and number of fluorophores that are used to detect the presence and signaling state of the internalized nanostructures. Thus, further studies are needed in order to have a better control on cellular localization.

12.4 The micrograph semi-automatic analysis

Even though that visual analysis is usually the best option for characterizing intracellular distribution, we also performed a semi automatic micrograph analysis (see Section 2.4.2.2 for details). Based on the measurement of the average fluorescence intensity of defined areas inside the cells and also considering the background intensity for each micrograph for all the filters (off-peak, on-peak, FRET and Cy5). We performed the statically evaluation, where we could determine the average fluorescence for each cell and the fluorescence from the background for all the filters, then the background was subtracted leading to the single fluorescence; however this value also contains the autofluorescence coming from the off-peak, so was also subtracted. This evaluation was done to determine the net fluorescence from the FRET, Cy3 and Cy5 filters for a series of micrographs of the same cellular field.

Statistical analysis of those data (not shown here) evidence an unexpected behavior where since the Cy3 emission intensity is very high in comparison with the Cy5 emission intensity, we could not provide a consistent value of the single fluorescence of each cell. This could be due to the limited number of cells that we could measure or also to the likely fact that. The value of FRET emission could also include the tail the Cy3 emission which does not allow to simply deduce a net FRET value from Cy5. In addition, the generally low Cy5 emission intensity makes accurate quantification hard. Also further studies over the fluorescence microscopy parameters to acquire more quantitative micrographs are required to allow us to achieve better fluorescence statistical analysis.

12.5 TT:BAX15 and Staurosporine for cellular apoptotic evaluation

Human glioblastoma cells were also chosen to probe the *in vivo* biofunctionality of our designed TT:BAX nanostructure. As we described, Staurosporine induces the BAX transcription by RNA during the beginning of the apoptotic cycle of the cell, then the BAX strand that forms part of our nanostructure (TT:BAX) must detect the transcribed BAX sequence from RNA (BAX:RNA). When TT:BAX binds complementary to the BAX:RNA, the TT:BAX closes, the fluorophore pairs get close each other leading to the

FRET effect phenomena. Thus, if TT:BAX recognizes the BAX:RNA sequence effectively we could follow the FRET emission by fluorescence microscopy.

Human glioblastoma cells were treated with the TT:BAX15 structure after 6 h incubation, then, staurosporine [1 μ M] was added to the cells with the structure. Immediately, we were following the microscopically visualization, recording the FRET effect every 15 minutes for 3 hours. Previously we were following, as a control, the normal death cellular process due to the exclusion of their physiological conditions.

The BAX transcription by RNA was documented to occurs within the first 1.5 hours after the apoptotic cycle is induced, so, in this period time is when we expect to detect the FRET intensity increment. Nevertheless, the FRET signal was still very low through all the measurement (results not shown).

Probably, the BAX transcription happens too fast, which is hard to detect with this methodology; or even the amount of our TT:BAX structure inside the cells is too low to being detected by the BAX:RNA; or due the low FRET emission generated by the CY3/CY5 fluorophore pairs, we are no able to detect small intensity changes; or even could happen that our structure is digested somehow in the intrinsically apoptotic cycle.

From this point of view, we need a better understanding about the BAX:RNA process in the life cycle cell to design a suitable methodology in which we could detect the successful sensing signal about the biofunctionality of our nanostructures.

References Part IV

- [1] Goodman R.P., Schaap I.A.T., Tardin C.F., Erben C.M., Berry R.M., Schmidt C.F., Turberfield A.J., *Science* **2005**, 310.
- [2] Goodman R.P., Berry R.M., Turberfield A.J., *Chem. Commun. (Camb.)* **2004**, 1372–1373.
- [3] Bergamini C., Angelini P., Rhoden K.J., Porcelli A.M., Fato R., Zuccheri G. *Methods* **2014**, 67:185–192
- [4] Demidov Vadim V. and Frank-Kamenetskii Maxim D., *TRENDS in Biochemical Sciences* **2004**, 29; 2.
- [5] Demidov, V.V. *Trends Biotechnol* **2003**, 21; 148–151
- [6] Demidov, V.V. et al. *Methods* **2001**, 23; 123–131
- [7] Kuhn, H. et al. *Angew. Chem. Int. Ed. Engl* **1999**, 38; 1446–1449
- [8] Gondeau C., Maurizot J. C. and Durand M., *Nucleic Acids Res.*, **1998**, 26; 21.
- [9] Xodo L. E. *FEBS lett.*, **1995**, 370, 153-157.
- [10] Brucale M., Zuccheri G., Samori B., *Org. Biomol. Chem.*, **2005**, 3; 575-577
- [11] D. P. Millar, *Current Opinion in Structural Biology* **1996**, 6, 322.
- [12] J. L. Hecht, B. Honig, Y. K. Shin, W. L. Hubbell, *Journal of Physical Chemistry* **1995**, 99, 7782.
- [13] H. Pei, L. Liang, G.B. Yao, J. Li, Q. Huang, C.H. Fan, *Angew. Chem. Int. Ed.* **2012**, 51; 9020–9024.
- [14] A.S. Walsh, H.F. Yin, C.M. Erben, M.J.A. Wood, A.J. Turberfield, *ACS Nano* **2011**, 5; 5427–5432.
- [15] K.R. Kim, Y.D. Lee, T. Lee, B.S. Kim, S. Kim, *Biomaterials* **2013**, 34; 5226–5235.
- [16] H. Lee, A.K.R. Lytton-Jean, Y. Chen, K.T. Love, A.I. Park, E.D. Karagiannis, A. Sehgal, W. Querbes, C.S. Zurenko, M. Jayaraman, C.G.

- Peng, K. Charisse, A. Borodovsky, M. Manoharan, J.S. Donahoe, J. Truelove, M. Nahrendorf, R. Langer, D.G. Anderson, *Nat. Nanotechnol.* **2012**, 7; 389–393.
- [17] Liang L, Li J, Li Q, Huang Q, Shi J, Yan H, Fan C., *Angew Chem Int Ed Engl.*, **2014**, 10; 1002.
- [18] Wonbae Lee, Peter H. von Hippel, Andrew H. Marcus, *Nucleic Acids Research* **2014**, 42; 5967–5977
- [19] Grunwell J.R., Glass J.L., Lacoste T.D., Deniz A.A., Chemla D.S., Schultz, P.G. *J. Am. Chem. Soc.* **2001**, 123; 4295–4303.

PART V

Conclusions and Appendixes

Conclusions and Outlook

13. Conclusions

Along the previous three chapters, I presented two particular of novel DNA self-assembly nanostructures with the ability to perform a sensing response in live cells.

We described the theoretical and experimental tools that make possible the design, synthesis, characterizations and performance of DNA nanomachines. Feeding the emergency of revolutionized DNA nanostructures, we tried to developed two particular DNA biosensors: an intracellular pH response nanostructure and a nucleic-acids sensitive nanostructure. Here I describe some important remarks from our results that can help us to understand the full project presented in this thesis, leading us to come up with further achievements.

a) About the design

The accurate structural modeling and sequences design of our two functional DNA nanostructures were achieved by the use of NANEV and NUPACK. It is important to remark that both the structural modelling and the sequence design are crucial steps to program the outcome of successful self-assembly structures and assisted by computer software.

b) About the self-assembly

By the use of PAGE gel electrophoresis technique, we have verified the thermally annealing of our DNA nanostructures, probing that the most intense band in each lane

corresponded to the desired structure for both cases. Using this characterization technique, we have also adjusted the oligonucleotide stoichiometry in the assembly. Thereby we have probed the successful self-assembly of our two model designs in the established conditions.

c) About the sensing response

i) The pH nanosensor

By means of the PAGE gel technique, first we have successfully identified the formation of the triple helix conformation (closed state) in an acidic running buffer solution, while the open state was identified at basic conditions. We have also probed that the structure and its transition is stable and exhibits a good performance at cellular physiological conditions (37°C with 10 nM Mg²⁺ and 140 mM NaCl). We have also determined that the amount of Mg²⁺ ions present in the running buffer solution is of great importance to distinguish better the electrophoretic mobility of the TT:TFO structure among its positive (TT:PC) and negative controls (TT:nTFO) structures.

Using the fluorescence spectroscopic technique, we have evaluated the structural conformation response at certain pH environments, through the emission intensity of the Cy3 fluorophore. Performing a series of acidic- basic titrations, we have determined the successful TT:TFO structural change conformation from the open to the closed state when pH changes from basic to acid conditions; the TT:TFO does FRET upon reducing the pH, while the open and closed stationary nanostructures have a pH independent fluorescence. In addition it was shown the TT:TFO opened-closed cyclic conformational changes at different conditions, like the cellular physiological medium. We concluded that at physiological conditions, the unfolded conformation is much more preferred; the structure opens easily but takes more time to close. Due to the very low emission intensity of the BPY650 dye, when the FRET phenomena happens, we could not performed quantitative measurements based on this effect.

ii) The nucleic-acids sensitive nanosensor

First, by the use of PAGE gel technique, we have checked out the binding between the BAX oligonucleotide assembled in our DNA structure and the respective target's

sequences. We concluded that the longer strand (BAX15) binds easily inducing a conformational change, at normal TBE 1X running buffer solution, when it binds to 15's length target series. However, it requires a modified running buffer solution, enriched with Mg^{2+} ions, to be able to distinguish the binding with the 10's length target series. In addition at 37°C only 15+15-nt and 10+10-nt target sequences bind to BAX15, while 8+8-nt is not stable enough to bind. We concluded that due the 8's length target is too short, it does not to bind to BAX15 neither BAX10. BAX with length 15 is much more specific to target with 15-nt length. On the other hand, BAX10 binds preferentially to 10's series target rather than the 15's series target.

Characterizing the performance as a functional sensor was done through its the FRET behavior. First, by titrations we determined its BAX:Target quantitative binding, concluding that it is required around one equivalents of the target to completely binds to the BAX sequence in the structure. The conformational change was followed by means of its FRET response, concluding that when the structure is in the closed conformation, the FRET occurs, quenching the Cy3 emission intensity while the BPY650 emission intensity is increased; we have noticed that the highest FRET emission intensity is obtained BAX10 is closed with the target 10 with 5 gap. So, we conclude that the recognition is much more specific when we have two short DNA probes instead of a longer single one.

d) About the cell uptake

The treatment of our nanostructures with HeLa are perfectly internalized after 6 hour incubations and the structure remains inside with their fluorescence response without producing any negative effect inside the cells after more than 8 hours incubation. Renal and glioblastoma type cells also internalize the structures and are stable.

Glioblastoma cells treated with TT:PC containing the Cy3/Cy5 fluorophore pairs, after 6 hours incubation, leads to their uptake by cells and internalizing in the cytoplasmic organelles, by the inside cell morphological distribution of our structures, it appears that some end up in lysosomes and some in either mitochondria or Golgi apparatus. We conclude that Cy3 and Cy5 are both co-localized and some few FRET emission is also seen. We also conclude that the presence of Cy5 dye in the structure intensifies the emission intensity of Cy3 dye.

When glioblastoma cells are treated with the TT:BAX15 structure, which contains the Cy3/Cy5 fluorophore pairs, it is also perfectly internalized and localized around the peripheral nucleus, probably in lysosomes and mitochondria or Golgi apparatus. We also detected a few FRET emission intensity. Similarly to the pH structure, the Cy3 dye emission is intensified by the presence of Cy5 dye when they are in the same strand.

The quantitative characterization by the micrograph analysis did not provide a relevant value about the fluorescence distribution in each cell, we need to optimize the parameters of excitation-emission detections and to investigate deeper the fluorophore pairs distribution in the fully assembled structure and their interactions when are inside the live cells.

We tried to perform the sensing response by the TT:BAX structure in live cells, acting together with staurosporine to recognize the transcript BAX:RNA sequence when its expressed at the beginning of the apoptotic cycle. However we could not succeed because our FRET emission is very low to be able to follow in time.

13.1 Future Perspectives

Through this project we have demonstrated how two DNA nanostructures could work as a potential biosensors in live cells. Our pH sensing nanostructure could be used in localized acidic cellular organelles like lysosome, to sense its pH changes or use it as a switching device for carrying and delivering localized therapy agents. However, more advanced and interdisciplinary researching are requires.

On the other hand, to probe the TT:BAX sensing during the apoptotic cycle inside the cell we need first to characterize a suitable fluorophore pairs with the ability to perform a distinguishable FRET emission by fluorescence microscopy. Later we need to understand better the apoptotic mechanism for the specific recognition of the BAX:RNA transcript by our TT:BAX strand. One possibility could be the evaluation of expression of BAX in time by the qPCR technique. Also, to accomplish a more quantitative data we need appeal to another technique like flow cytometry, that provide quantitative information on the fluorescence of a cell population of a size by measuring the fluorescence intensity of each cell together with their light scattering properties that inform about cell size and morphology

It is eminent that DNA nanotechnology is emerging as a potential discipline, it is setting the bases for the improvement in many biomedical fields that certainly, in a near future could be successfully applied, providing significantly achievements in the way to use the medicine.

14 Appendixes

15.1 Filter microscope characterization

In this section is described the characterization of the FRET filter when was mounted in our fluorescence microscope. The aim was to ensure that when the DNA nanostructures generate the FRET effect, the detected emission is coming exclusively from Cy5 and not from the emission tail of the Cy3 fluorophore.

Procedure

To achieve this characterization we considered three samples; TT:nTFO, TT:PC that contains the Cy3/Cy5 fluorophore pairs and the single REP strand, not being part of the structure, that contains both fluorophores.

Measurements were done using the following excitation-emission parameter ranges for each set of filters:

Table 1. Excitation-emission parameters for the different filter sets

Excitation/ Emission	Filter
515/565 nm ; Cy3/Cy3	Cy3
543/650 nm ; Cy5/Cy5	Cy5
515/650 nm ; Cy3/Cy5	FRET
405/515 ; off-peak	FRITC

To determine the fluorescence intensity for each filter, we have tried with four different apertures of the excitation light from the mercury lamp; 1/1 (the highest intensity), 1/4,

1/8 and 1/32 (the lowest intensity). Imagine acquisitions were carried out from the one with lower light exposure to the highest for each filter. In this way, also the light exposure is reduced to avoid the photobleaching effect. The gain was maintained constant at 4.8X for 150 ms exposure time. We mounted a single drop at 1 μ M of each sample on the microscope stage and focalized both a section inside the drop and other outside, this means considering in the same image, the background emission.

The qualitative intensities from the images suggested that the FRET of the single REP strand is of lower intensity than the Cy3 and Cy5 by their selves. Also the same behavior is shown for TT:nTFO (the FRET intensity is lower) and we hardly notice a difference between TT:nTFO and TT:PC

The quantitative analysis was done by measuring automatically a defined area both the inside drop and from the background, so we obtained an average value of the area for both sections.

We determined statistically the dispersion rate of the values for all the filters in each sample and was also removed the average background value.

The imagine analysis were done using the program Image J which automatically provides the fluorescence intensity value of a defined pixel section. We obtained values from different fields; considering measurements inside the drop and outside the drop (the background). Measurements done for all the filters with all the samples.

The statistically evaluation was done by obtaining the deviation standard intensity value for each drop with their corresponding background. Then the background value was subtracted from the drop intensity to obtain the net fluorescence intensity value. This operation was done individually for all the micrographs with all the aperture variations.

Cy3, Cy5 and FRET intensities were obtained by taking the intensity average value for each filter set in the next ratios: Cy3/Cy5, Cy3/FRET and FRET/Cy5. Results are presented in **Figure 1**.

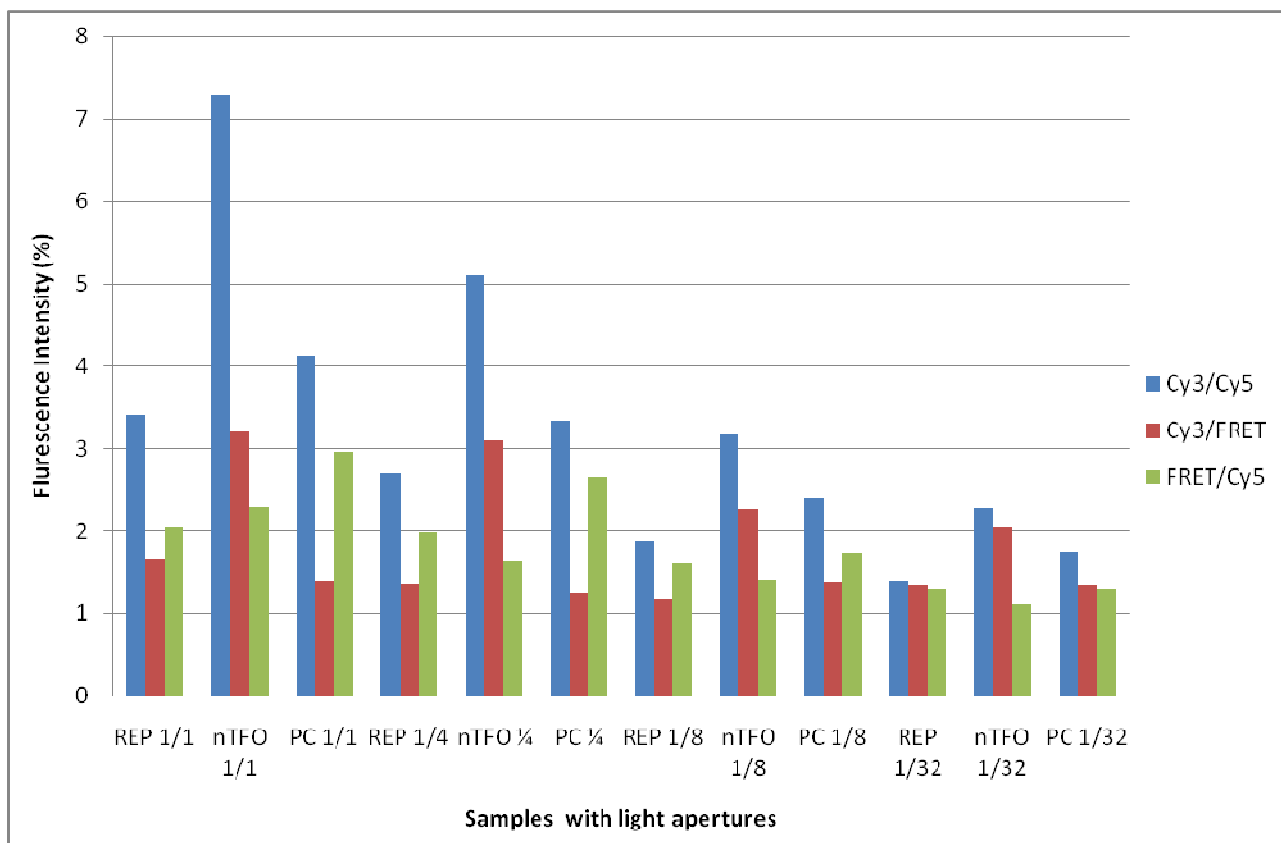


Figure 1. Fluorescence intensity values for each sample at different light apertures

Fluorescence intensity values presented in **Fig. 1** are described as follow:

- Cy3/Cy5 in all the cases the intensity ratio is higher for nTFO structure, then lower for PC structure and the lowest for the single REP strand that contains the two flurophores.

- Cy3/FRET the intensity ratio is higher in all the cases for nTFO structure and both the PC structure and the REP strand describe the same intensity value

- FRET/Cy5 the intensity ratio is always higher for the PC structure, then for the REP strand and sometimes the lowest for nTFO structure.

From the previous values, as we expected, the higher FRET/Cy5 intensity ratio becomes from the PC structure, which is more intense when the structure is closed, while the higher Cy3/Cy5 and Cy3/FRET come from the nTFO structure as we expected, when they are in the open state; this behavior is the same, even though that the illumination was rotated. With those values we can deduce the net FRET emission intensity by subtracting from the PC structure intensities the nTFO intensity values; in this way, we

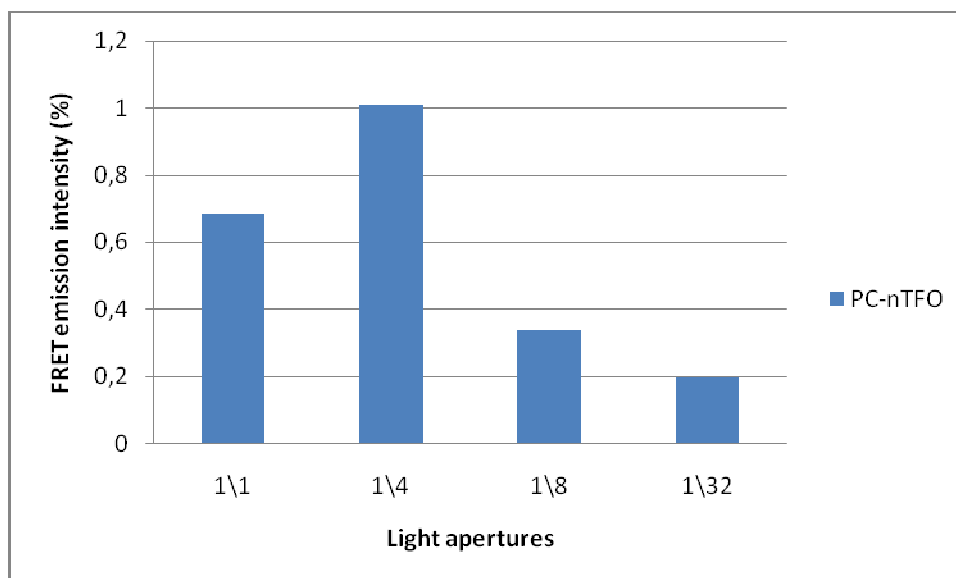


Figure 2. Net FRET intensity values at different light apertures.

suppressed the fluorescence intensity value from the tail Cy3 intensity over the FRET. The net FRET values are represented in Figure 2.

In conclusion, by the filter characterizations we have notice that with the Cy3/Cy5 emission value from the nTFO structure, being higher, we could deduce the net FRET emission intensity value for all the samples. However, the fact that it also depend on the illumination shows that it is difficult to have quantitative results with the microscope set-up as the cells will be illuminated differently from the drops of nanostructure solution and will presumably contain nanostructures at lower concentrations.

15 Acknowledgments

Two years ago I started one of the most amazing trips in my life, my first time in Europe, it was the beginning of one of the most enrichment opportunities for my professional, personal and spiritual life. I was afraid when I left home but at the same time, very anxious to discover all the experiences, places, people, knowledge and culture that this Master was preparing for me; experiences that have enriched one of the most important chapters in my life. Along my stay in Europe there were a lot of people that helped me during this period. They gave me all the support, time, knowledge, smiles, patience, courage and love to success in this voyage.

My parents, Ma del Carmen and Alejandro; since I was a child, they gave me all the motivation, security and confidence to do whatever I wanted. You are still a great source of inspiration.

My sisters (Yolanda, Genoveva) and my lovely nieces (May, Ma.Josè, Mimis). Day by day were here to providing me all the love and emotional support to continue even at adverse circumstances. We are a great family.

My “secta” Lidia, Vero, Rosita, Bruno, Daniel. From the other part of the ocean, you were with me all the time as a big source of motivation, inspiration friendship and happiness. Thanks for trust on my; you are a fundamental part in my life.

My admire Italian friend, Stef. Italy and its life would have been so different without you. Thank you for all the support, courage and your time to show me a lot of amazing places, people and culture of Italy.

It was a fantastic experience to meet a lot of interesting people during my two years Master, Leipzig and Bologna, people from around the world that once we started with the same objective and hopefully we will meet again in a near future. Thanks to share with me a little part of your culture.

All my Mexican friends that I was finding on the road of this two years, you made me feel again at home; thank you for sharing experiences, food, advises and happiness that is part of us.

Dr. Giampaolo Zuccheri, thank you for giving me the opportunity to be part of your research group and for providing me a lot of knowledge and support during this thesis. Also to all teh guys at the lab, thank you for your patient, support and great

moments during this time. Christian, thank you for your time and dedication with the cell experiments in this project.

To the Erasmus Mundus Association, anything of this dream would have not been reality without this opportunity. I am enormously grateful for giving to third world students a chance to learn, discover and interchange professional and personal experiences.

In Lak'ech Ala K'in

Isidro